EVALUATION OF SURFACE SOIL GEOCHEMICAL DATA AND STATISTICAL MODELING OF AKARCA FULA TEPE LOW SULFIDATION EPITHERMAL AU-AG MINERALIZATION, BURSA, TURKEY

A THESIS SUBMITTED TO
THE GRADUATE SCHOOL OF NATURAL AND APPLIED SCIENCE
OF
THE MIDDLE EAST TECHNICAL UNIVERSITY

BY

DERYA BAL

IN PARTIAL FULFILLMENT OF THE REQUIREMENTS
FOR
THE DEGREE OF MASTER OF SCIENCE
IN
GEOLOGICAL ENGINEERING

SEPTEMBER 2015

Approval of the thesis:

EVALUATION OF SURFACE SOIL GEOCHEMICAL DATA AND STATISTICAL MODELING OF AKARCA FULA TEPE LOW SULFIDATION EPITHERMAL AU-AG MINERALIZATION, BURSA, TURKEY

Submitted by **DERYA BAL** in partial fulfillment of the requirements for the degree of **Master of Science in Geological Engineering Department, Middle East Technical University** by,

Prof. Dr. Mevlüde Gülbin Dural Ünver _____
Director, Graduate School of Natural and Applied Sciences

Prof. Dr. Erdin Bozkurt _____
Head of Department, Geological Engineering

Prof. Dr. Nurkan Karahanoğlu _____
Supervisor, Geological Engineering., METU

Examining Committee Members:

Prof. Dr. Erdin Bozkurt _____
Geological Engineering Department., METU

Prof. Dr. Nurkan Karahanoğlu _____
Geological Engineering Department., METU

Assist. Prof. Dr. Fatma Toksoy Köksal _____
Geological Engineering Department., METU

Prof. Dr. Yurdal Genç _____
Geological Engineering Department., Hacettepe University

Assist. Prof. Dr. Erkan Yılmazer _____
Geological Engineering Department., Aksaray University

I hereby declare that all information in this document has been obtained and presented in accordance with academic rules and ethical conduct. I also declare that, as required by these rules and conduct, I have fully cited and referenced all material and results that are not original to this work.

Name, Last Name: DERYA BAL

Signature:

ABSTRACT

EVALUATION OF SURFACE SOIL GEOCHEMICAL DATA AND STATISTICAL MODELING OF AKARCA FULA TEPE LOW SULFIDATION EPITHERMAL AU-AG MINERALIZATION (BURSA), TURKEY

Bal, Derya

M.S., Department of Geological Engineering

Supervisor: Prof. Dr. Nurkan Karahanoğlu

September 2015, 99 pages

The Akarca property is dominated by Triassic sedimentary units that tectonically overlie Pre-Triassic basement rocks (schists and marbles). The property displays characteristics of a low sulfidation Au-Ag deposit type in terms of alteration, mineralization and vein textures. The Akarca property is characterized by six primary mineralized zones. Among these zones, Fula Tepe Zone formed the subject of this thesis. The main aim of this dissertation is to evaluate the results of surface soil geochemistry data and to create statistical model based upon indicator and pathfinder elements to generate new gold targets for further exploration in the mineralized zone. A geochemical dataset was obtained from 195 surface soil samples, which were evaluated using univariate and bivariate statistical methods. Seven elements, namely, Au, Ag, As, Hg, Sb, Se, and Te are considered. Descriptive statistics, histograms, and Q-Q plots reveal that Au, Ag, As, Hg, and Sb display non-normal distribution. Pearson correlation matrix identifies silver as the best indicator for gold. Gridding maps show that Au, Ag, As, Sb and Se have strong anomalies in the area. The strong gold anomalies nearly coincide with the strong silver anomalies

at the center of area. As and Se appear to be enclosed to main Au anomalies. As and Se could therefore be used as pathfinder elements for prospecting gold. In order to identify new target zones, higher background population was separated from the datasets for Au and Ag. Consequently, new three gold targets were identified for further exploration.

Keywords: Statistical analysis, surface soil geochemistry, epithermal gold, Akarca, Turkey

ÖZ

AKARCA FULA TEPE DÜŞÜK SÜLFİTLİ EPİTERMAL AU-AG MİNERALİZASYONUNUN YÜZEY JEOKİMYASAL TOPRAK VERİLERİNİN DEĞERLENDİRİLMESİ VE İSTATİSTİKSEL MODELLEMESİ, BURSA, TÜRKİYE

Bal, Derya

Yüksek Lisans, Jeoloji Mühendisliği Bölümü

Tez Yöneticisi: Prof. Dr. Nurkan Karahanoğlu

Eylül 2015, 99 sayfa

Akarca bölgesinde Triyas öncesi temel kayalar şist ve mermerden oluşan ve bu kayaları tektonik olarak üzerleyen Triyas tortul birimleri yüzeyler. Bölgedeki alterasyon, mineralizasyon ve damar dokusu tipik düşük sülfitli Au-Ag cevherleşmesinin özelliklerini gösterir. Akarca altı temel mineralizasyon zonlarından oluşmaktadır. Bu altı zondan Fula Tepe Zon tezin çalışma konusunu oluşturur. Tezin temel amacı Akarca Fula Tepe zonunda ki toprak jeokimyası verilerini değerlendirerek yol gösterici elementlere dayılı istatistiksel bir model oluşturmak, elde edilen sonuçlara göre ise altın için yeni hedef alanlar belirlemektir. Tek ve iki değişkenli istatistiksel yöntemler kullanılarak değerlendirilen 195 toprak örneğinden jeokimyasal veri üretilmiştir. Çalışmada yedi elemente, Au, Ag, As, Hg, Sb, Se ve Te'ye odaklanılmıştır. Tanımlayıcı istatistikler, histogramlar, ve Q-Q grafikleri Au, Ag, As, Hg ve Sb'nin normal bir dağılıma sahip olmadığını göstermektedir. Pearson korelasyon matriks analizine göre gümüş altın için en iyi indikatör olarak belirlenmiştir. Anomali haritaları Au, Ag, As, Sb ve Se gibi elementlerin sahada

güçlü anormallikleri gösterdiğini ortaya koymaktadır. Güçlü altın anomalileri çalışma alanının merkezindeki güçlü gümüş anomaliler ile neredeyse örtüşmektedir. As ve Se anomalileri, Au anomalilerini çevrelemiş şekilde görülür. Bu nedenle, As ve Se elementleri altın yol gösterici elementler olarak kullanılabilinir. Yeni hedef bölgelerini tespit etmek amacıyla, yüksek popülasyonlu anomaliler Au ve Ag veri setlerinden ayrılmıştır. Sonuçta, ilerideki arama çalışmaları için yeni üç altın hedef bölgesi belirlenmiştir.

Anahtar Sözcükler: İstatistiksel analiz, toprak jeokimyası, epitermal altın, Akarca, Türkiye

Dedicated to my family for their love, support and education throughout my life.

To my loved ones-the people who support and believe in me.

ACKNOWLEDGEMENTS

I would like to thank my supervisor Prof. Dr. Nurkan KARAHANOĞLU for his valuable suggestions and guidance. I could not have imagined having a better advisor for my M.Sc. study.

I also would like to thank Dr. Mesut SOYLU for his constant support, guidance, valuable comments, continues encouragement, and patience. His guidance was always with me in every stage of this research and thesis writing. It is a great honor to work with him and our cooperation always influence my business, academical, and world view highly. Without his helps, this study would not have been finished.

I wish to express my sincere gratitude to Dean D. TURNER for his valuable suggestions and valuable comments.

I would like to thank Eurasian Minerals Inc., Dr. Cengiz DEMİRCİ (General Manager of Asia Minor Mining) and Asia Minor Mining for giving me the chance to work with them at the Akarca Project for my Master's thesis. I am grateful to Mr. Michael P. Sheehan (Exploration Manager), Mr. Eric JENSEN (General Exploration Manager), and all of my colleagues in Eurasian Minerals for their recommendations.

I thank to Miss Burcu ŞAHİN, Mrs. Birce BAKDI ÖZBALABAN, and Miss Yelda DİNEROL for their help and continues moral support.

I also thank to one who, directly or indirectly, have lent me their helping hand.

Finally, I owe a special gratitude to my family for their great support and generous help.

TABLE OF CONTENTS

LIST OF TABLES

TABLES

LIST OF FIGURES

FIGURES

LIST OF ABBREVIATION

CRM : certified reference material

GIS : geographic information systems

H/S : high sulfidation

ICM/AES : inductively coupled plasma atomic emission spectroscopy

ICM/MS : inductively coupled plasma mass spectrometry

L/S : low sulfidation

LH : lower hinge

LW : lower whisker

MAD : median absolute deviation

MSL : mean sea level

Q1 : first quartile

Q2 : second quartile

Q3 : third quartile

QA/QC : quality assurance/quality control

SRM : standard reference material

UH : upper hinge

UIF : upper inner fence

UW : upper whisker

CHAPTER 1

INTRODUCTION

1.1. Purpose and Scope

The aim of this thesis is to evaluate the results of surface soil geochemistry data and to create a statistical model based upon indicator and pathfinder elements to identify new target zones for further exploration in Akarca Fula Tepe Zone low sulfidation (L/S) epithermal Au-Ag mineralization.

In this study, univariate (histograms, Q-Q plots, box-and-whisker plots, and probability graphs) and bivariate methods (e.g. correlation coefficients) were applied with geographic information system (GIS) technique to interpret geochemical results and investigate geochemical anomalies in a geochemical dataset. The statistical study covers following elements; Au, Ag, As, Hg, Sb, Se, and Te. According to studies in literature, these elements are regarded as indicator and pathfinder elements for low sulfidation (L/S) gold-silver deposits. The geochemical results were evaluated by using IBMSPSS22, Microsoft Excel, and ArcGIS software.

The dataset contains chemical analyses of 195 surface soil samples. All samples were analyzed by ALS Laboratory Services. During the geochemical survey, QA/QC (Quality Assurance/Quality Control) samples (standards, blanks, and duplicates) were used for the data assurance reliability, accuracy, precision and reproducibility of assay results and analyses.

1.2. Geographic Location of the Study Area

The Akarca property is located 20 km south of Mustafakemalpaşa in Bursa, west Turkey (Figure 1). It is located approximately 450 kilometers west of Ankara, the capital city of Turkey, and 70 kilometers southwest of Bursa, a major industrial city and namesake of the province. The property corresponds to UTM zone 35, ED50 coordinates of 4,421,420 meters north and 624,370 meters east. Akarca, Kömürcükadı and Şapçı villages are the closest residential areas to the study area and are accessible via paved road from Mustafakemalpaşa town center.

Physiography of the Akarca property is gently to moderately steep, with subdued mountain ranges and valleys with elevations ranging from 50 to 820 meters above mean sea level (MSL). The property is dominated by a forest cover of mostly oak and pine, and grasslands. The vegetation and the forest cover are dense at some localities within the study area and its vicinity.

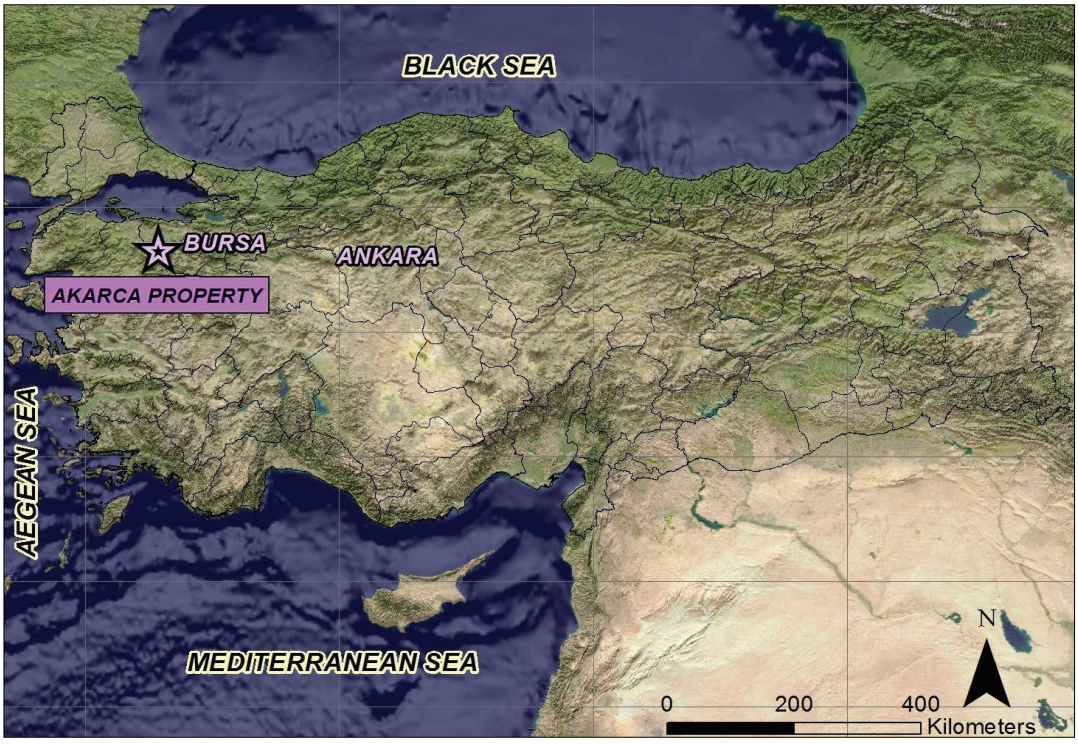

Figure 1. Location of Akarca property, Bursa, Turkey.

1.3. Previous Studies

Some researchers studied the geology, stratigraphy, lithology, mineralization and structural geology of the property, and some of them include the study area.

Yalçınkaya and Avşar (1980) studied the lithological units of Mustafakemalpaşa and surrounding region and mapped the area at a scale of 1:25,000.

Chadwick (2009) studied the general geology and the mineralization of the property. As a result of his study, he determined that the Neogene (?) clastic sediments unconformably overlie the Paleozoic metamorphic rocks. He stated that the vein type low sulfidation (L/S) gold-silver mineralization has reached to surface by parallel normal faults.

Tosdal (2010) aimed to create geological model on mineralization of the Akarca property based upon field observations, core studies, and geochemical database. His observations can be summarized as follows:

- The mineralization in the Akarca property is typically of L/S epithermal type,
- The geochemical data suggest that Au and Ag are observed between 400 meters relative level (mRL) and 175 mRL. However, the best horizon for Au with consistently higher grades lies between ~260 and 330-340 mRL. An apparent base to the Au lies at 175 mRL. Below this point, Au appears be lower grades and uneconomic.

Hedenquist (2011) studied on geology, and mineralization using diamond drill cores of the Akarca property and his conclusions are as follow;

- Akarca Au-Ag mineralization is a L/S epithermal system formed in shallow paleo-depths hosted in Neogene (?) clastic sediments.
- Neogene sediments are pebble stones, sandstones, and siltstones whose base includes carbonaceous mudstones.

- Silicified halos around the veins and breccia zones are not well developed; their thickness could be related with permeability and porosity of the sandstones and conglomerates.

- The conglomerates and sandstones without an argillaceous component are the best to host the best-developed veins.

- The Akarca L/S epithermal system shows several similarities with the known L/S style of vein mineralization around the world; forming in an extensional setting, the common association of classical L/S vein textures with Au mineralization, Se anomalies with Au, and halos of As, Sb and Hg.

Davies (2012) conducted a geological field study and core analyses. His evaluations can be summarized as follows:

- Neogene units that host mineralization indicate a proximal depositional environment.

- The units are generally composed of coarse clasts. Most of the pebbles are derived from limestone and marble. Granite gravel is not found among pebble stones.

- The property is divided into two base sections. One of them is schist, which is composed of high grade metamorphic rocks while the other one is lower grade phyllite.

- There are many faults in the area. All of these faults are post-mineralization faults and they are not related to the mineralization and alteration in the property.

- According to the core surveys, significant cataclastic zones are observed. A distinct foliation, brecciated rocks, and curved structures are usual in this zone. According to the researcher, these structures may indicate a “detachment fault” in the area. If this detachment fault exists, it might possibly truncate veins in Neogene units.

Ferguson (2013) conducted a detailed field study and diamond drill core analysis. He carried out lithological mapping based upon the different rock types exposed in the property. He mapped the lithological units as follows:

- Neogene (?) sedimentary rocks,
- Permo-Triassic carbonate and Mesozoic-Tertiary phyllite and meta-sediment, and
- Mylonitic granitoid, paragneiss, and marble.

Toprak (2014) studied lithological units and structures of the Akarca property and surrounding region and mapped the area at a scale of 1:25,000. His evaluations can be summarized as follows:

- Pre-Neogene (Jurrassic and Cretaceous) two overthrust faults and late-Neogene three-phased faults were observed in the area.
- The age of the sedimentary units that host the mineralization was determined to be Triassic. The units are generally composed of conglomerate, sandstone, siltstone and claystone.
- The pre-Triassic metamorphic units are tectonically overlain by the Triassic sedimentary units along the southern boundary of the property.

CHAPTER 2

GEOLOGICAL SETTING

Geological setting chapter is compiled from the studies of Delaloye and Bingöl (2000), Dreier and Soylu (2011), Ferguson (2013), Hedenquist (2011), Helvacı (1994), Okay and Göncüoğlu (2004), Sapancı (2011), Toprak (2014), and Yalçınkaya and Avşar (1980). The simplified geologic map and tectonostratigraphic columnar section are modified from Toprak (2014) (Figures 3 and 4).

2.1. Regional Geology

The Akarca property occurs in the Sakarya Composite Terrane of the Pontides, where deformation and magmatism occurred during Cretaceous to Neogene Alpine orogenic event (Figure 2).

There are several rock units which ages ranging from the Paleozoic to Quaternary (sedimentary sequences, metamorphic rocks, intrusions, and ophiolitic units) with recent alluvium cover around the Akarca property (Figure 3). There are some overthrust faults mapped in an area near to the property. These overthrust faults are represented in Figure 4. They are observed between the Triassic Karakaya Formation and pre-Triassic metamorphic rocks as well as being observed at the base of Upper Cretaceous ophiolitic rocks. Rocks exposed within and around the property can be divided into nine units. They are, from oldest to youngest, pre-Triassic metamorphic rocks, Triassic clastics and carbonates (Karakaya Formation), Jurassic limestone and clastic rocks, Upper Cretaceous ophiolites, Oligo-Miocene granitic intrusions, Miocene continental clastic rocks, Pliocene continental clastic rocks, and Pliocene and Quaternary terrace deposits, and recent alluvium covering them (Toprak,2014).

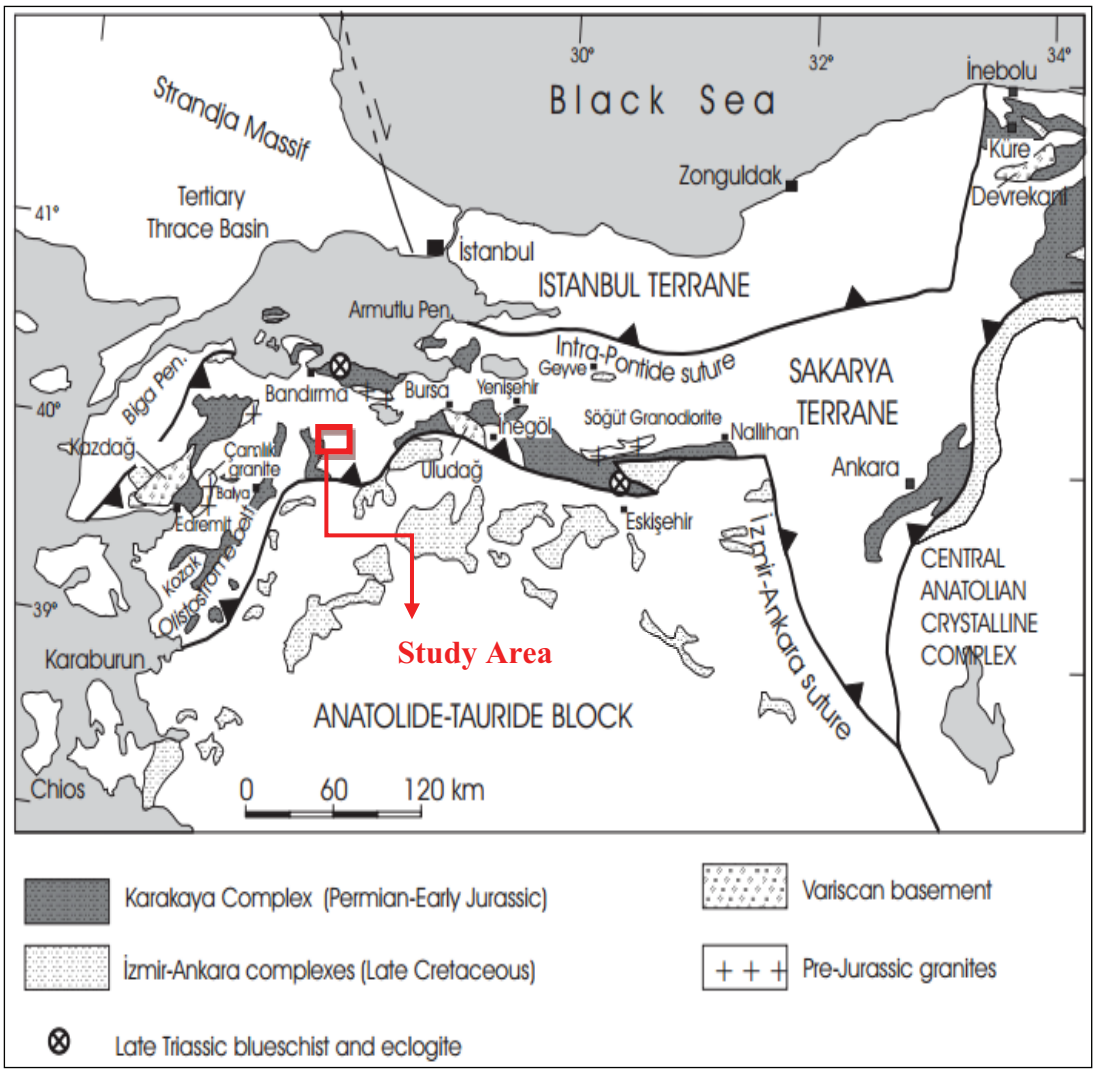

Figure 2. Regional tectonic setting of the Akarca property (Okay and Göncüoğlu, 2004).

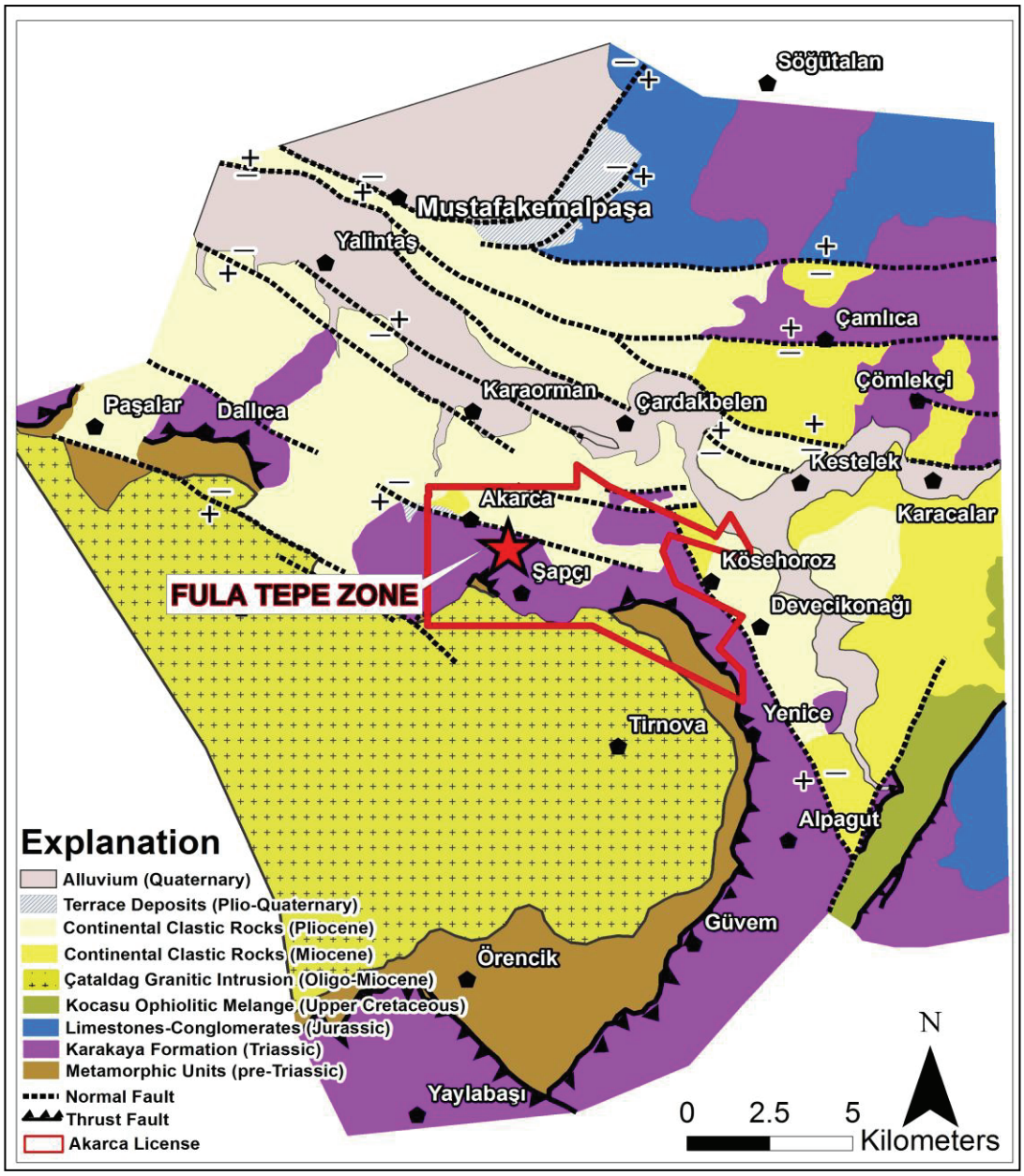

Figure 3. Geological map of the Akarca property and surrounding region (Toprak, 2014).

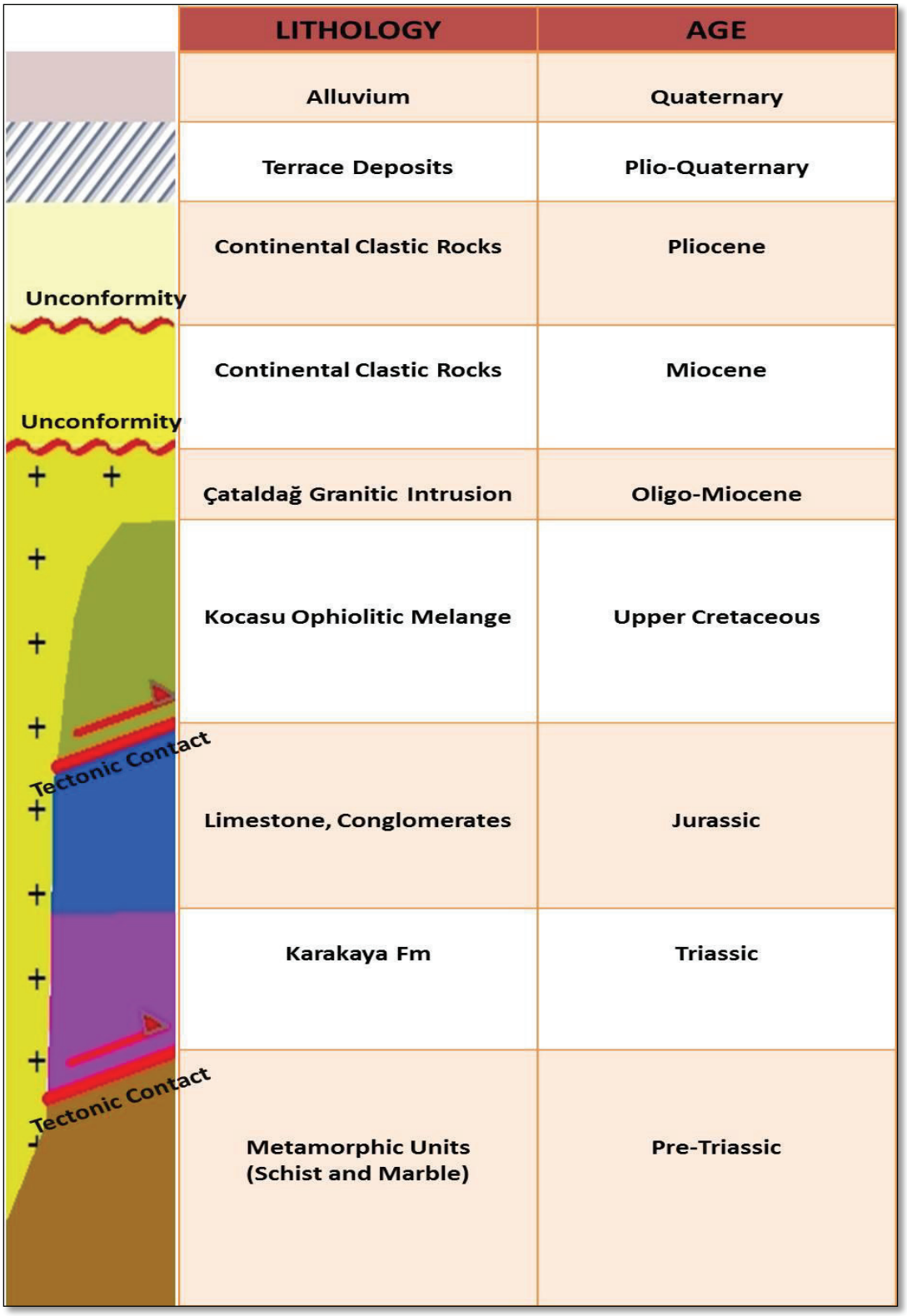

Figure 4. The tectonostratigraphic columnar section of the Akarca property (Toprak, 2014) (This section is not to scale).

2.1.1. Metamorphic Units (pre-Triassic)

Yalçınkaya and Avşar (1980) defined metamorphic units as two packages. Both packages include metaclastic rocks in the lower section while they include crystallized limestones and/or marbles in the upper section.

Metamorphic units display three types of contact with younger units: 1) The units are tectonically overlain by the Triassic Karakaya Formation, 2) They are intruded by Oligocene granite, and 3) They are uncomformably overlain by Pliocene terrestrial clastics.

2.1.2. Karakaya Formation (Triassic)

Triassic Karakaya Formation is defined in Sakarya Zone and composed of conglomerate, sandstone, siltstone, shales, block structured limestones, volcanic rocks, which contain tuffs and lavas, and pyroclastic rocks (Okay and Göncüoğlu, 2004). This formation tectonically overlies the metamorphic units (Yalçınkaya and Avşar, 1980).

Karakaya Formation is exposed along E-W direction within the property. The southern portion of the property is covered by the pre-Triassic metamorphic rocks and Oligocene granite. The northern contact is faulted through Güveçdere-Akarca-Kömürcükadı corridor.

2.1.3. Sedimentary Units (Jurassic)

The Jurassic sedimentary units are composed generally of gray colored, medium-thick bedded sandstones, conglomerates, and limestones.

These units are exposed on the northeast and southeast side of the Akarca property. Yalçınkaya and Avşar (1980) are the first to name the clastic units under these units as Dağakçe Formation, and limestones above these units as İnatlar Formation.

2.1.4. Kocasu Ophiolitic Melanjic Units (Late Cretaceous)

Yalçınkaya & Avşar (1980) defined ophiolitic rocks as Kocasu Melange. Kocasu Melange is composed of pyroxenite, serpentinite, gabbro, diabase, diorite, and tuff. The mélange units are tectonically in contact with the Jurassic sedimentary units. The Triassic Karakaya Formation, metamorphic rocks, and the mélange also contain older units as blocks.

2.1.5. Granitic Intrusion (Oligo-Miocene)

Granitic rocks cover Çataldağ and surrounding area. Delaloye and Bingöl (2000) dated the granitic stock using K-Ar dating and obtained an age of 20.8 ± 0.4 Ma. The granites intrude metamorphic rocks, Karakaya Formation, the Jurassic Sedimentary units, and the ophiolitic melanjic units. They also are unconformably overlain by the Pliocene units.

2.1.6. Continental Clastic Rocks (Miocene)

Terrigenous clastic rocks are composed of conglomerates, volcanic rocks and fine terrestrial clastics. This assemblage uncomformably overlie the Upper Cretaceous ophiolitic mélange and the Triassic Karakaya Formation. The Pliocene terrigenous units unconformably overlie these units. Carbonaceous levels are observed on top of the clastic section that contains some lignite seams (Helvacı, 1994).

2.1.7. Continental Clastic Rocks (Pliocene)

The Pliocene units expand from south-eastern to northern part of the Akarca property. These units unconformably overlie the Miocene units. The Quaternary alluviums unconformably overlie this assemblage. The dominant lithology of the Pliocene units is coarse clastic rocks such as conglomerate, sandstone and siltstone. In general, they are deposited as alluvial fan.

2.1.8. Terrace Deposits (Plio-Quaternary)

The Plio-Quaternary terrace deposits are located at the eastern Mustafakemalpaşa and the south of the Karaorman village. Terrace sediments generally have a smooth morphology, which is low sloped and not very slit.

2.1.9. Alluvium (Quaternary)

The Quaternary alluviums give two outcrops separated by Mustafakemalpaşa horst. These alluvial deposits are located almost in the central part of the Pliocene sediments. According to this evident, the tectonic phase, which began in the Pliocene, still continues today.

2.2. Local Geology

The Akarca property is dominated by development of the Triassic sedimentary rocks (Karakaya Formation) that tectonically overlie the pre-Triassic metamorphic rocks, (schist and marble) (Yalçınkaya and Avşar, 1980). The Karakaya Formation is unconformably overlain by the Pliocene continental clastic rock (Yalçınkaya and Avşar, 1980). The metamorphic rocks are intruded by Oligo-Miocene granitic stock at the southern portion of the property (Figure 5).

The pre-Triassic metamorphic units (basement) are made up of schist and marble. The units are exposed at the southwest corner of the property. The basement is tectonically overlain by the Triassic sedimentary rocks of Karakaya Formation. Schist consists of quartz, mica, chlorite, and amphibole and its color varies from dark brown to green. The marbles are observed as massive or poorly bedded. These vary in color from dark beige to dark grey.

The Triassic sedimentary rocks (Karakaya Formation) are made up of conglomerate, sandstone, siltstone, and claystone. This formation covering most part of the Akarca property is exposed along Akarca, Şapçı, Kömürcükadı, and Kösehoroz villages. These rocks tectonically overlies the pre-Triassic metamorphic basement rocks (schist, and marble). It is the main host unit for the epithermal L/S Au-Ag mineralization (Dreier and Soylu, 2011). The lithological distribution

analyses show that the poorly sorted conglomerate is the dominant rock type of this formation in the prospect. Clasts of the conglomerates are derived from volcanic, sedimentary, and metamorphic rocks. The clasts of conglomerate are polygenetic and subrounded to rounded. The clast size ranges from sand to boulder. The roundness analyses present that the subrounded grains are dominant in the area. According to sorting analyses, the whole area includes poorly sorted conglomerates. Sandstone is second dominant lithology in this formation and is generally observed as massive and thin bedded. Claystone is the least observed sedimentary units in the area. The eastern part of the property includes relatively high amounts of claystone. In the western part of the property, tuffaceous units are also observed. Due to extensive alluvial cover and vegetation, it is hard to measure and observe structures. However, measurements from the limited rock exposures show that the dips of bedding range between 20° and 40°.

The Oligo-Miocene granitic stock is exposed at the southwest corner of the property. It intrudes metamorphic rocks and Karakaya Formation. It is unconformably overlain by the Pliocene units. The granitic stock ismade up of medium to coarse in crystal size and its composition ranges from granite to granodiorite. Near the contacts with the basement rocks, the granite appears to be foliated and displays gneissic texture (Ferguson, 2013).

The Pliocene continental clastics crops out in the south-eastern to northern part of the Akarca property. These units unconformably overlie the pre-Triassic basement rocks. The dominant lithology of the Pliocene units is coarse clastic rocks. The depositional environment of the continental clastics has similar properties with an alluvial fan system (Toprak, 2014). In view of the present morphology and regional tectonics, the south of the area is uplifted along normal fault system and the alluvial fan is developed from south to north (Toprak, 2014).

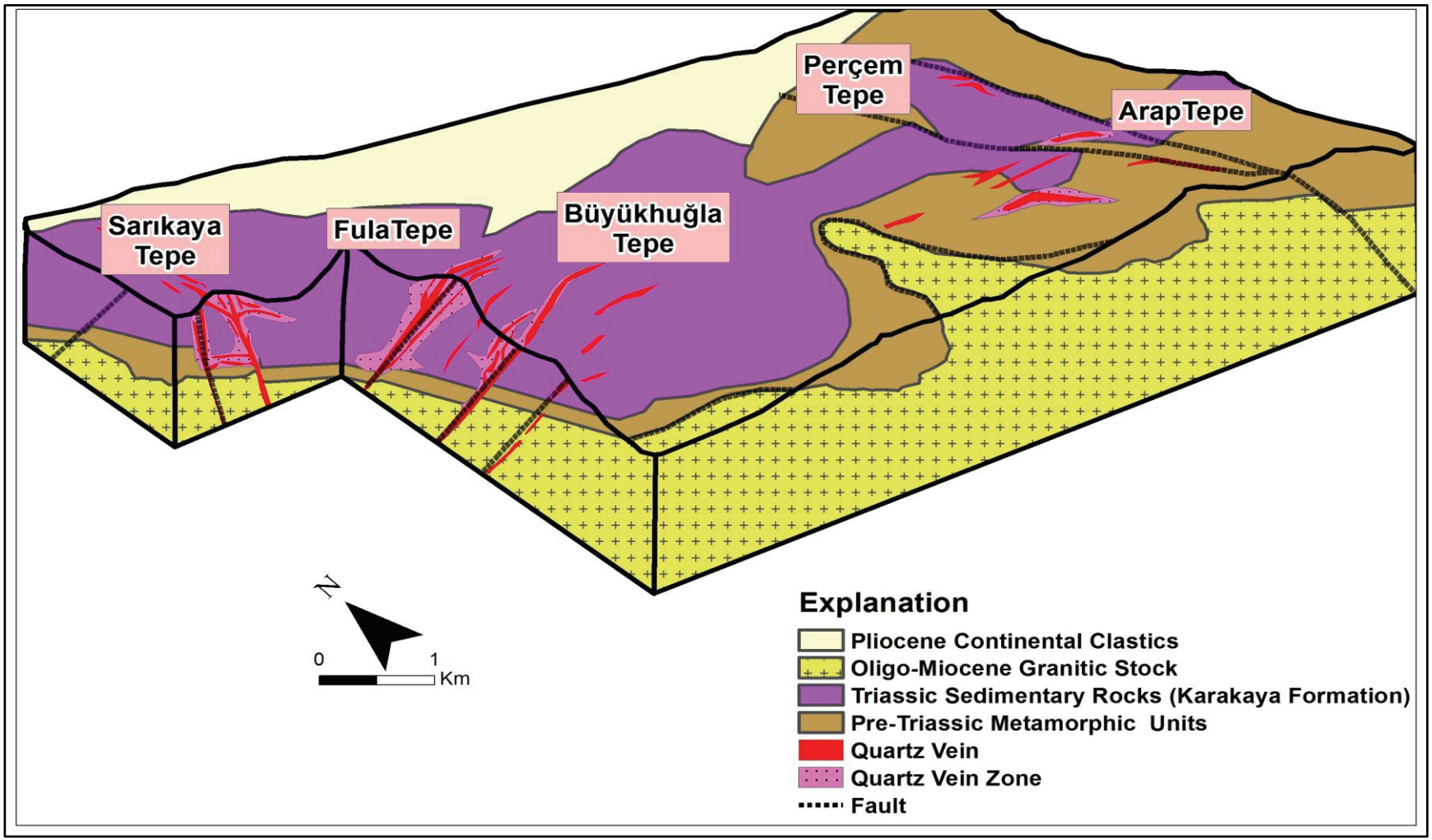

Figure 5. The perspective view of Akarca property.

CHAPTER 3

MINERALIZATION

3.1. Deposit Type

Epithermal deposits are important sources of gold and silver that form within hydrothermal systems associated with magmatic activity (Sillitoe and Bonham, 1984). They develop at low temperatures (100-320 C), moderate pressures (<100 bars), and shallow crustal levels (typically <1 km below the water table) (Lindgren, 1933). Epithermal deposits are divided into two main types on the basis of fluid types, and sulfidation states of hypogene sulfide assemblages (Sillitoe and Hedenquist, 2003), namely high sulfidation (H/S) and low sulfidation (L/S) deposits (Hedenquist, 1987, 2000) (Figure 6). L/S deposits form from neutral-pH and reduced hydrothermal fluids, a mixture of meteoric water and magmatic water, at relatively low temperatures (<220 C) and shallow depths (<250 m) (Corbett and Leach, 1998).

In L/S type, ore zones form in structures and in permeable lithologies (Panteleyev, 1996). Most of the L/S deposits comprise cavity-filling veins with sharp boundaries, or stockworks, dissemination, and replacements (White and Hedenquist, 1995). L/S deposits exhibit a wide variety of textures, including comb, crustiform, colloform, chalcedony, lattice bladed, massive silica, etc (Figure 7).

Clay alteration is dominant alteration type in L/S deposits and clay minerals are the best indicators of paleo-temperature (Sillitoe and Hedenquist, 2003). Silicification (replacement of wall rocks by quartz or chalcedonic silica) is common alteration type in the inner zone (Taylor, 2007). Kaolinite and smectite (argillic alteration) is common alteration minerals. Besides, chlorite and carbonates occur in many low sulfidation deposits (Figure 8).

"L/S precious metal deposits contain pyrite (< 1-2%), or the low-temperature variant marcasite, ± minor amounts of galena, arsenopyrite, chalcopyrite, silver sulfides sphalerite, and sulfosalts, and rare pyrrhotite" (Sillitoe, 1993). Ag, As, Sb, Hg, Se, Zn, Pb, Te and K are closely associated with gold in L/S precious metals deposits (Sillitoe 1993).

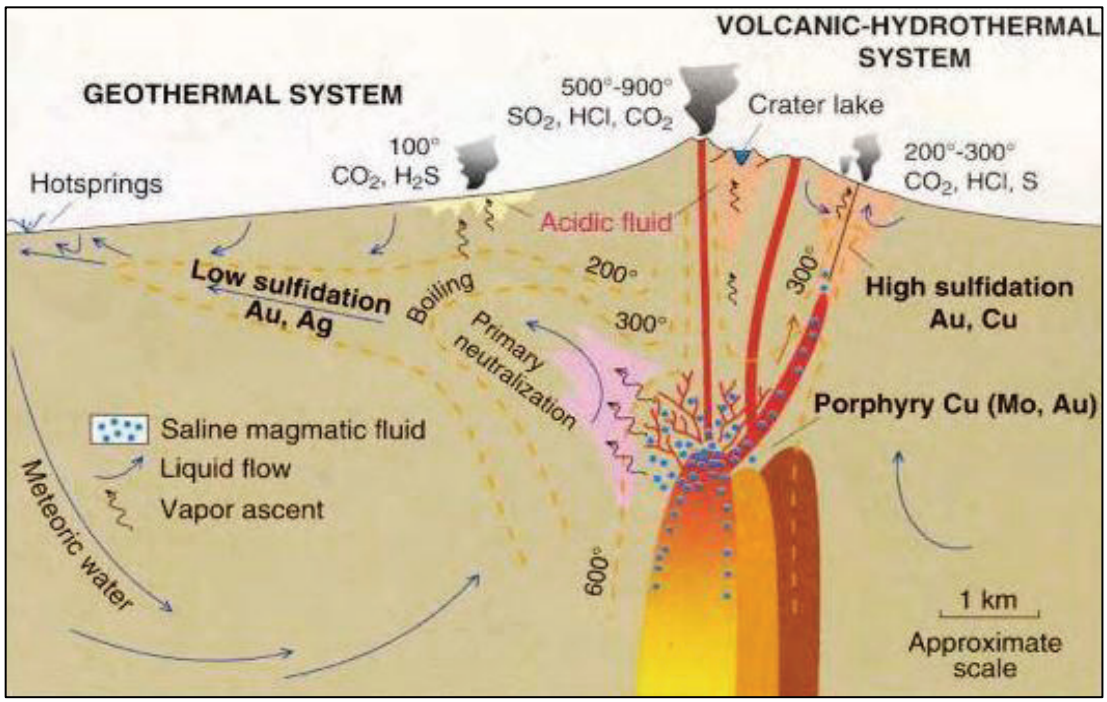

Figure 6. The environments of H/S and L/S style epithermal deposits (Hedenquist, 2000).

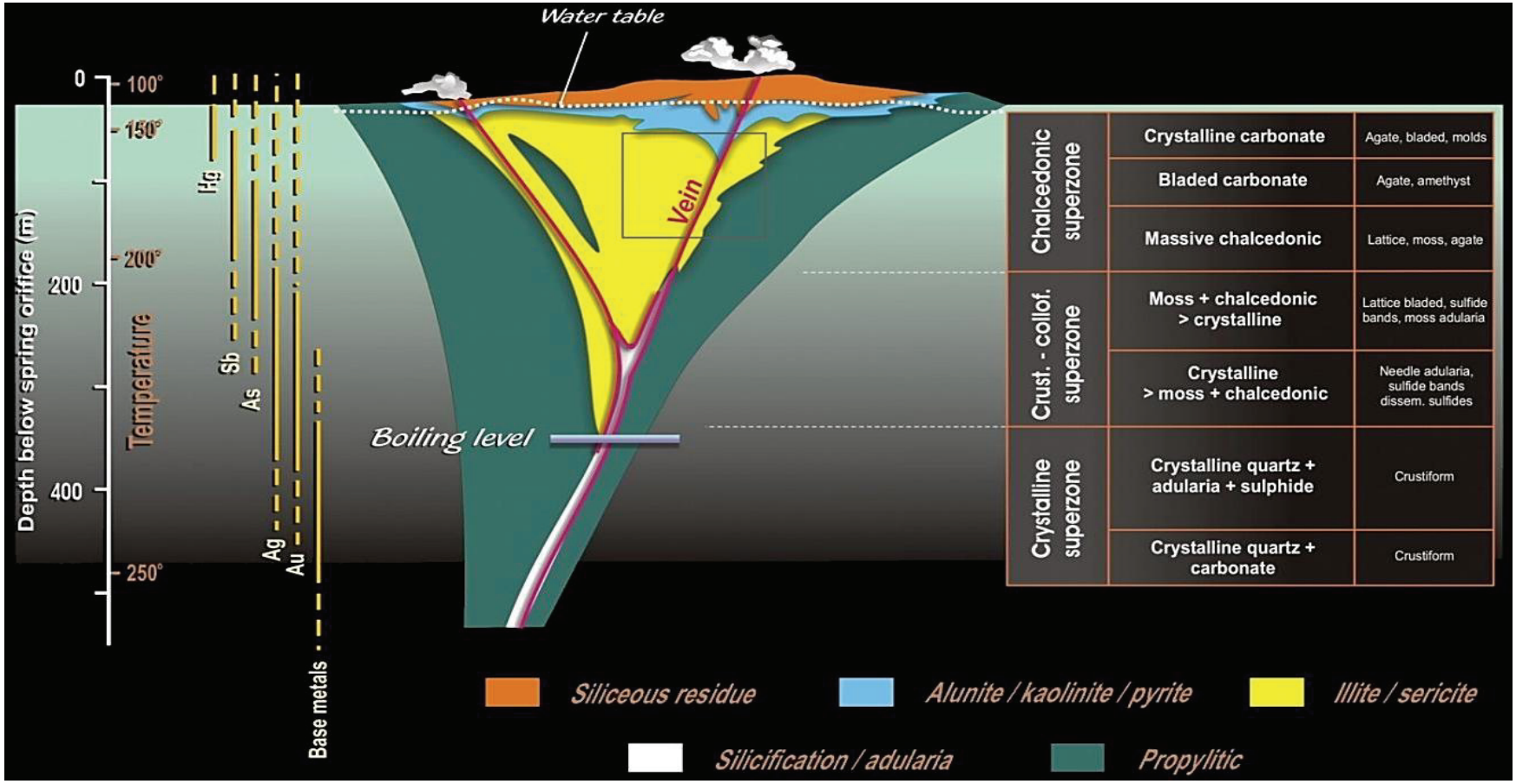

Figure 7. The texture zoning model for low sulfidation deposits (adapted from Berger and Eimon, 1983; Buchanan, 1981; Corbett & Leach, 1998; Hollister, 1985).

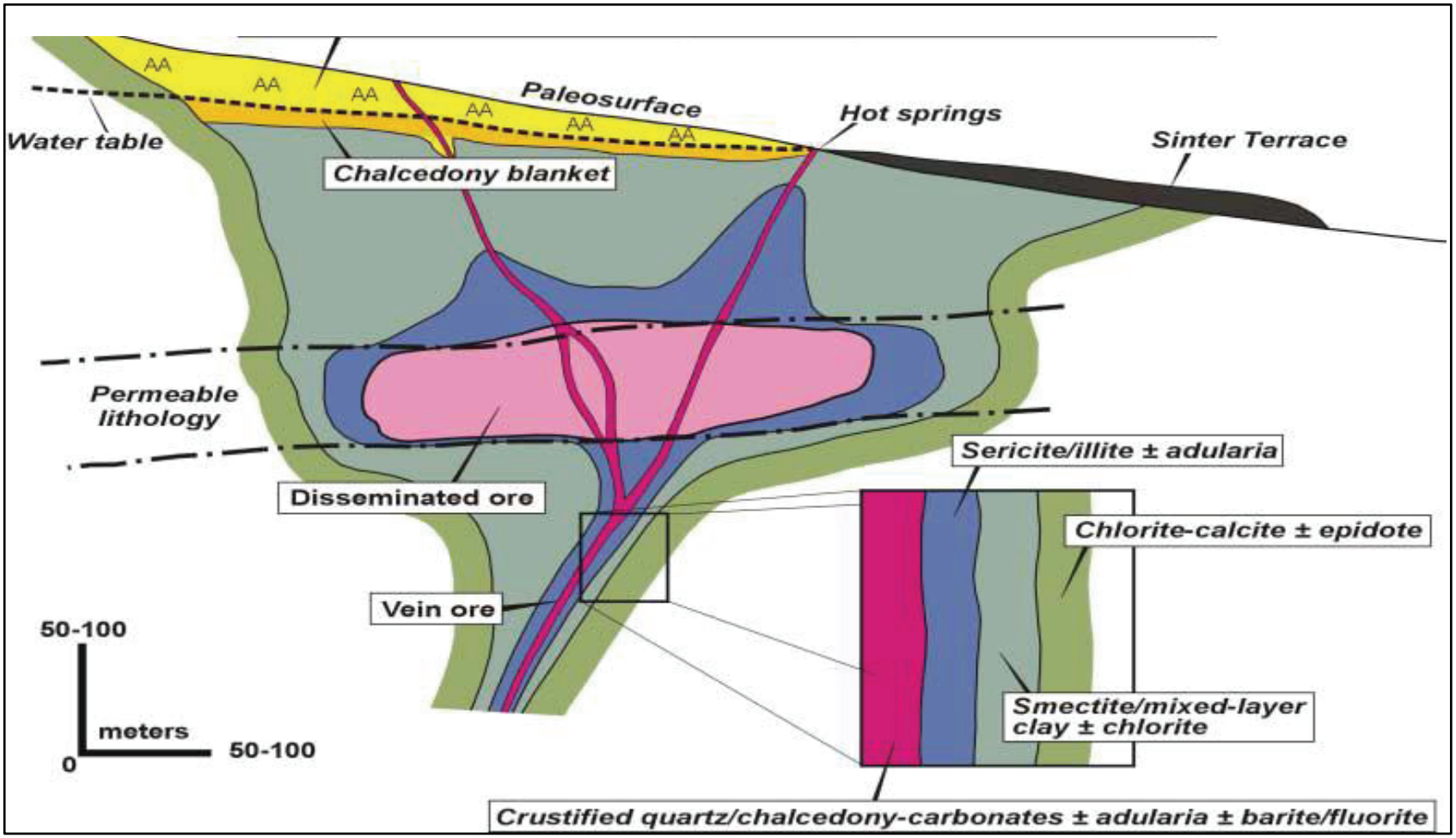

Figure 8. Schematic section showing typical alteration and mineralization patterns in low sulfidation system (Hedenquist, 2000).

The Akarca property displays characteristics of L/S Au-Ag deposit in terms of alteration, mineralization and vein textures. Mineralization occurs as both structurally controlled vein-style and lithologically controlled disseminated-style (Dreier and Soylu, 2011). The alteration consists of clay alteration, quartz veining, silicification, and iron oxidation. Silicification occur as both quartz veins with fine quartz veinlets and moderate silica flooding surrounding the veins. Akarca L/S quartz veins show wide variety of textures, including crustiform-colloform banding, massive silica, comb, chalcedonic silica, lattice bladed, and moss texture. Calcite veining can be observed with increasing depth.

The Akarca property is divided into six principal mineralization zones. These are Küçükhuğla Tepe Zone, Büyükhuğla Tepe Zone, Fula Tepe Zone, Sarıkaya Tepe Zone, Arap Tepe Zone, and Perçem Tepe Zone (Figure 9). All these zones are characterized by development of L/S Au-Ag veins. However among these zones, Fula Tepe Zone has been subjected to more systematic exploration in terms of geochemical survey, drilling, and trenching.

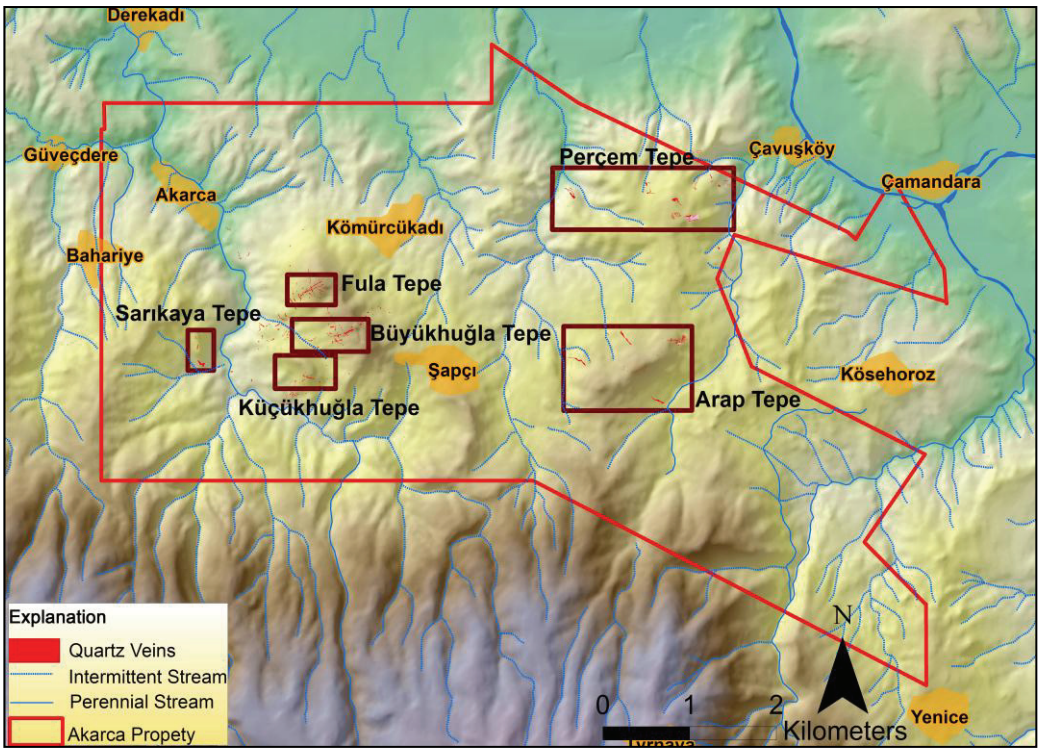

Figure 9. Six principal mineralized zones of the Akarca property.

3.2. Akarca Main Zones

The Küçükhuğla Tepe Zone, at the southern part of the Akarca property, consists of a 698m by 380 m area of anomalous gold and silver, veining, and alteration. There are two sub-parallel main vein zones that strike N100°-110° and dips 85°-90° to the NE. Veins mainly display banding, massive, carbonate lattice blades textures, are locally composed of oxidized silica and brecciated zones. The Büyükhuğla Tepe Zone is located between Kücükhuğla Tepe Zone and Fula Tepe Zone. It consists of 881 m by 370 m corridor of gold and silver anomalous. Average 5 m thickness of 400 m long vein zone, trending N60°-70° and dipping 70°-80° to the SE, displays banding, massive, colloform and crustiform textures and hematite cemented silica breccia textures. The Sarıkaya Tepe Zone, at the west of the property, is characterized as a 295 m by 461 m zone of anomalous, quartz veining and moderate to strong silicification. The zone contacts both limestone and conglomerate, trending N340°-350°. The Arap Tepe Zone is located at the east-southeast of the Akarca property. The zone includes W-NW trending veins similar to those that form Küçükhuğla, Büyükhuğla and Fula vein systems. Veins display carbonates lattice bladed, saccharoidal, massive, chalcedonic banded, strongly hematitic altered quartz textures. The Perçem Tepe Zone, located at north of the Arap Tepe Zone, is characterized by 1,000 m by 707 m corridor of gold-silver mineralization. The NW trending corridor is represented at the surface by three mineralized quartz vein zones having strike length of 85 to 110 meters, and ranging 1 to 18 meters in width (Dreier and Soylu, 2011).

3.2.1. Fula Tepe Zone

The study area, the Fula Tepe Zone, is located at north of the Akarca property. The zone is covered by the Triassic conglomerates, sandstones, and siltstones that host L/S Au-Ag mineralization (Figure 10).

Fula Tepe Zone is characterized by a 557 m by 345 m corridor of gold-silver mineralization. It consists of quartz veins, quartz vein zones, and silicified outcrops.

The veins cut the sedimentary rocks with strikes N50°-60° to NE, dips 80°-85°. Vein textures and silica polymorphs in the veins of the property are typical for L/S style epithermal veins (Chadwick, 2009). Veins display coarse comb, carbonate lattice bladed, micro-crystalline quartz, crustiform, colloform, and banding textures. Banded recrystallized chalcedony and micro-crystalline quartz texture are dominant at higher elevations. Local amethystine and coarse comb quartz are dominant at lower elevation.

Silicification and clay alteration are two main hydrothermal alteration types in the study area accompanied with moderate to strong iron oxide development.

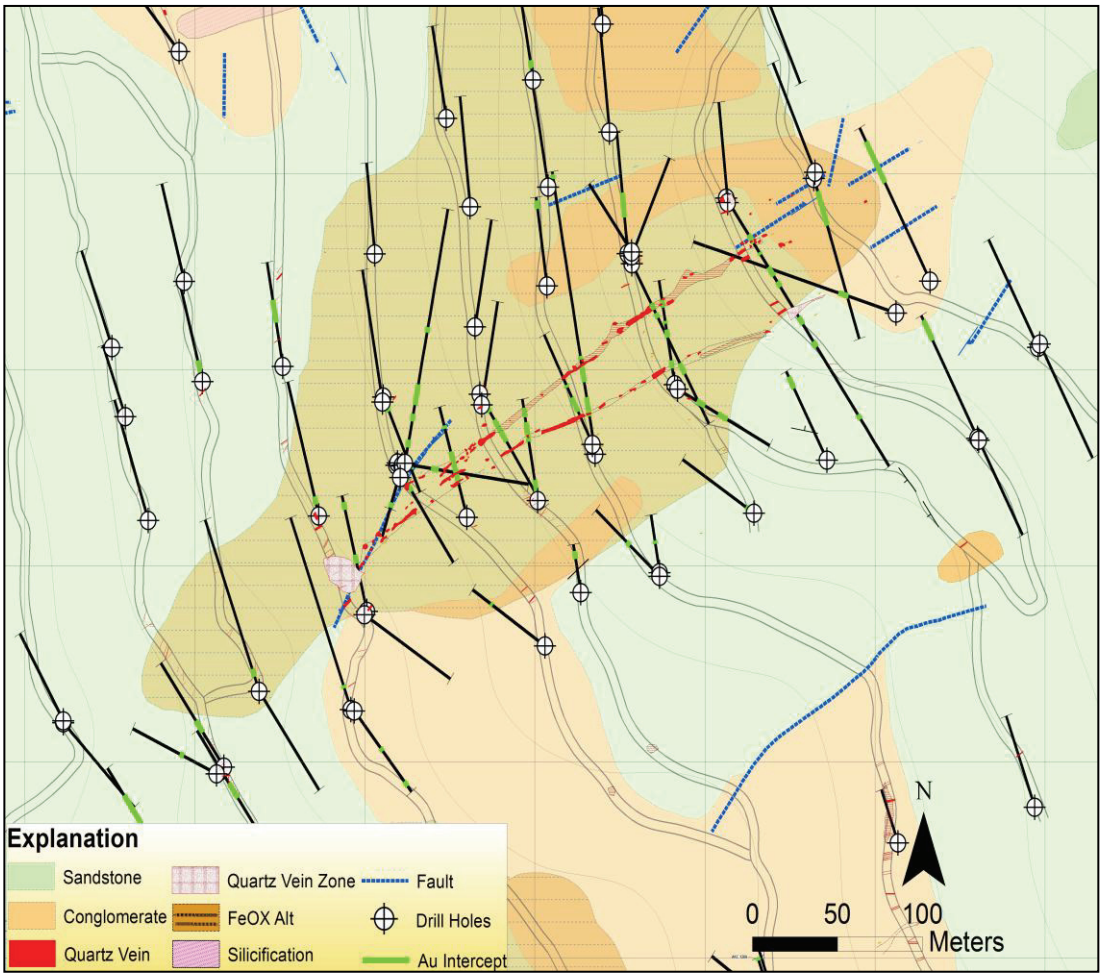

Figure 10. The geology of Fula Tepe Zone (Created by Eurasian team).

CHAPTER 4

METHODOLOGY

4.1. Field Methods and Sample Analyses

The study area is predominantly covered by soil and rock exposures are quite limited. For this reason, soil survey was conducted to test existence of a possible covered gold-silver mineralization. A total of 195 soil samples were collected on 100 meters spaced lines with 50 meters sample spacing to transect the vein and structural orientation perpendicularly.

The soil sampling procedure can be summarized as follows (Dreier and Soylu, 2011):

i. sample area is cleaned from vegetation and the top layer of debris is removed.
ii. at each site 50 by70 cm hole is excavated down to reach the ‘’B horizon’’,
iii. samples are collected from B horizon due to containing high metal concentration,
iv. unsieved samples (3-4 kilograms) were bagged, tagged, and coordinates recorded,
v. parameters (color, texture, abundance and profile type) and geologic notes were recorded and
vi. a group of samples are transported to a central collection point in preparation for shipment to the ALS Chemex sample preparation laboratory in Izmir.

The sample preparation of the soils consists of logging, drying (at <120 C), disaggreating, and dry screening to -80 mesh (plus and minus fraction saved, minus fraction split for assay).

Soil samples were fire assayed to measure concentration of Au by inductively coupled plasma atomic emission spectroscopy (ICP/AES) finish. Ag, base metals, and multi-elements were determined with an aqua regia digestion and inductively coupled plasma mass spectrometry (ICP/MS). For all of the analyses, standard reference material (SRM) and blank sample were used to monitor lab performance and duplicate sample which is a second portion of the same sample was used to evaluate the precision of analysis.

4.2. Evaluation of Data and Presentation of Results

4.2.1. Descriptive Statistics

Descriptive statistics can be conducted to obtain information on the main statistical properties of the datasets. They indicate significant departure, the degree of differences, among mean, median and mode of the datasets from normality. The statistics are concerned with measures of central tendency and measures of variability or dispersion. Measures of central tendency include mean, median, and mode, while measures of dispersion include standard deviation, minimum-maximum values of the variables, kurtosis, and skewness (Davis, 1973).

i. Mean is the average value of data, determined by dividing the sum of all data by the number of data.
ii. Median is the central value that divides data into two groups.
iii. Mode is the most abundant value. If datasets are grouped into classes, the mode is taken as middle of the class.
iv. Standard Deviation measures of dispersion around the mean. It is square of root of the variance.
v. Kurtosis is a measurement of the degree of peakedness or flatness of data distribution. Positive kurtosis represents a peaked distribution and negative kurtosis represents a flat distribution.
vi. Skewness is a measurument of asymmetry of the distribution shape.

4.2.2. Univariate Statistical Methods

Univariate statistical methods can be used to obtain information from dataset of values for a single element. These methods are histograms, Q-Q plots, box-and-whisker plots, and probability graphs.

I. Histograms

Histograms are the commonly used method of analyzing the data distribution. The histograms are used to obtain a simple visual display of range of data, and general form of probability density function, modes, and anomalous. The normal distribution data is displayed as a symmetric bell shaped in the histogram.

II. Q-Q Plots

Normal Q-Q plots examine datasets graphically whether geochemical data follow normal or log-normal distribution (Sinclair, 1991).

In Q-Q plot, expected and observed values are assigned to y and x axis, respectively. Plotted values are compared with a linear line. If observed values follow a normal distribution, they are plotted close to the linear line and clustered along a straight line.

III. Box-and-Whisker Plots

The box-and-whisker plot (Figure 11) was created by John W. Tukey (1970). It is very useful univariate graphical method to show the distribution of datasets.

Tukey (1977) defined the box and whisker plot as five-number summary statics; minimum, lower-median-upper hinge, and maximum. He also described the most important characteristics of a univariate dataset for box and whisker plot, namely;

i. Location and central tendency
ii. Spread
iii. Skewness
iv. Length of tails
v. Outliers

The interquartile range (IQR) is the width of the box, the difference between the third Quartile (Q3) and the first Quartile (Q1) (Tukey, 1977). The line in the middle of the boxes represents the second Quartile (Q2), the median. The spacing between the different parts of the box represents the degree of dispersion and skewness in the data. In addition, it shows the degree of outliers that have no effect on the IQR (McGill, Tukey, and Larson 1978).

Box-and-whisker plot is also used to determine threshold values of datasets. In box-plot, upper inner fence (UIF) value is usually accepted as threshold value that separates background values and anomalies (Bounessah and Atkin, 2003; Reimann et al., 2005). This method is best applied when the data contain less than 10% outliers. Data values in the UH (upper hinge Q3)-UW (upper whisker) class can be accepted as high background. Data values in the LH (lower hinge Q1)-UH (upper hinge) class represent background value and data values in the LW (lower whisker)-LH represent low background value.

$$UIF = Q1 + (1.5\ IQR)$$

Apart from the boxplot-defined threshold (UIF), a threshold can be estimated from median+2MAD. The MAD is the median absolute deviation (Tukey, 1977).

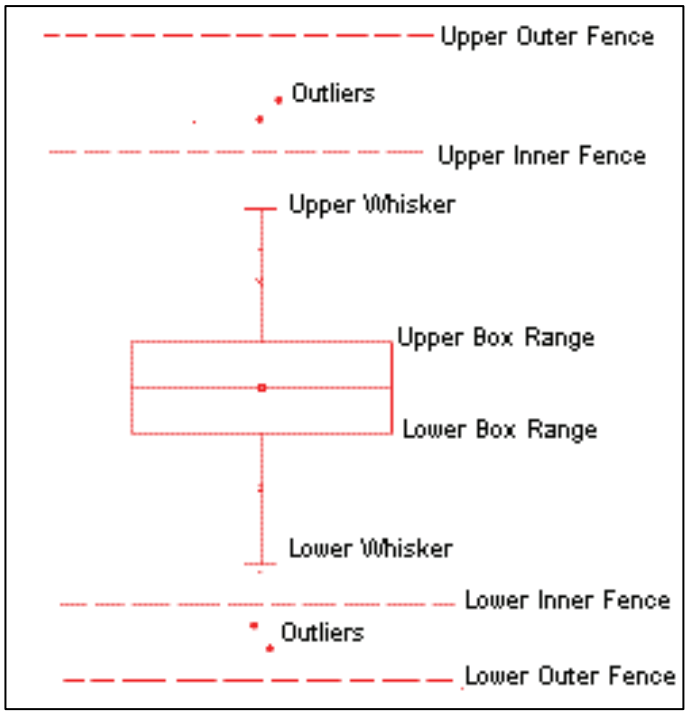

Figure 11. Box-and-Whisker Plot (Tuker, 1977).

IV. Cumulative Frequency Probability Graph

The cumulative frequency probability graphs are used to divide the data into sub-populations and define the background, threshold, and anomalous values of datasets. This type of graph is very sensitive to departure from normality (Lepeltier, 1969). The cumulative frequency probability graph is a useful method to determine the combinations of multiple populations (Sinclair, 1974; Lepeltier, 1969). If the datasets have polymodel distribution, many inflection points can be observed. Each inflection point in a probability graph represents a sub-population in the data population. Each sub-population shows different geologic event such as mineralization. The stages of the creating probability graph are;

i. Calculation of limit of class interval
ii. Calculation of cumulative frequency percentile
iii. Plotting them on logarithmic probability graph
iv. Identifying inflection points and estimation of threshold values

4.2.3. Identifying Geochemical Anomalies

Generally, geochemical anomalies are identified by setting threshold and background values. The normal concentration, non-mineralized element is referred as background. The upper limit of the background is accepted as the threshold. The threshold value is used to divide the distribution into background data and anomalous data. Anomalous data indicate an enriched value for mineralization (Rose et al., 1979). The value of the anomalies depends on the degree of mineralization and the intensity of geologic event. The detection of threshold is very important in mineral exploration. If the value of detected threshold is too high, some deposits would have been ignored. If the value of detected threshold is too low, time and money would be wasted during following up unspecified anomalies.

There are various methods that can be used to identify threshold values:

- Using simple statistical methods, such as percentiles. For example, the values which are greater than 75^{th} percentile are anomalies and values less than 25^{th} percentile are backgrounds.
- Calculating the mean plus or minus twice standard deviation for threshold value. In some cases, this method might be adequate. However, if dataset involve more than one sub-population and does not follow a normal distribution, estimated threshold can be spurious.
- Using box-and-whisker plot. The upper inner fence (UIF) value is usually accepted as threshold value.
- Setting the threshold at 2MAD from the median.
- Using a histogram and a probability graph.

4.2.4. Bivariate Methods- Pearson Multivariate Correlation and Scatterplots

The Pearson multivariate correlation analysis is a useful tool to determine of multi-element relationships and to select a suite of pathfinder and base metal elements

(Edwards, 1976). The high and significant positive correlation value between two elements can be considered as derived from the same source.

The significance of correlation indicates the associations between elements. If the correlation coefficient is close to ± 1, the association is close to a perfect linear relation (Belkhiri et al., 2010).

The scatterplot is also a useful tool for visual exploration of element relationship. If two variables follow a straight line, they exhibit a linear correlation. If two variables follow some arbitrary function, they exhibit a non-linear correlation.

4.2.5. Spatial Analysis

Spatial analysis is a comprehensive part of this study. The GIS mapping technique is carried out to produce the spatial distribution maps. There are various ways to produce geochemical maps as described below:

1. The thematic maps for the raw data; thematic maps show not only the location of each sampling point but also the relative concentration of the elements. Points are colored based on the concentration range of the element value. Hot colors are used for the highest values and cool colors are used for the lowest values. Thematic maps aid to provide quick understanding of the distribution of anomalies in an area.
2. Grid maps derived by gridding the point data; the geochemical data for soil samples are interpolated in grid format to represent the regional variation in geochemical values. Kriging is a commonly used interpolation technique. It is provides to estimate the unknown value of any variable of a sample from surrounding samples with variables of known values (Matheron, 1971). Similar color-scheme is used with used in the point map.
3. Maps produced by color-coding contours in a geological map; the geochemical data are contoured by drawing isograds or lines of equal composition. This type of maps emphasizes possible mineralization trends.

4.3. Quality Assurance (QA) and Quality Control (QC)

The main purpose of the QA/QC program is to prevent introducing errors into the database, and provide assurance of the accuracy of data. In this study, QA/QC compilations were reported for gold and silver.

For this study, QA/QC program included the use of standard, blank and duplicate samples. One each of these QA sample types were inserted into the sample stream at a set interval, in general every 30 samples. Blank samples are known to be barren of mineralization. They were inserted to identify contamination issues and they were added to the beginning of a sample batch to determine whether a laboratory is clean or not. Field blank samples purchased from ACME labs. Standard blank samples are comprised of limestone-rich, silty, and sandy soil. Duplicate samples were used to evaluate the precision of analysis. Duplicate samples were collected at the same time and from same location as the original sample. Standard Reference Materials (SRM) were used to monitor for analytical accuracy, which is the closeness of a result to its "true" value, as estimated by results of round-robin testing. All certified reference materials are purchased from Geostat Pty Ltd. SRM samples were selected to reflect the metal of interest, the level of expected metal grade and the general characteristics of the host rock. A total of five standards were used during geochemical survey. Two high grade (G304-9 and G900-8C), two moderate grade (G901-11C and G303-1), and one low grade (GLG303-3C) were inserted into the sample stream, normally with one low grade and one high grade per group of 30 samples.

For blank QC monitoring, detection limit for the element is important. The baseline blank gold value is on the order of 3 ppb or less, and the baseline silver is 0.10 ppm, which are at, or near, the respective detections limits for each element.

For duplicates QC monitoring, 10% tolerance limit was applied for original-duplicate sample pairs. Sample pairs falling beyond this tolerance limit were rejected. The scatter plots were used to determine original-duplicate sample pairs.

For SRM QC monitoring, QC nomogram charts were plotted for each Certificate Reference Material (CRM), and evaluated with the following general criteria (Dreier and Soylu, 2011):

i. CRM assays within ± 2 standard deviations (SD) are acceptable,
ii. single, non-consecutive CRM assays between ± 2SD and ± 3 SD are acceptable while consecutive CRM assays between ± 2 SD and ± 3SD are not acceptable (systematic bias outside of tolerance).
iii. CRM assays outside of ± 3 SD are always rejected.

CHAPTER 5

GEOSTATISTICAL STUDIES

5.1. Quality Assurance (QA) and Quality Control (QC) Results

There were 10 SRMs analyzed for Au. All SRM QC results were reported within two standard deviations of the expected value, with only isolated, non-sequential cases occurring between two and three standard deviations. Accordingly, SRM analysis for Au passed the QC tests, and it is concluded that the ALS Chemex assays are within acceptable limits of precision and accuracy. All SRMs results are given in Figure 12-16.

The performance of the QC blank samples indicates that there are no significant issues for Au and Ag. Generally, Au and Ag consistently reported at, or less than 2 to 3 times the baseline blank value. For Au soil blanks, the samples were at, or near the 0.005 ppm detection limit. The soil blank Ag assays consistently reported at 0.08 ppm silver, and showed no significant issues with contamination at the low end. All blank results are given in Figure 17 and 18.

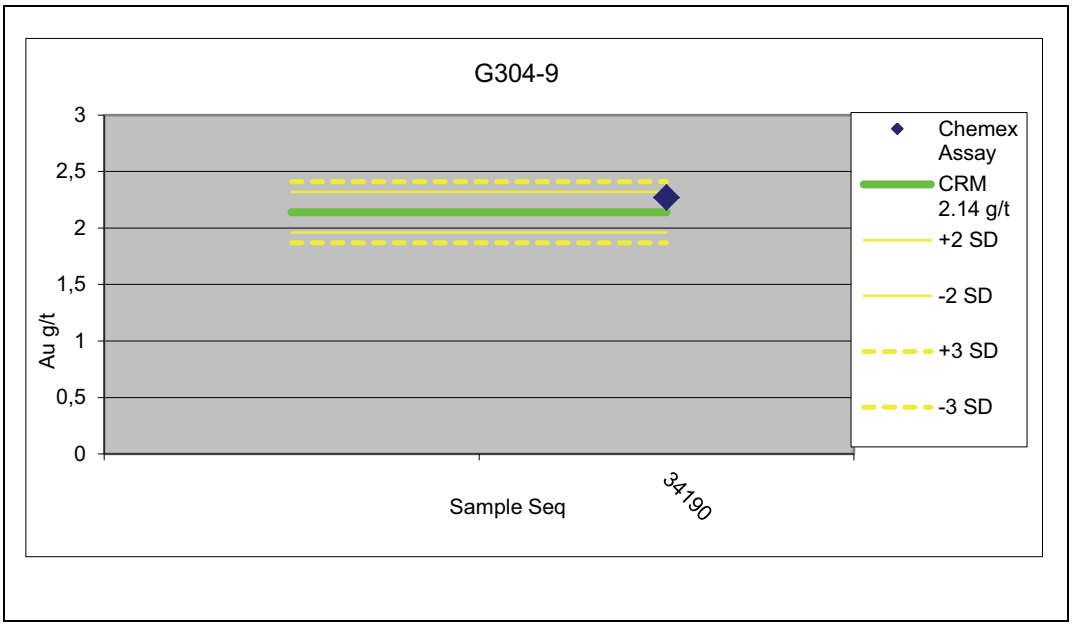

Figure 12. G304-9 SRM QC plots for Au.

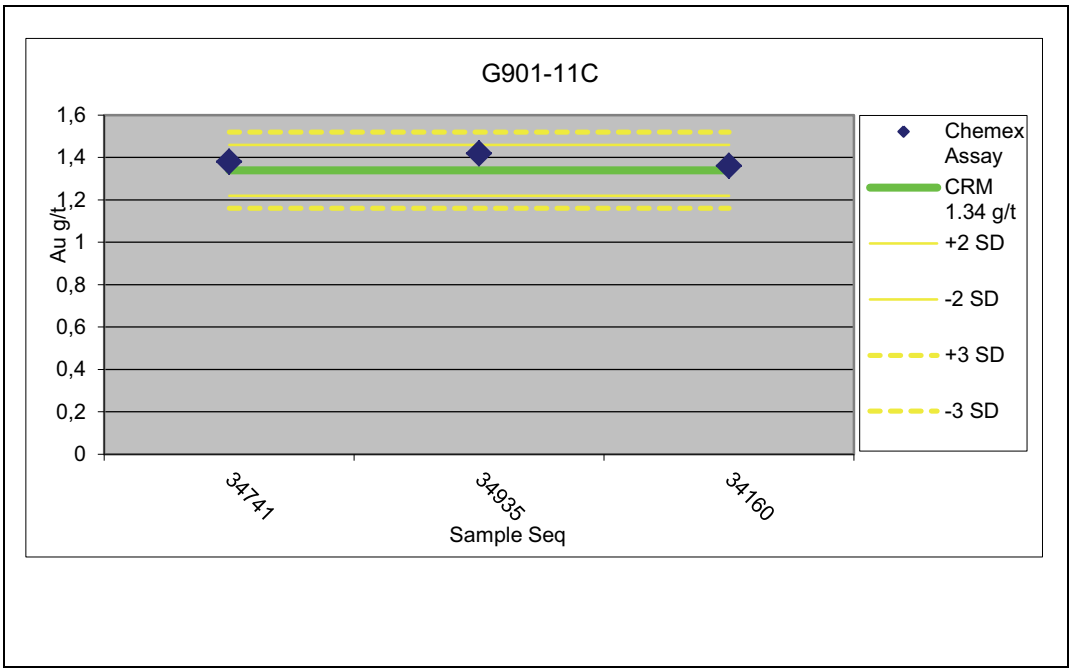

Figure 13. G901-11C SRM QC plots for Au.

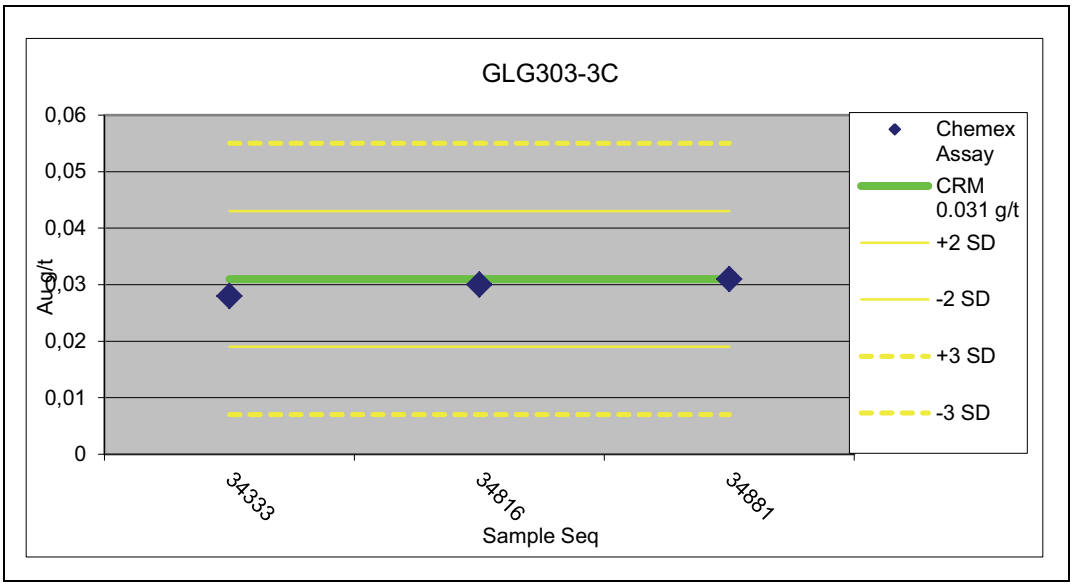

Figure 13. GLG303-3C SRM QC plots for Au.

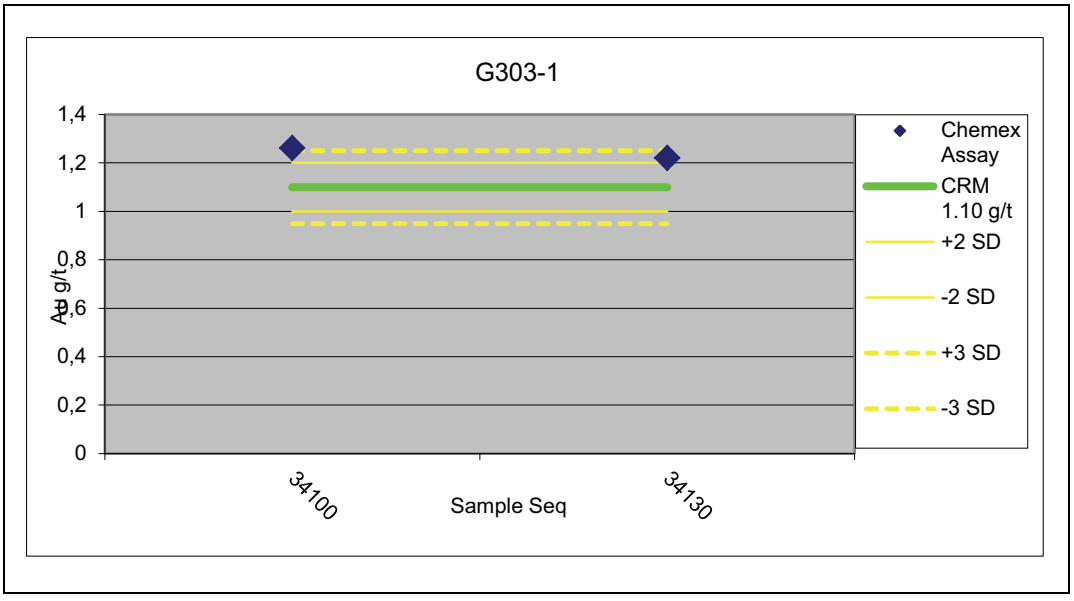

Figure 14. G303-1 SRM QC plots for Au.

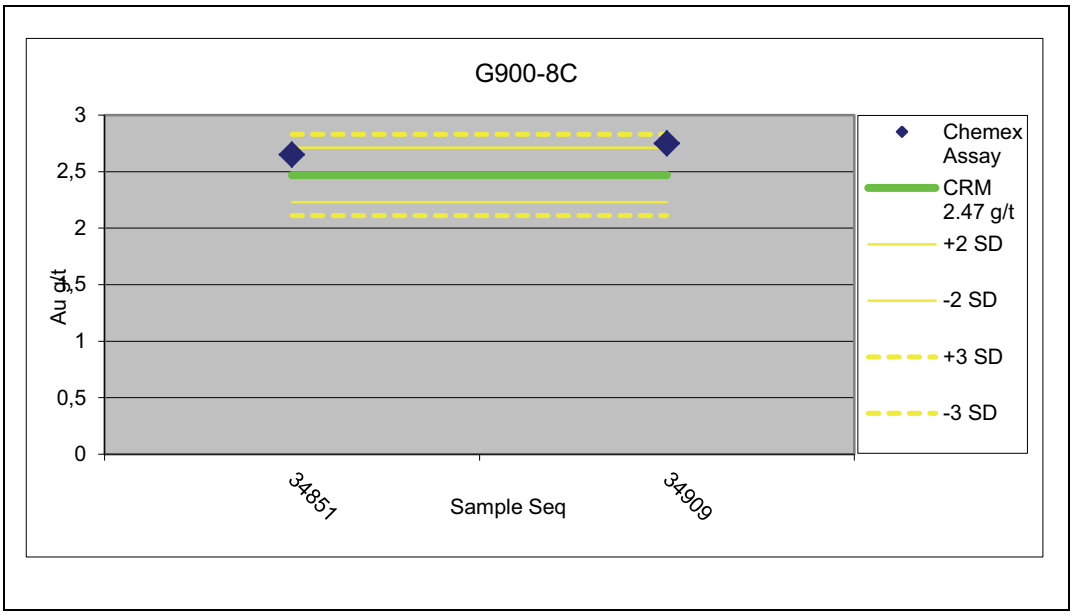

Figure 15. G900-8C SRM QC plots for Au.

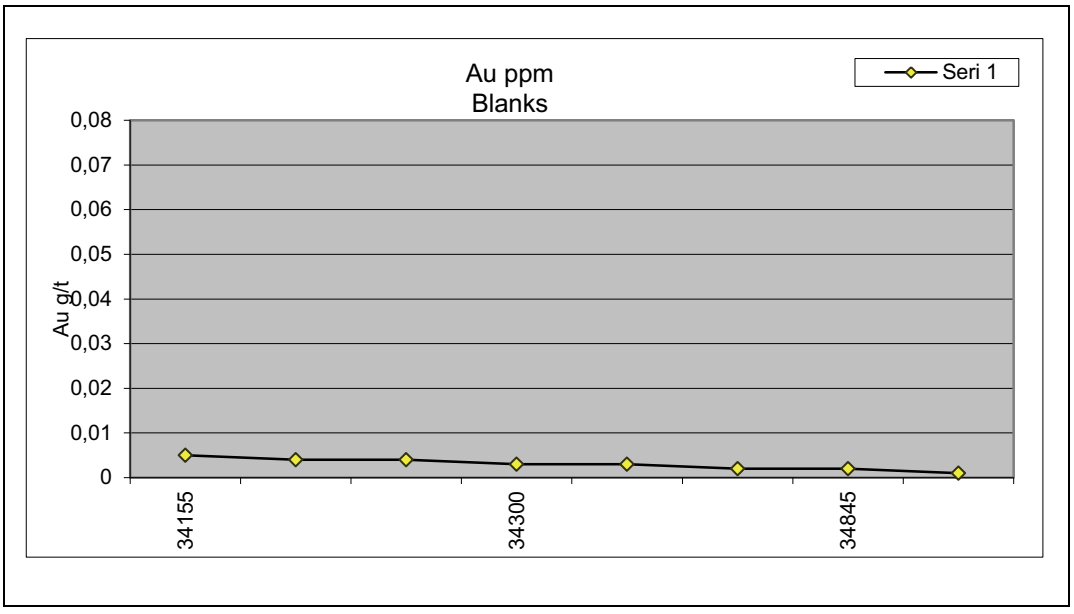

Figure 16. Soil sample blank QC plots for Au.

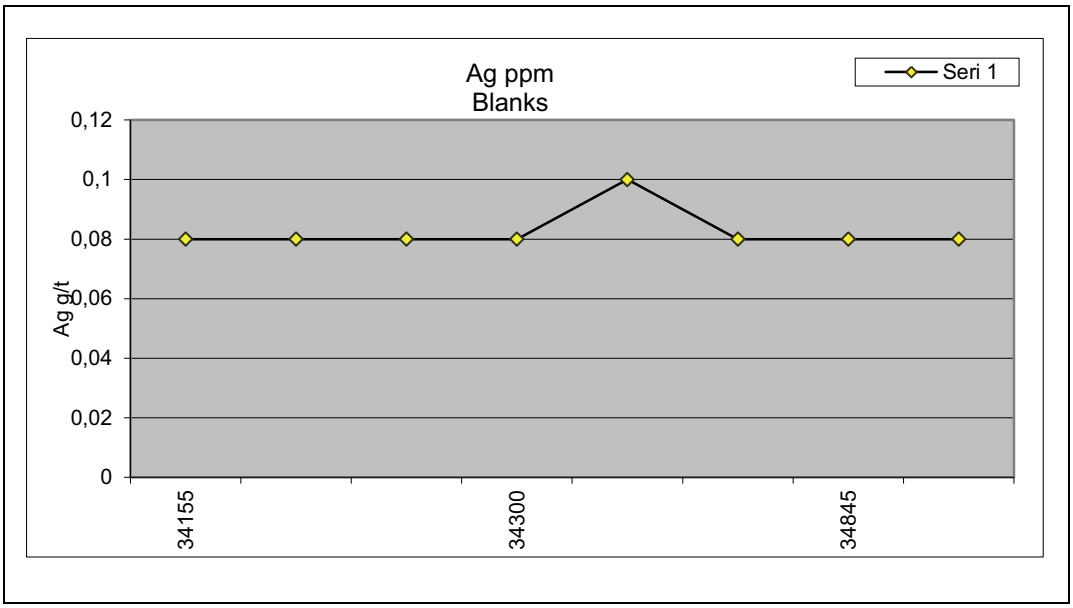

Figure 17. Soil sample blank QC plots for Ag.

The duplicate soil samples reflect an acceptable reproducibility as portrayed by linear relationships on the scatter plots for Ag. However, the Au analyses indicate some substantial scatter in the data. This result is consistent with Au in nuggets or small free gold fragments. To identify the problem, the reject samples should be re-analyzed. Duplicate samples results are given in Figure 19 and 20.

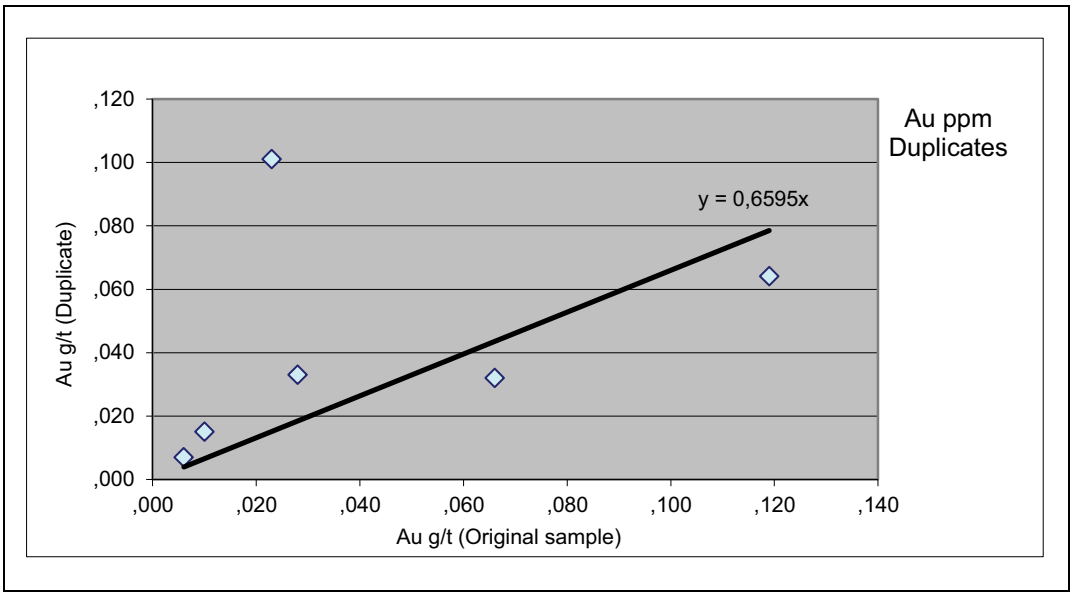

Figure 18. Soil QC duplicate scatter plot for Au.

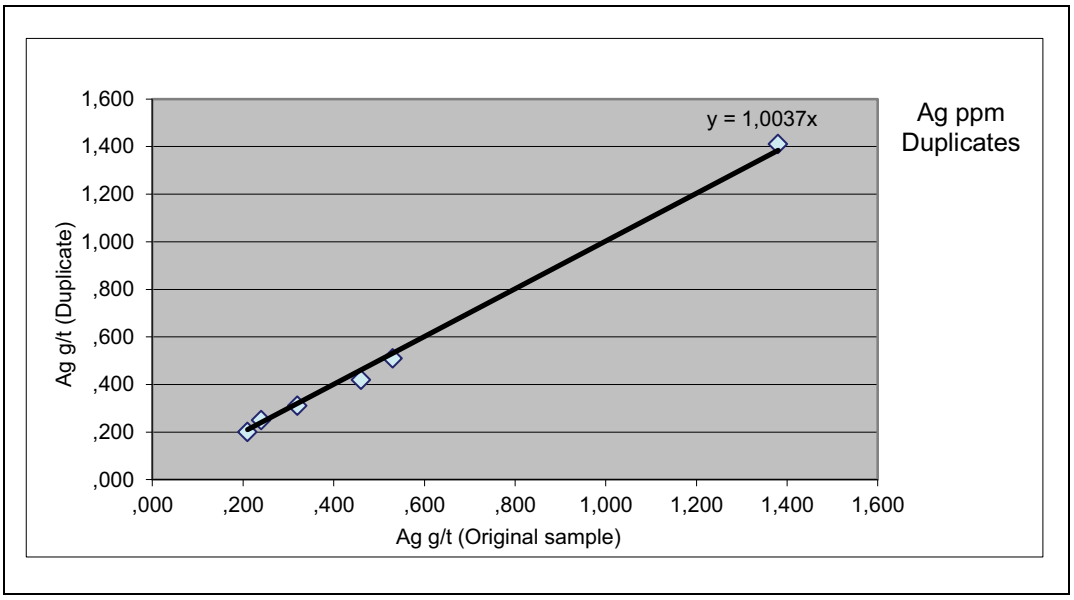

Figure 19. Soil QC duplicate scatter plot for Ag.

5.2. Evaluation of Surface Soil Geochemistry Data

Results of surface soil samples (N: 195) were analyzed by descriptive statistics. In order to describe the shape and the flatness of data distribution, skewness and kurtosis coefficients were used. Histograms and box-plots were examined for the possible anomalies that affect the characterization of spatial variation and the descriptive statistics. The Q-Q plots were prepared to examine datasets graphically whether geochemical data follow normal or log-normal distribution. The Pearson multivariate correlation analysis was performed to determine of multi-element relation and select suite of indicator and pathfinder elements. The probability graphs were carried out to define background, threshold and anomalous values. The statistical study covers following elements; Au, Ag, As, Hg, Sb, Se, and Te.

Results of descriptive statistics such as maximum, minimum, median, mean, geometric mean, standard deviation, skewness, and kurtosis for Au, Ag, As, Hg, Sb, Se, and Te are shown in Table 1 and descriptive statistics results for all elements are given in the Appendix A.

Table 1. Descriptive statistics for the selected elements.

	Au (ppb)	Ag (ppm)	As (ppm)	Hg (ppm)	Sb (ppm)	Se (ppm)	Te (ppm)
Mean	87.80	0.88	53.92	0.057	4.95	0.67	0.04
Std. Error of Mean	20.65	0.06	2.30	0.002	0.15	0.02	0.0009
Median	32.00	0.62	46.30	0.05	4.64	0.60	0.04
Mode	15.00	0.52	20.20	0.05	5.12	0.60	0.04
Std. Deviation	288.31	0.82	32.18	0.03	2.04	0.27	0.013
Variance	83,123.5	0.67	1,035.49	0.001	4.17	0.07	0
Skewness	9.68	3.29	1.97	4.38	1.47	0.95	0.88
Kurtosis	106.29	18.73	5.54	31.99	4.52	0.83	1.66
Range	3,488	7.08	217.60	0.33	14.37	1.30	0.08
Minimum	2	0.12	8.40	0.02	1.58	0.20	0.01
Maximum	3,490	7.20	226.0	0.35	15.95	1.50	0.09
Sum	17,121	171.47	10,514	11.16	966.21	130.60	8.07

The mean and median values are different for some variables, such as Au, As, and Ag, which were strongly and positively skewed. This aspect is also seen in their histograms shown in Figure 21-27. The kurtosis results of elements show that As, Sb, Se, and Te have a narrow range of concentration while Au, Ag, and Hg have a wide range of concentration. It is a known fact that the raw data deviates far from a normal distribution when data have high kurtosis and skewness values. High kurtosis and high skewness values are caused by outlier values. The data are therefore normalized using logarithmic transformation to reduce the asymmetry of the distributions for multivariate analyses. In fact, no dataset is exactly normally distributed, instead, " it is only necessary for the data to be near normal " (Shapiro, 1990). According to statistics results, Au, Ag, As, Hg, and Sb have high kurtosis and high skewness values. These elements have non-normal distribution pattern while Se and Te have normal distribution pattern. This aspect may also be seen in the histograms. To approach normal distribution, raw data of Au, Ag, As, Hg, and Sb were logarithmically transformed (log10). The descriptive statistical results and histograms for log transformed datasets are shown in Table 2 and Figure 28-32, respectively.

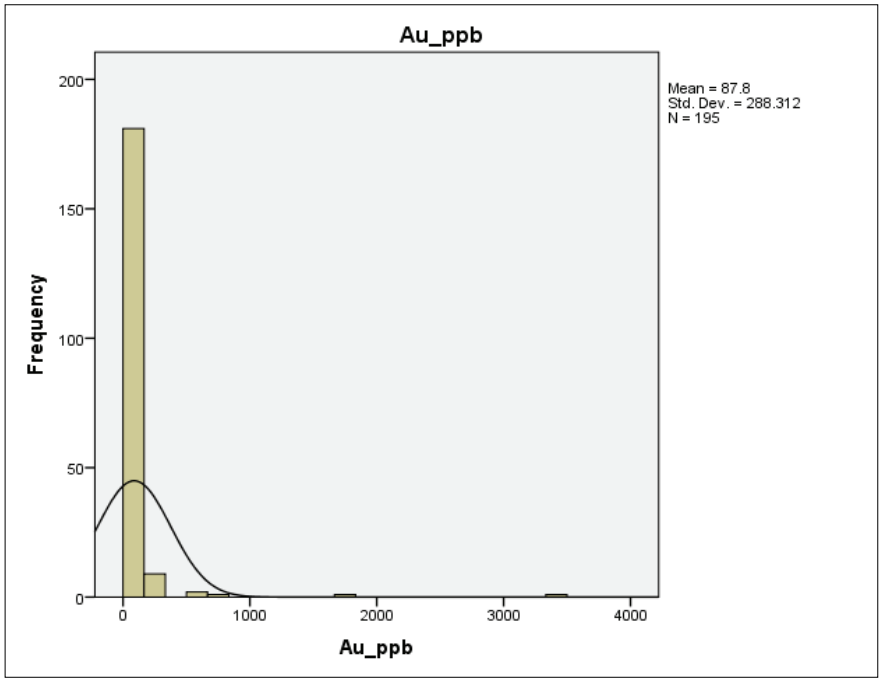

Figure 21. Frequency histogram for Au.

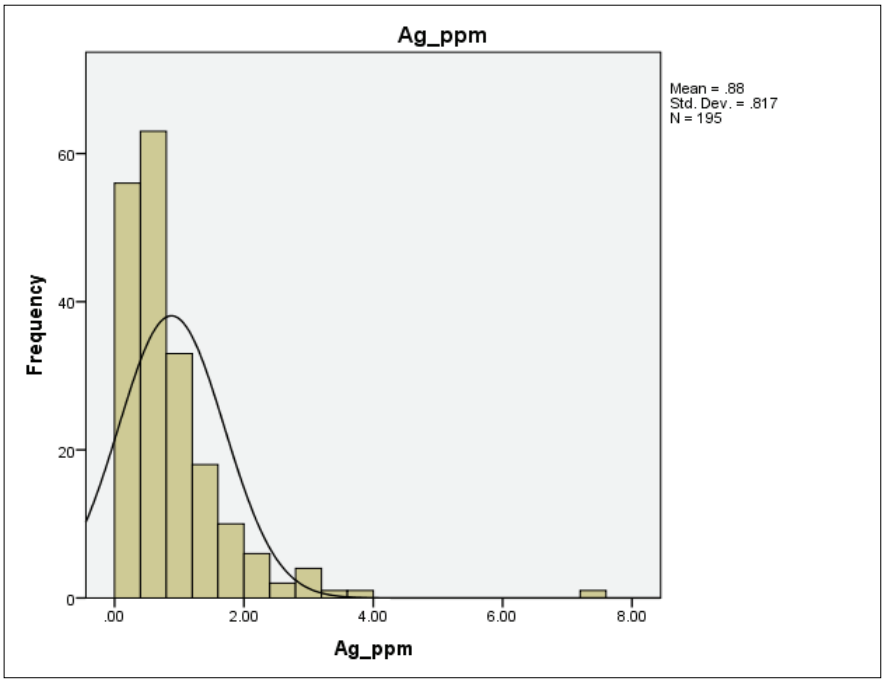

Figure 20. Frequency histogram for Ag.

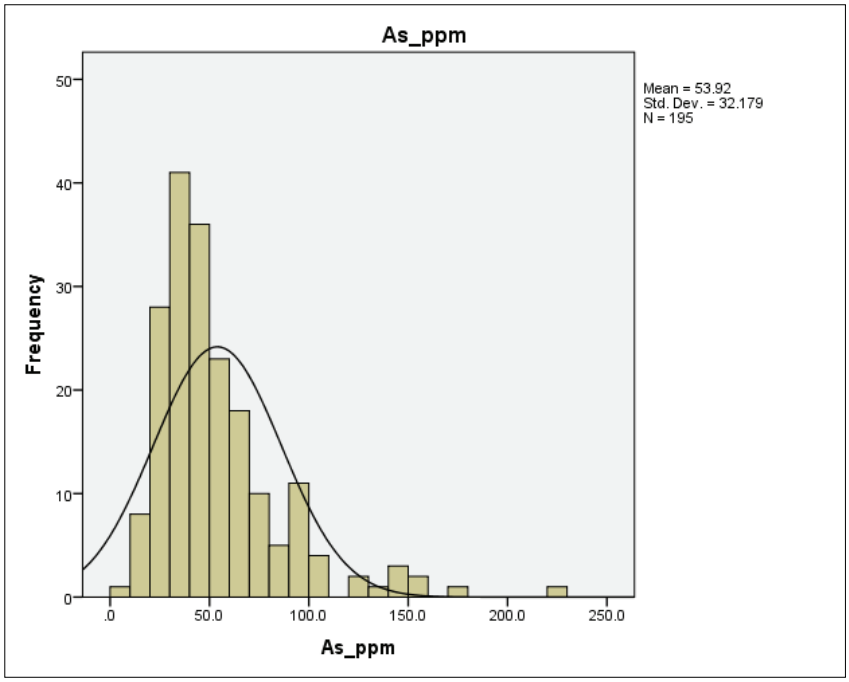

Figure 21. Frequency histogram for As.

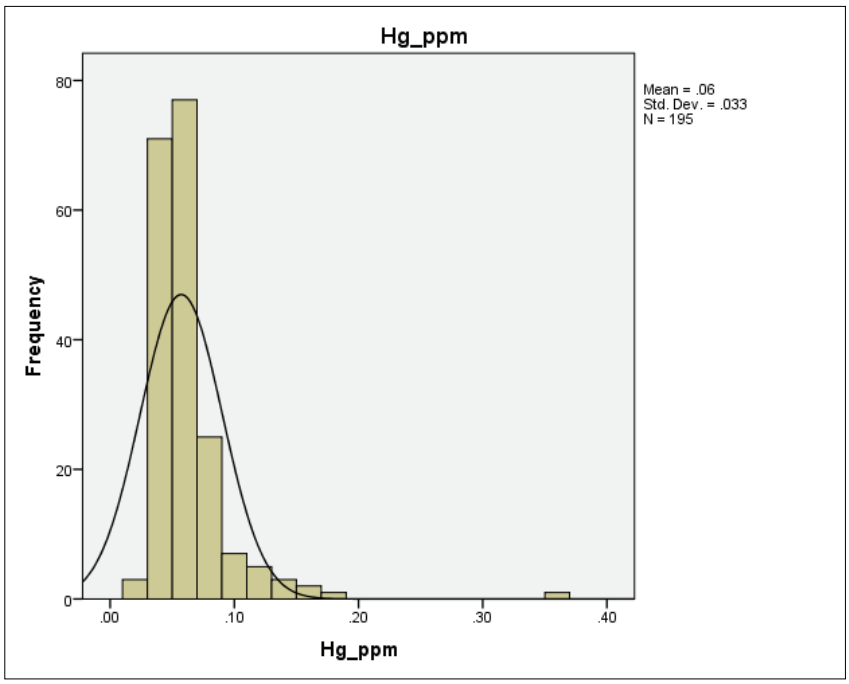

Figure 22. Frequency histogram for Hg.

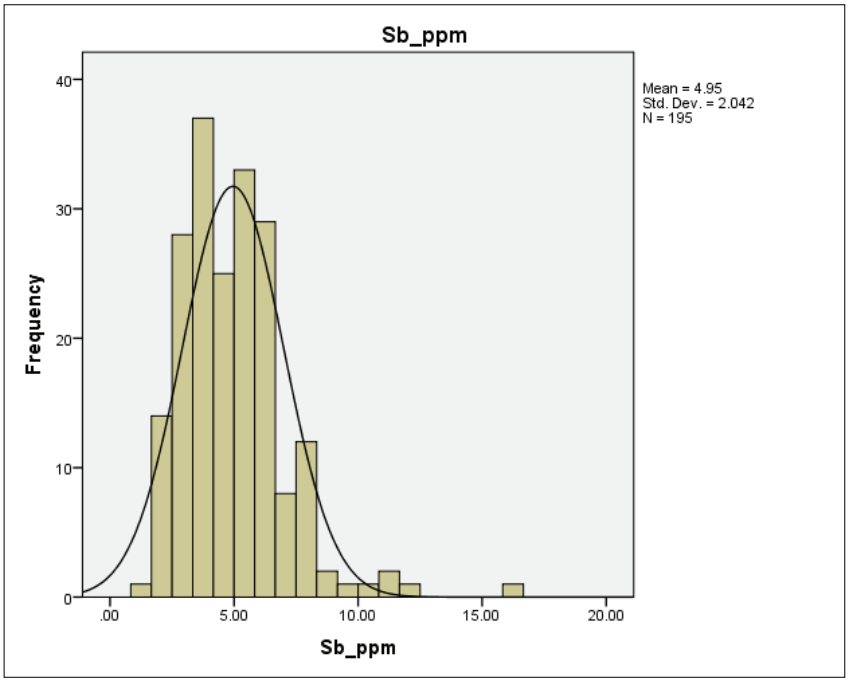

Figure 23. Frequency histogram for Sb.

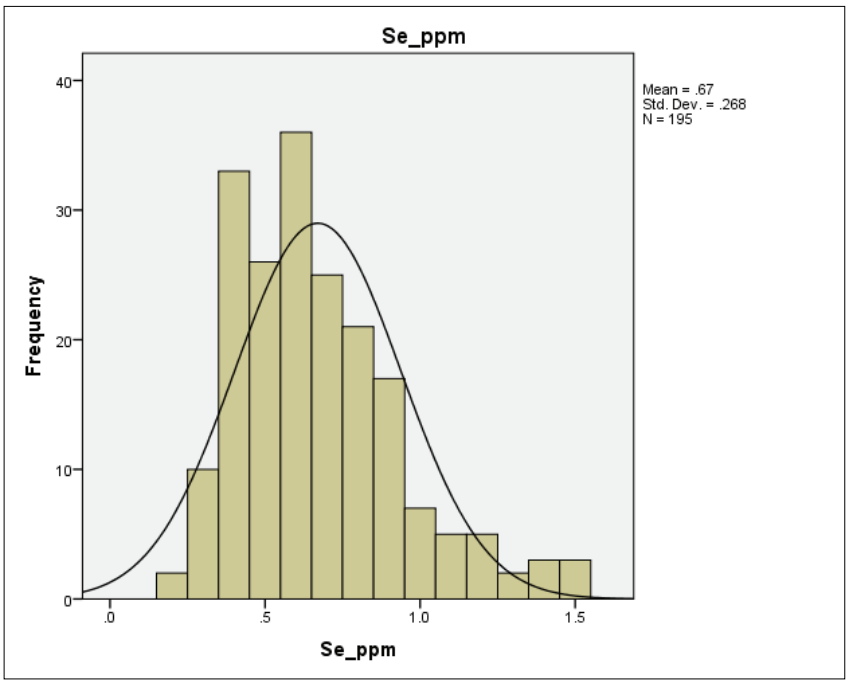

Figure 24. Frequency histogram for Se.

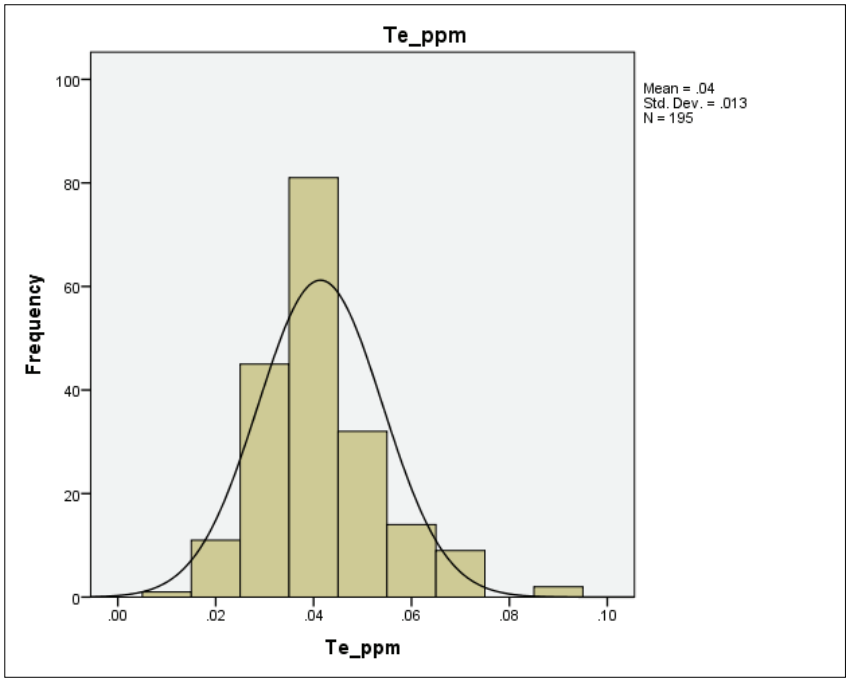

Figure 25. Frequency histogram for Te.

Table 2. Descriptive statistics for logarithmically transformed Au, Ag, As, Hg, and Sb.

	Au (ppb)	Ag (ppm)	As (ppm)	Hg (ppm)	Sb (ppm)
Mean	1.55	-0.19	1.67	-1.29	0.66
Std. Error of Mean	0.04	0.02	0.02	0.01	0.01
Median	1.51	-0.21	1.67	-1.30	0.67
Mode	1.18	-0.28	1.30	-1.30	0.71
Std. Deviation	0.49	0.34	0.23	0.18	0.17
Variance	0.25	0.11	0.05	0.03	0.02
Skewness	0.62	0.19	0.12	0.84	0.01

Table 2 (Cont'd)					
	Au (ppb)	**Ag (ppm)**	**As (ppm)**	**Hg (ppm)**	**Sb (ppm)**
Std. Error of Skewness	0.17	0.17	0.17	0.17	0.17
Kurtosis	1.26	-0.34	0.30	1.98	-0.04
Std. Error of Kurtosis	0.35	0.35	0.35	0.35	0.35
Range	3.24	1.78	1.43	1.24	1.00
Minimum	0.30	-0.92	0.92	-1.69	0.19
Maximum	3.54	0.86	2.35	-0.46	1.20
Sum	301.53	-36.87	325.38	-250.84	128.98

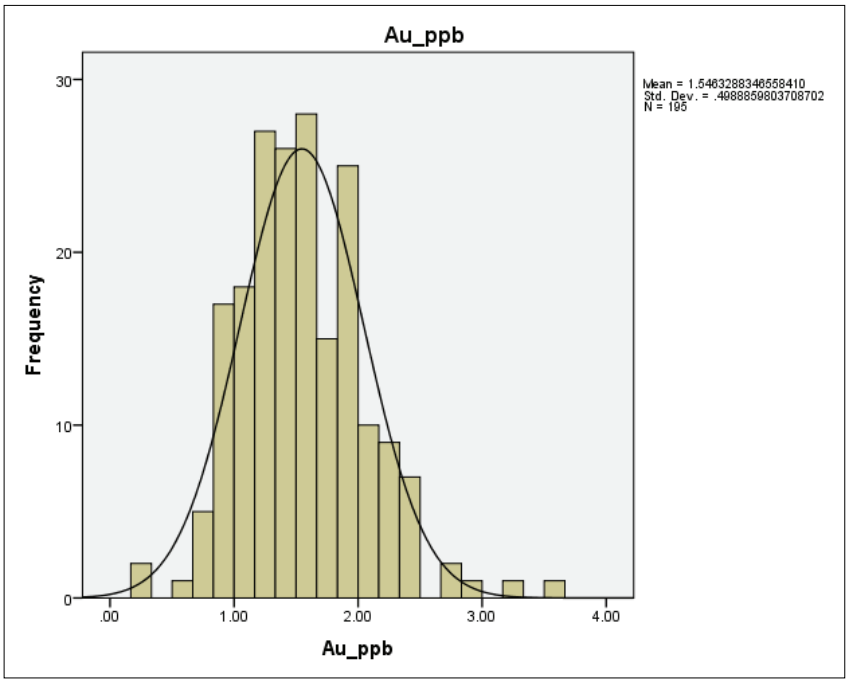

Figure 26. Frequency log 10 histogram for Au.

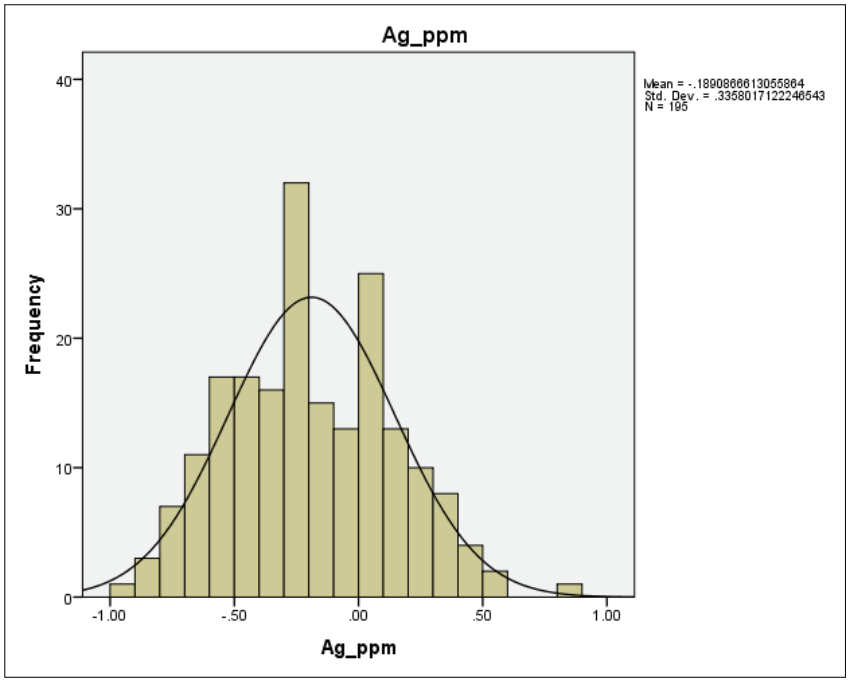

Figure 27. Frequency log 10 histogram for Ag.

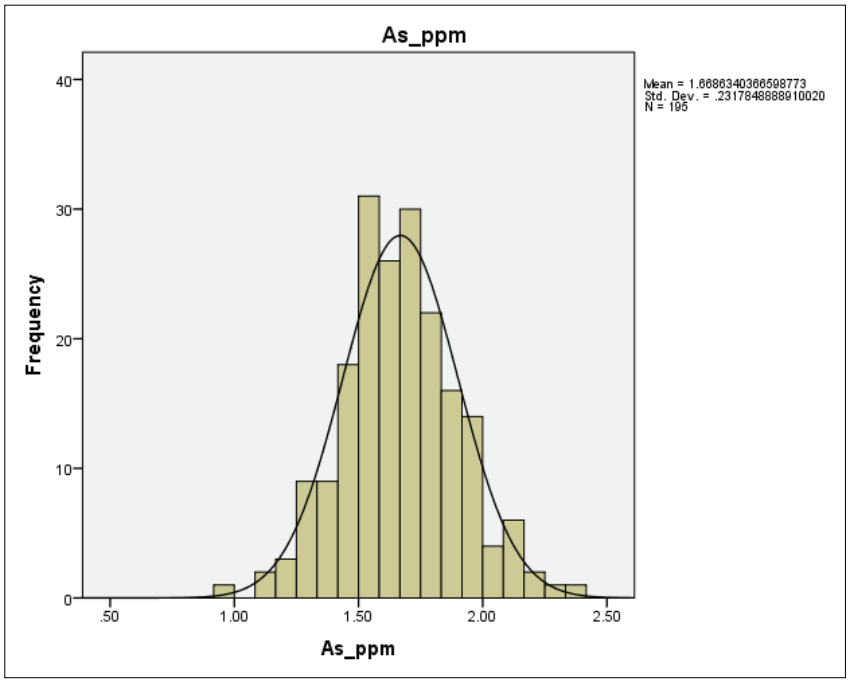

Figure 28. Frequency log 10 histogram for As.

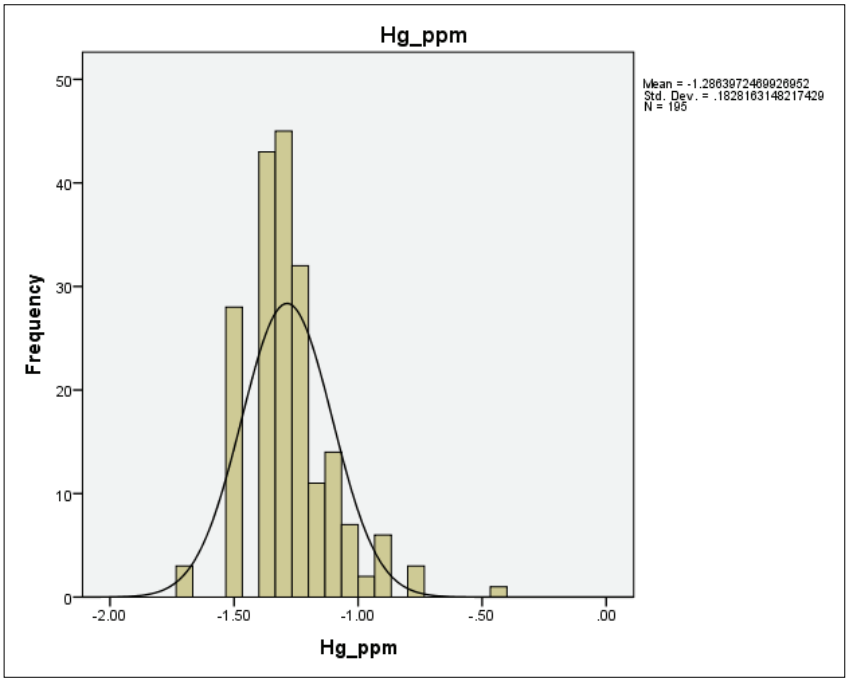

Figure 29. Frequency log 10 histogram for Hg.

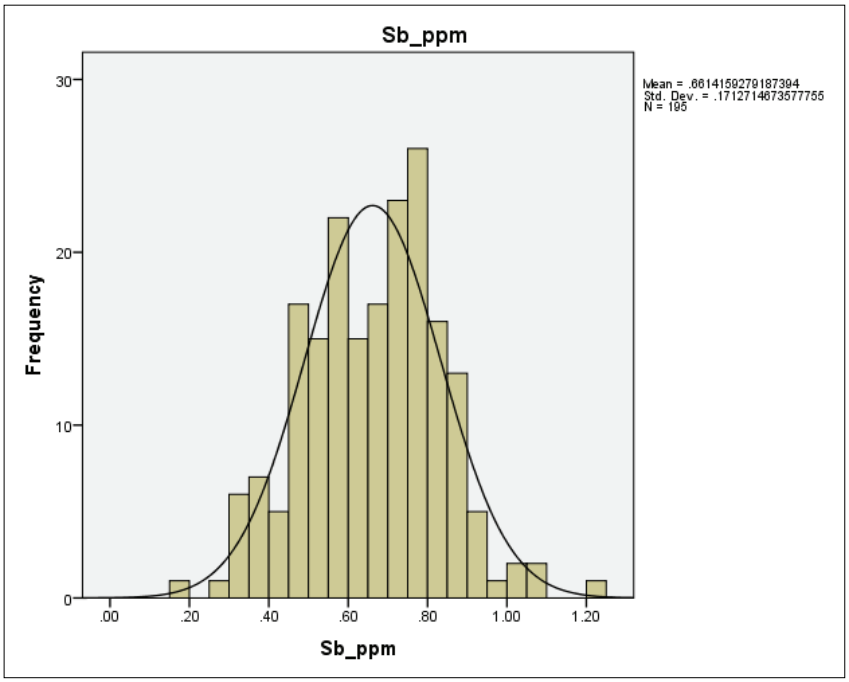

Figure 30. Frequency log 10 histogram for Sb.

In order to determine the probability characteristic of elements in soil samples, Q-Q plots of both raw and log-transformed data were prepared. Figure 33-39 represents Q-Q plot of raw datasets for selected elements.

It is clearly noticed that the dataset of Au, Ag, As, Hg, and Sb deviated far away from the normal distribution. However, Q–Q plots of Se and Te partly differ from those of other elements. Other property of this plot is that outliers are clearly distinguishable. Outliers plot far away from straight line. Au shows only two high values while Ag, As, Sb, and Se show more than two high values. These high values in the dataset may be result of mineralization, weathering, supergene enrichment or external contamination of samples.

Figure 40-44 illustrate the Q-Q plot of the log-transformed values for the Au, Ag, As, Hg, and Sb, respectively. The distributions of log-transformed elements are close to normal, they do approximate straight line.

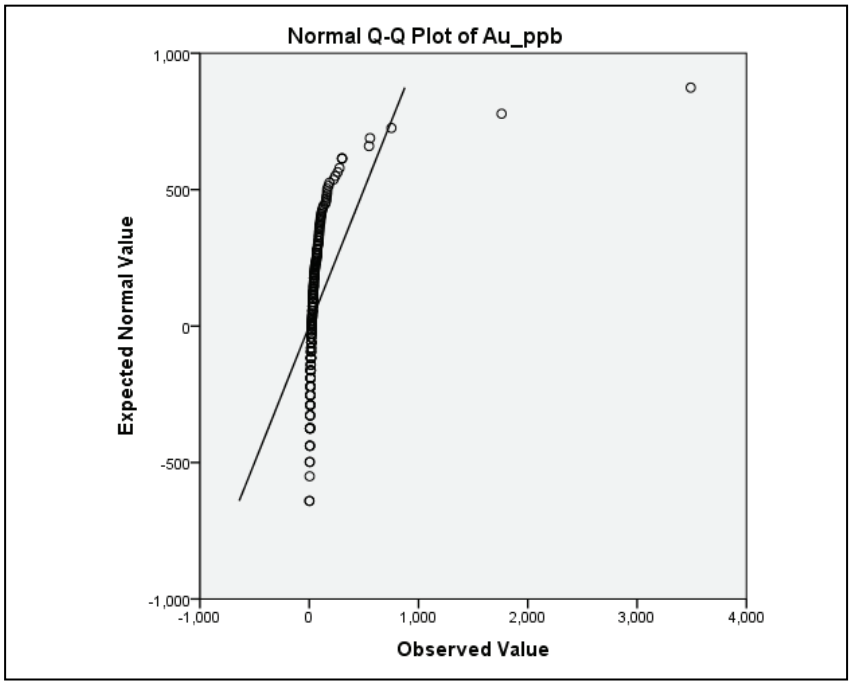

Figure 31. Normal Q-Q plot for Au.

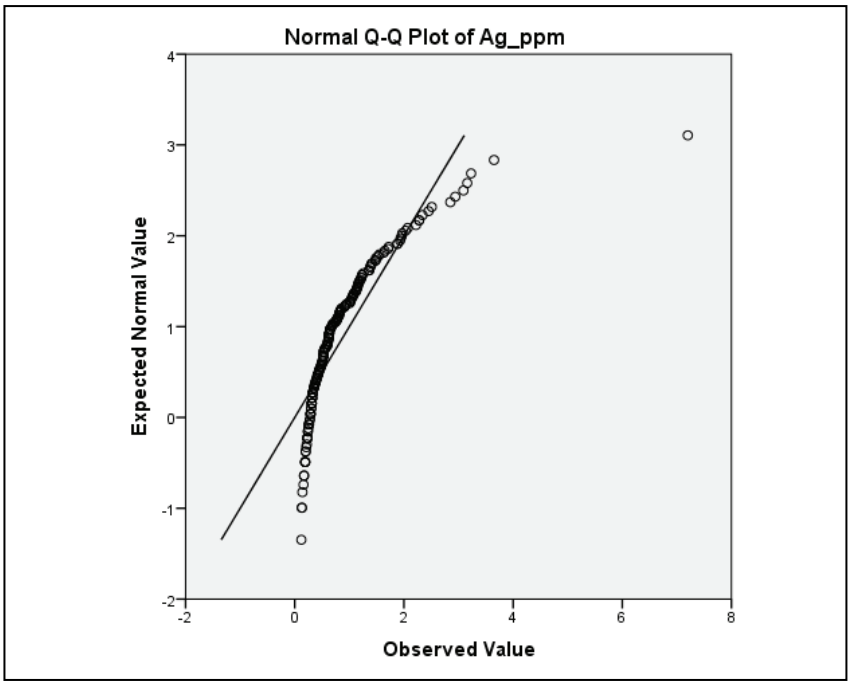

Figure 32. Normal Q-Q plot for Ag.

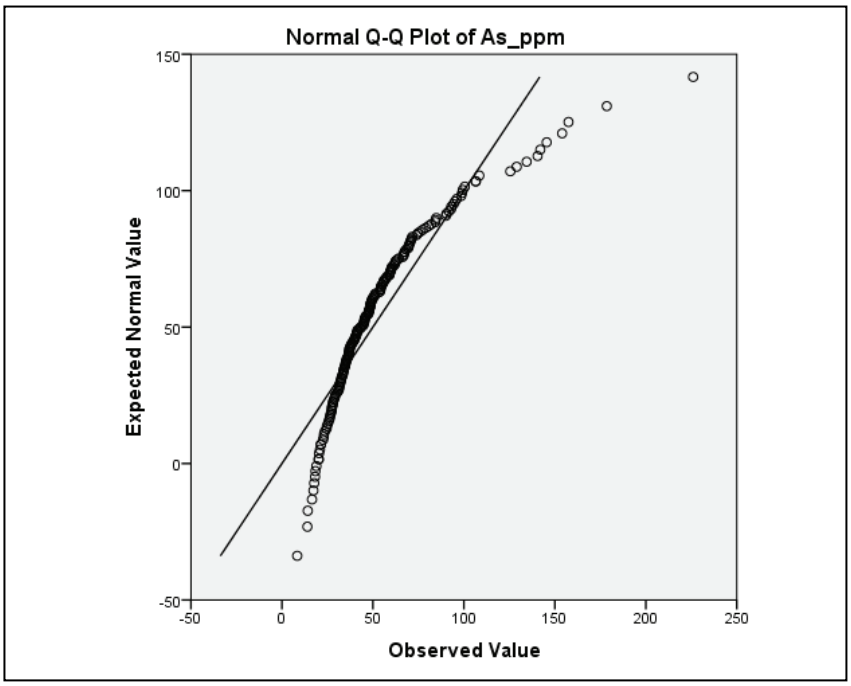

Figure 33. Normal Q-Q plot for As.

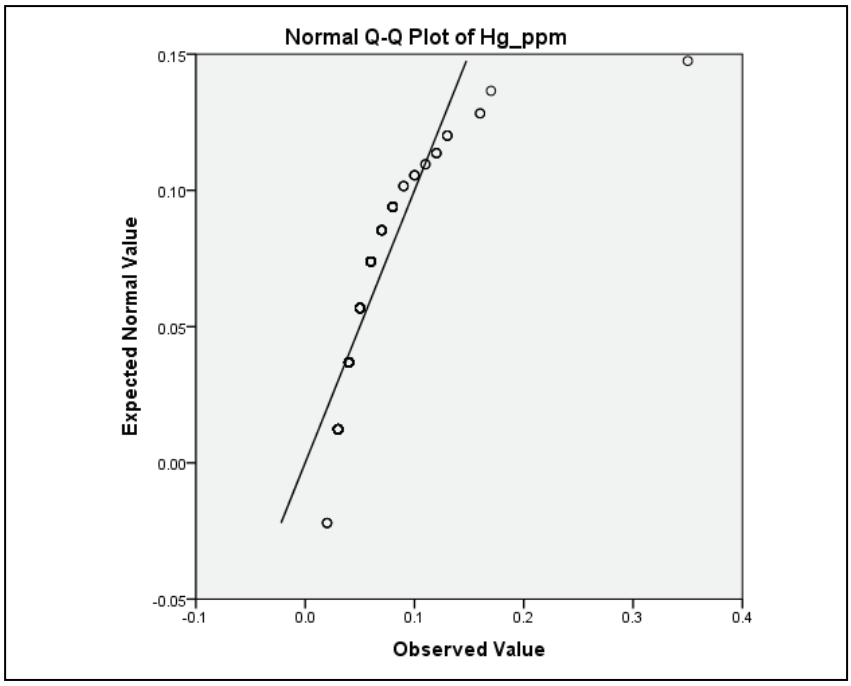

Figure 34. Normal Q-Q plot for Hg.

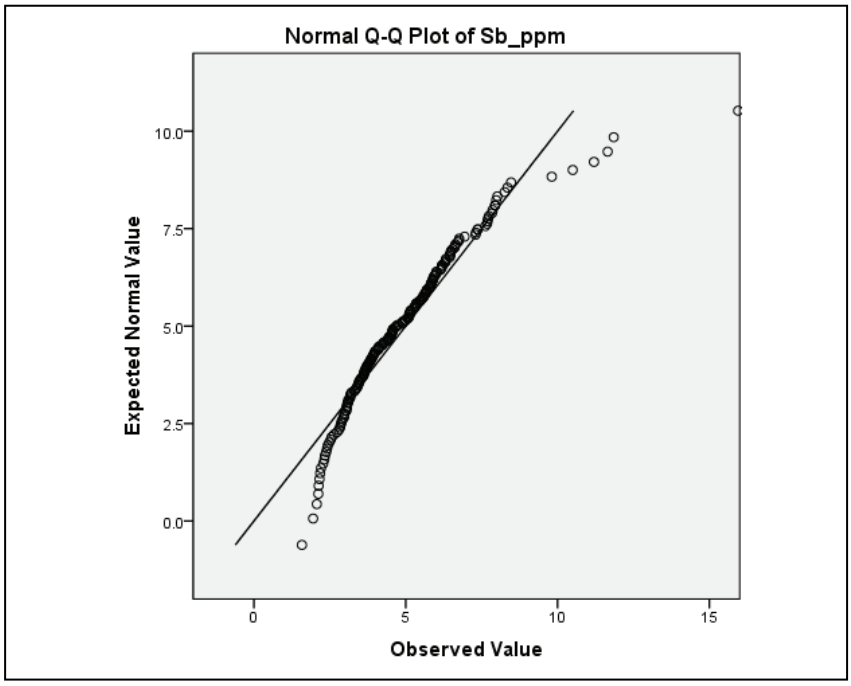

Figure 35. Normal Q-Q plot for Sb.

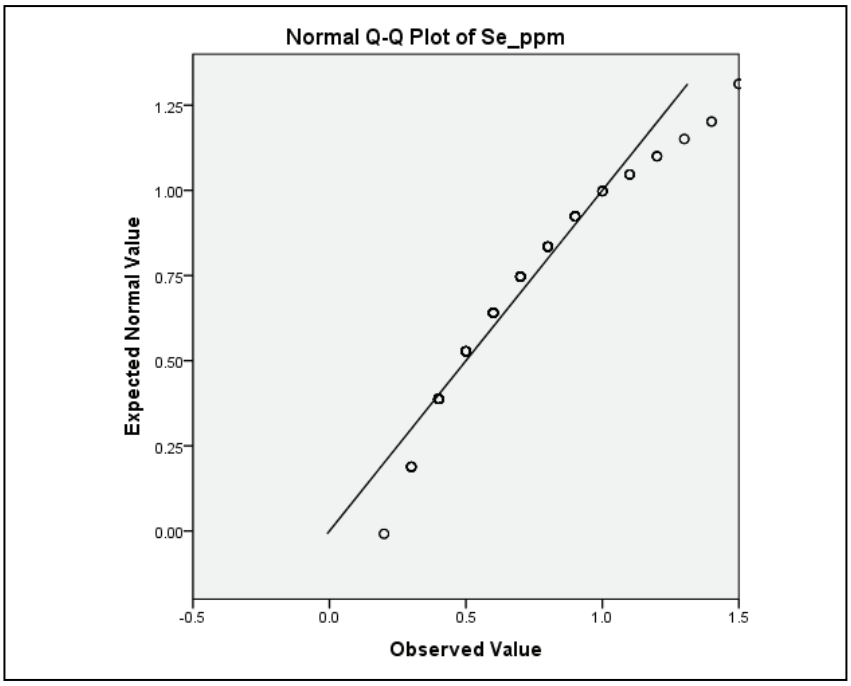

Figure 36. Normal Q-Q plot for Se.

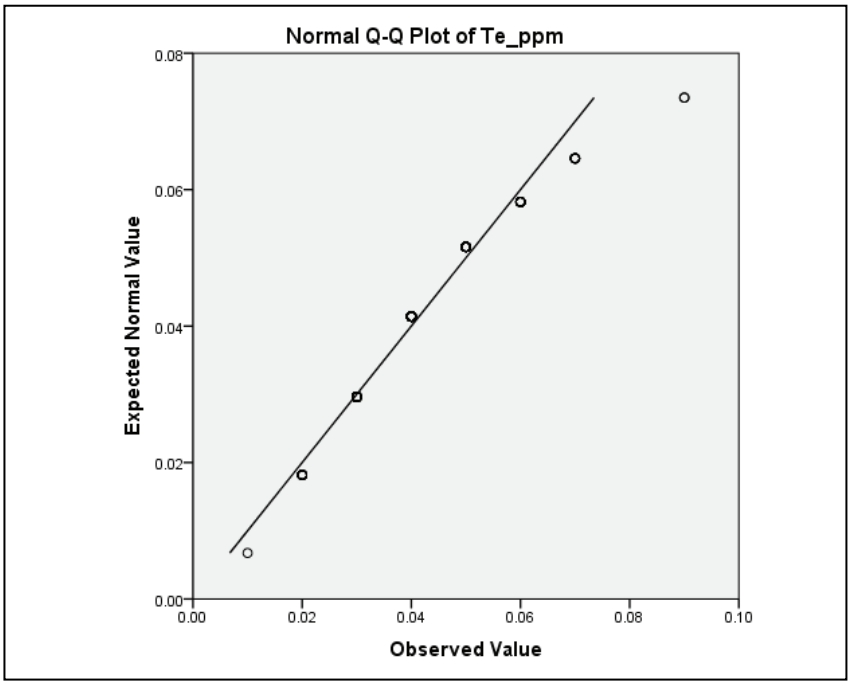

Figure 37. Normal Q-Q plot for Te.

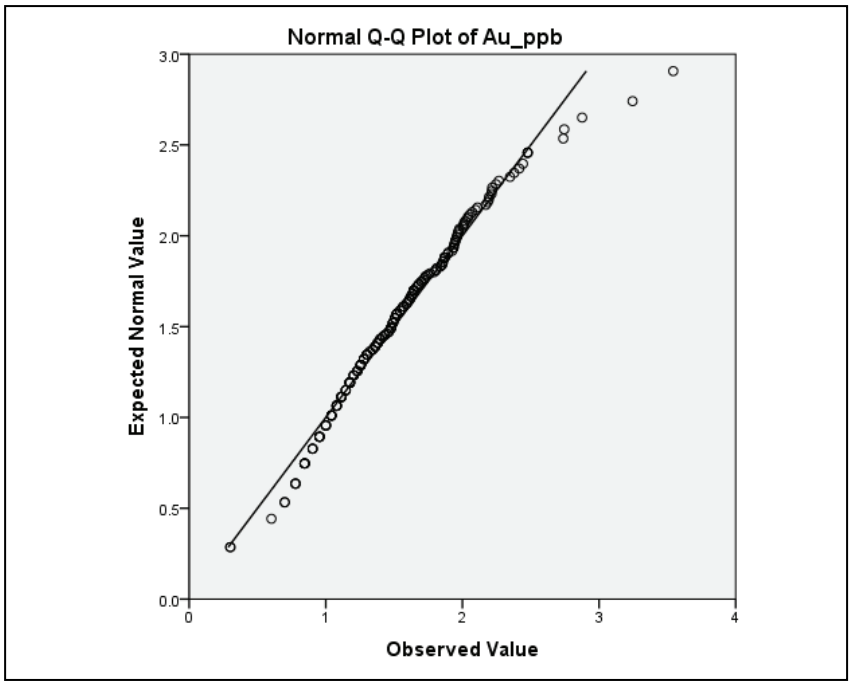

Figure 38. Log normal Q-Q plot for Au.

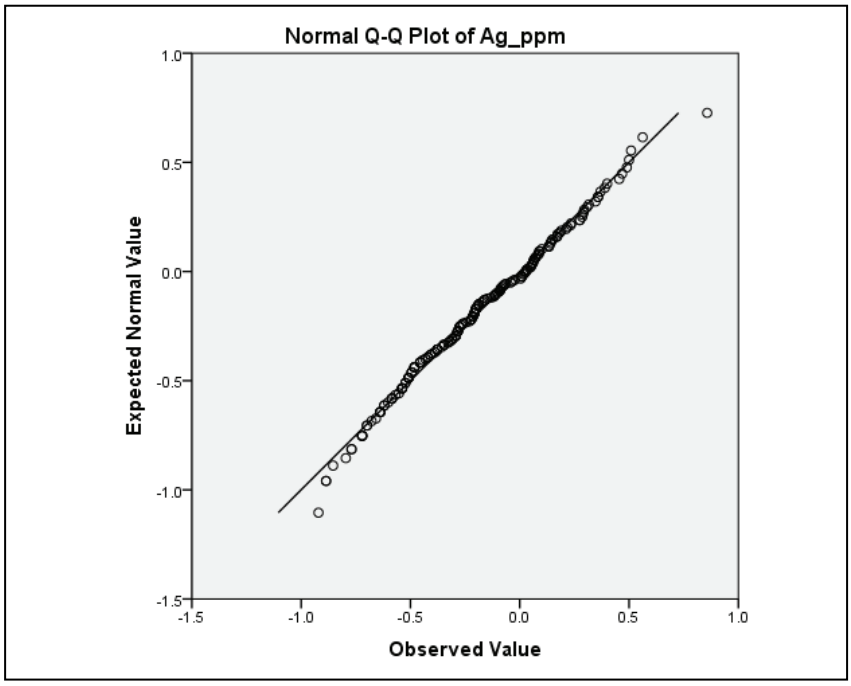

Figure 39. Log normal Q-Q plot for Ag.

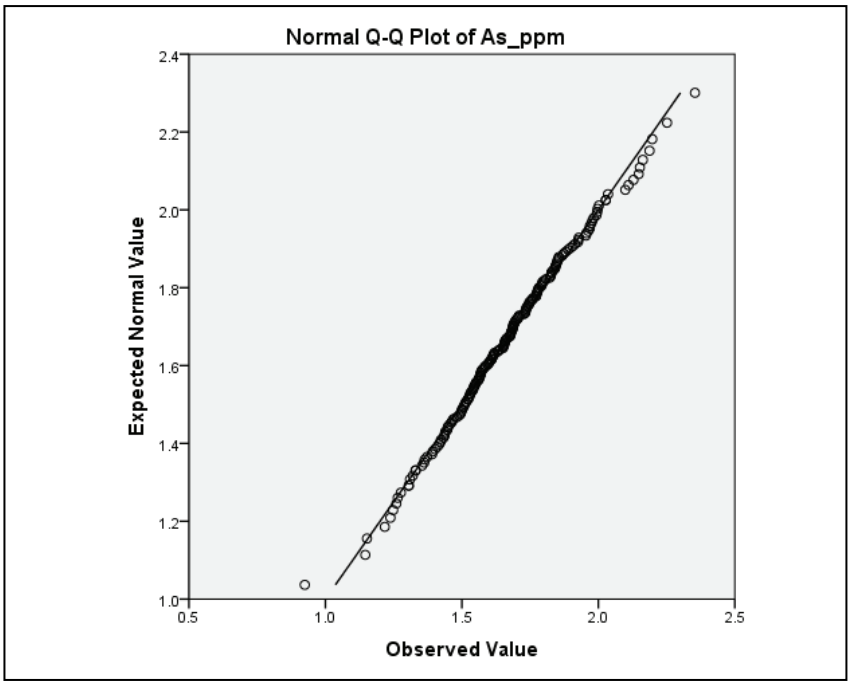

Figure 40. Log normal Q-Q plot for As.

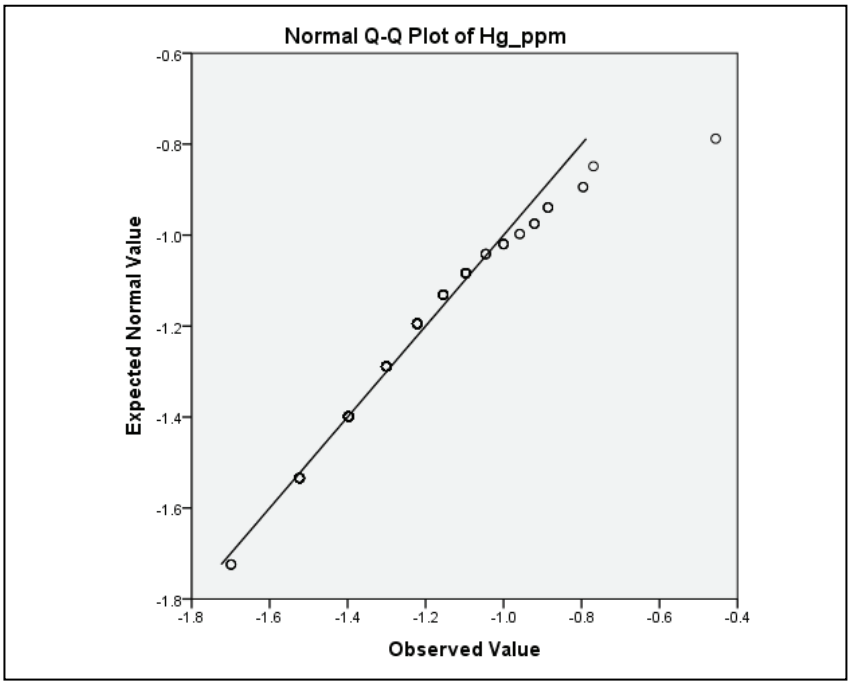

Figure 41. Log normal Q-Q plot for Hg.

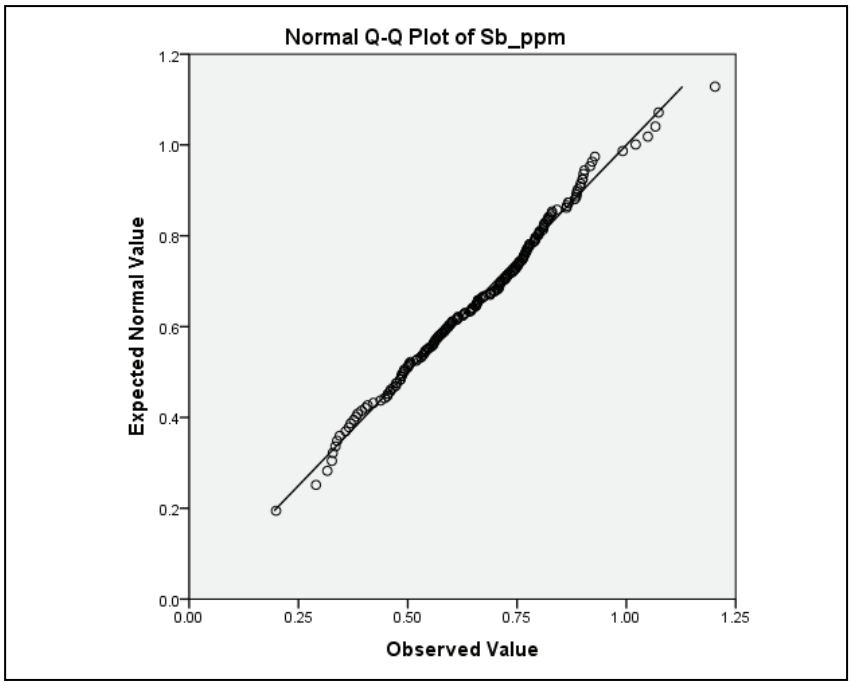

Figure 42. Log normal Q-Q plot for Sb.

Results of Box-and-Whisker plots for log-transformed Au, Ag, As, Hg, Sb, Se, and Te are represented in Figure 45. According to box plots, As-Sb, and Se-Te have quite similar trends between each other. The median plots near the center of Te boxes, indicating that data are close to normal distribution. However, the median of Au, Ag, As, Hg, Sb, and Se plots far away from the center showing that the distribution skewed. Au and Hg have narrow inter-quartile range (IQR) boxes and are positively skewed, which implies that a higher number of samples have similar concentrations. Se and Te have wide IQR boxes and are positively skewed, which implies a great variability in the concentrations found in the IQR. Maximum concentrations for these elements, as indicated by the outliers, occur in the Au, Ag, As, Hg, and Sb. In box-plot, upper inner fence (UIF) value is usually accepted as a threshold value. According to UIF results, the threshold values of Au, Ag, As, Hg, Se, Sb, and Te are 103.50 ppb, 0.86 ppm, 81.38 ppm, 0.07 ppm, 7.23 ppm, 0.95 ppm, and 0.06 ppm, respectively.

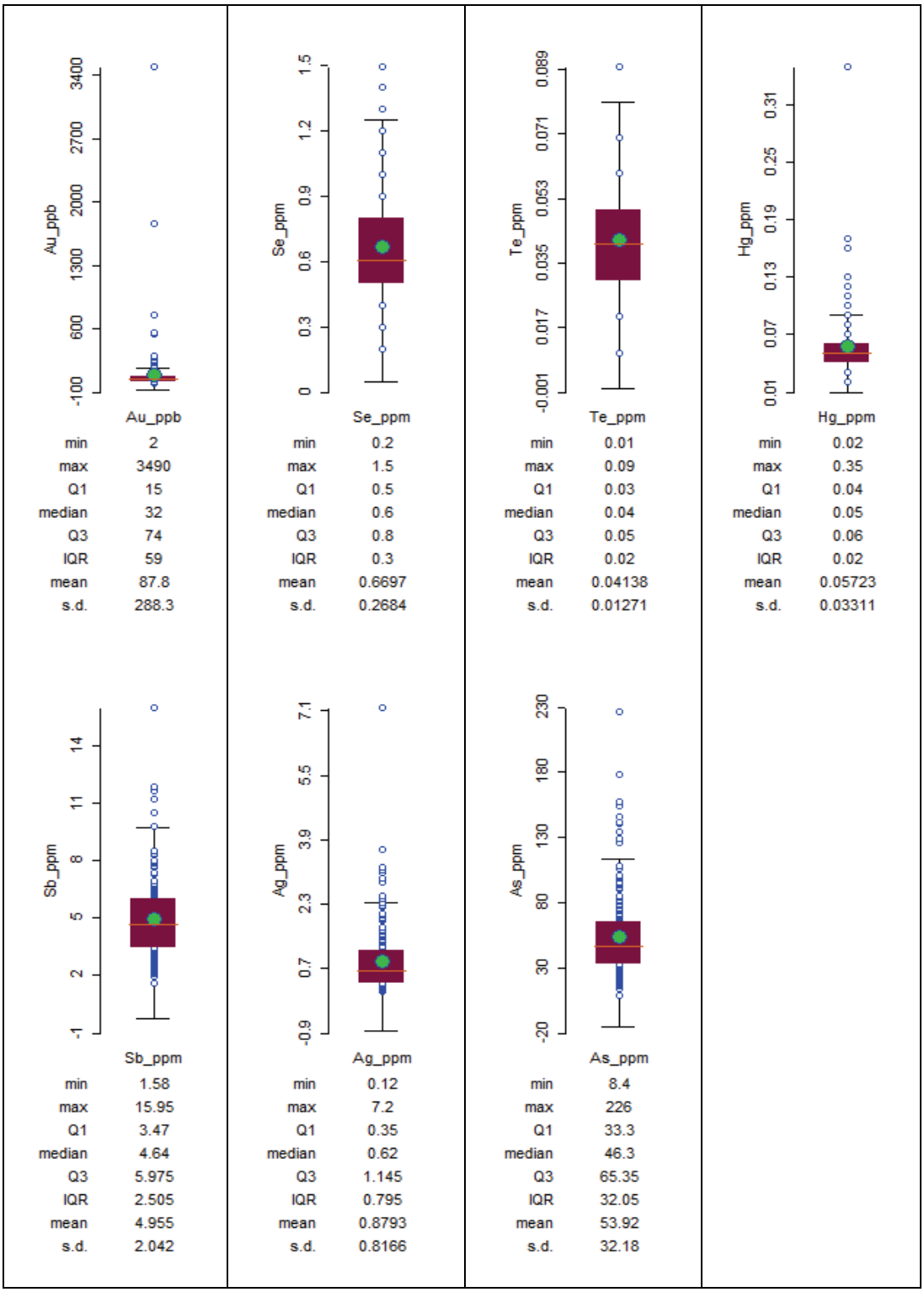

Figure 43. Box-and-Whisker Plot results for Au, Ag, As, Hg, Sb, Se and Te.

The correlation matrix indicates the association between elements. It summarizes the strength of the linear relationships between each of pair of variables. In the correlation coefficient matrix, the elements with correlation coefficient above ± 0.7 are regarded as highly correlatable and the elements with correlation coefficient between ± 0.5 and ± 0.7 are regarded as moderately correlatable (Davis, 1973). The results of correlation matrix are shown in Table 3. The correlation matrix shows that Au has positive moderate correlation with Ag. This aspect is also seen in the Au/Ag scatter plot shown in Figure 46. Because other elements had correlation coefficients less than an absolute value of 0.5 relative to Au, the relationship of these elements to Au was arbitrarily considered not significant in terms of prospecting value. The scatter plots of Au, Ag, As, Hg, Sb, Se and Te are given in the Appendix B.

Table 3. Pearson multivariate correlation matrix for Au, Ag, As, Hg, Se, Sb, and Te.

	Au (ppb)	**Ag (ppm)**	**As (ppm)**	**Hg (ppm)**	**Sb (ppm)**	**Se (ppm)**	**Te (ppm)**
Au (ppb)	1						
Ag (ppm)	0.68	1					
Al %	0.05	0.26					
As (ppm)	0.15	0.23	1				
Be (ppm)	0.27	0.35	0.49				
Bi (ppm)	-0.03	0.08	0.07				
Ca %	0.17	0.35	0.19				
Cd (ppm)	0.12	0.19	0.16				
Ce (ppm)	0.12	0.24	0.36				

Table 3 (Cont'd)

	Au (ppb)	Ag (ppm)	As (ppm)	Hg (ppm)	Sb (ppm)	Se (ppm)	Te (ppm)
Co (ppm)	0.24	0.35	0.42				
Cr (ppm)	0.11	0.09	0.52				
Cs (ppm)	0.19	0.37	0.40				
Cu (ppm)	0.30	0.22	0.35				
Fe %	0.12	0.22	0.44				
Ga (ppm)	0.14	0.29	0.48				
Ge (ppm)	0.02	-0.04	0.05				
Hg (ppm)	0.30	0.37	0.25	1			
In (ppm)	0.14	0.24	0.39	0.28			
K %	0.09	0.37	0.31	0.32			
La (ppm)	0.06	0.12	0.21	0.26			
Li (ppm)	0.05	0.06	0.36	0.11			
Mg %	0.004	-0.01	0.28	0.05			
Mn (ppm)	-0.02	0.19	-0.04	0.31			
Mo (ppm)	0.09	0.23	0.35	0.11			
Na %	3.55E-	3.84E-	8.54E-	-1.2E-			
Nb (ppm)	-0.03	0.19	-0.08	-0.02			
Ni (ppm)	0.13	0.19	0.48	0.29			

Table 3 (Cont'd)

	Au (ppb)	Ag (ppm)	As (ppm)	Hg (ppm)	Sb (ppm)	Se (ppm)	Te (ppm)
Pb (ppm)	0.25	0.29	0.27	0.19			
Rb (ppm)	0.08	0.44	0.31	0.29			
S %	0.09	0.24	0.26	0.42			
Sb (ppm)	0.24	0.21	0.28	0.05	1		
Sc (ppm)	0.23	0.35	0.45	0.29	0.14		
Se (ppm)	0.27	0.46	0.46	0.46	0.01	1	
Sn (ppm)	0.03	0.21	0.04	0.21	0.18	0.37	
Sr (ppm)	0.12	0.14	0.29	0.22	0.27	0.24	
Te (ppm)	0.25	0.34	0.52	0.29	0.37	0.67	1
Th (ppm)	0.073	0.17	0.33	0.07	-0.15	0.43	0.35
Ti %	0.001	0.19	0.05	-0.06	-0.01	0.19	0.16
U (ppm)	0.21	0.34	0.54	0.41	0.02	0.67	0.54
V (ppm)	0.14	0.31	0.35	0.16	0.48	0.43	0.56
W (ppm)	0.13	0.05	0.21	-0.002	0.77	-0.09	0.25
Y (ppm)	0.17	0.31	0.38	0.37	-0.10	0.86	0.52
Zn (ppm)	0.08	0.06	0.18	0.23	0.19	0.41	0.37
Zr (ppm)	0.09	0.33	0.18	0.36	-0.20	0.54	0.35

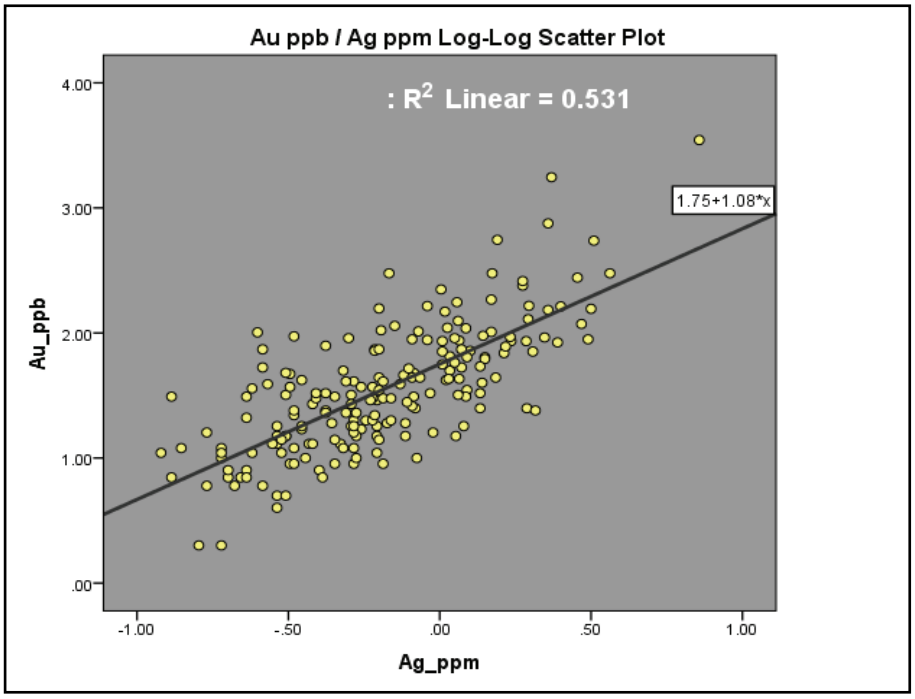

Figure 44. Au/Ag log-log scatter plot.

In order to divide data into sub-populations and define background, threshold and anomaly values of datasets, probability graphs were created. Since Au, Ag, As, Hg, and Sb have log-normal distribution, log-probability graphs were prepared. The results of the probability graphs for seven elements are given below.

- Gold has five sub-populations (Figure 47) which are indicated by four inflection point I1 (40 ppb), I2 (75 ppb), I3 (100 ppb), and I4 (155 ppb).Regional anomaly is between 27 ppb and 155 ppb, local anomaly values are above 155 ppb and the background values are below 27 ppb.
- Silver is also characterized by five sub-populations (Figure 48) indicated by four inflection points I1 (0.50 ppm), I2 (0.70 ppm), I3 (1,00 ppm), and I4 (1.90 ppm). The background values are below 0.30 ppm. Regional anomaly is between 0.30 ppm and 1.90 ppm and local anomaly values are above 1.90 ppm.
- Arsenic has four sub-populations (Figure 49) which are due to regional anomaly and local anomaly, indicated by three inflection points I1 (42 ppm),

I3 (77 ppm) and I3 (97 ppm). Regional anomaly is between 22 ppm and 97 ppm, local anomaly values are above 97 ppm. The background values are below 22 ppm.

- Mercury is characterized by two sub-populations (Figure 50) indicated by one inflection point I1 (0.16 ppm). Anomaly values are above 0.16 ppm, and the background values are below 0.07 ppm.
- Antimony has four sub-populations (Figure 51) which are indicated by three inflection point I1 (3.20 ppm), I2 (4.80 ppm), and I3 (7.2 ppm).Regional anomaly is between 2.70.00 ppm and 7.20 ppm, local anomaly values are above 7.20 ppm and the background values are below 2.70 ppm.
- Selenium is characterized by two sub-populations (Figure 52) indicated by one inflection point I1 (1.20 ppm). Anomaly values are above 1.20 ppm, which is same as anomaly value calculated by mean plus two standard deviations and the background values are below 0.90 ppm.
- Tellurium has two sub-populations (Figure 53) indicated by one inflection point I1 (0.07 ppm). Anomaly values are above 0.07 ppm which is almost same as anomaly value calculated by mean plus two standard deviations and the background values are below 0.04 ppm.

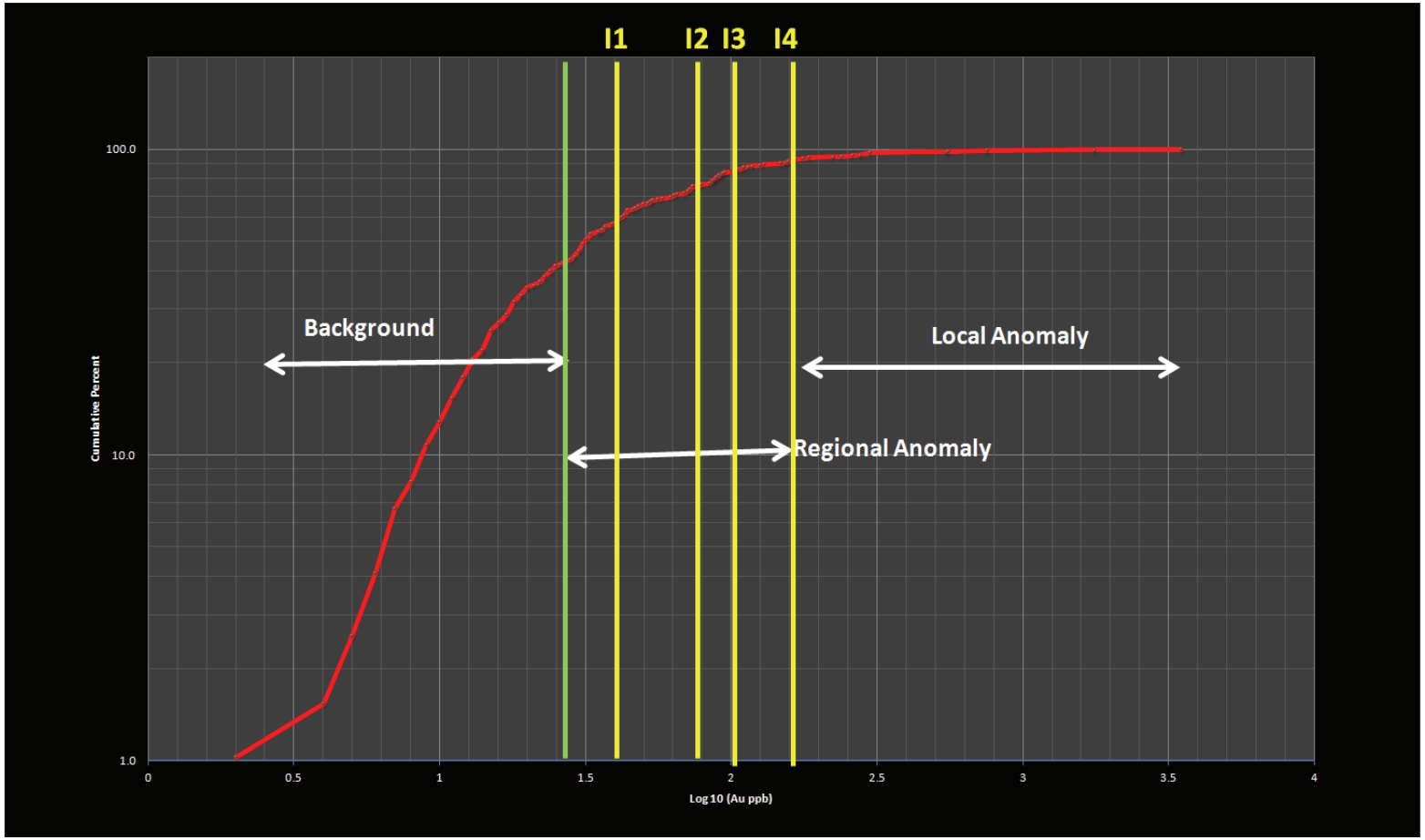

Figure 45. Au probability graph (I1, I2, I3, I4: inflection points).

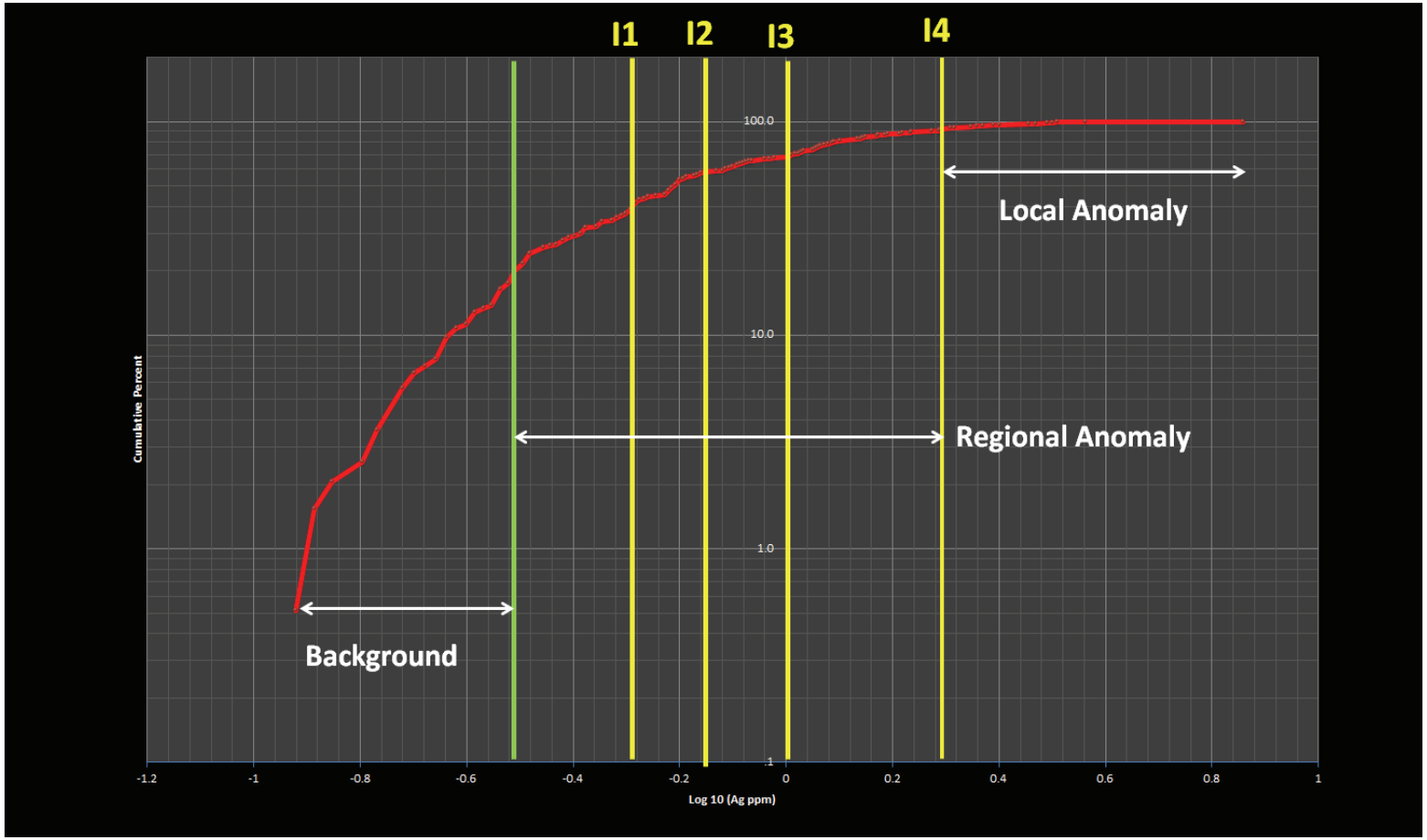

Figure 46. Ag probability graph (I1, I2, I3, I4: inflection points).

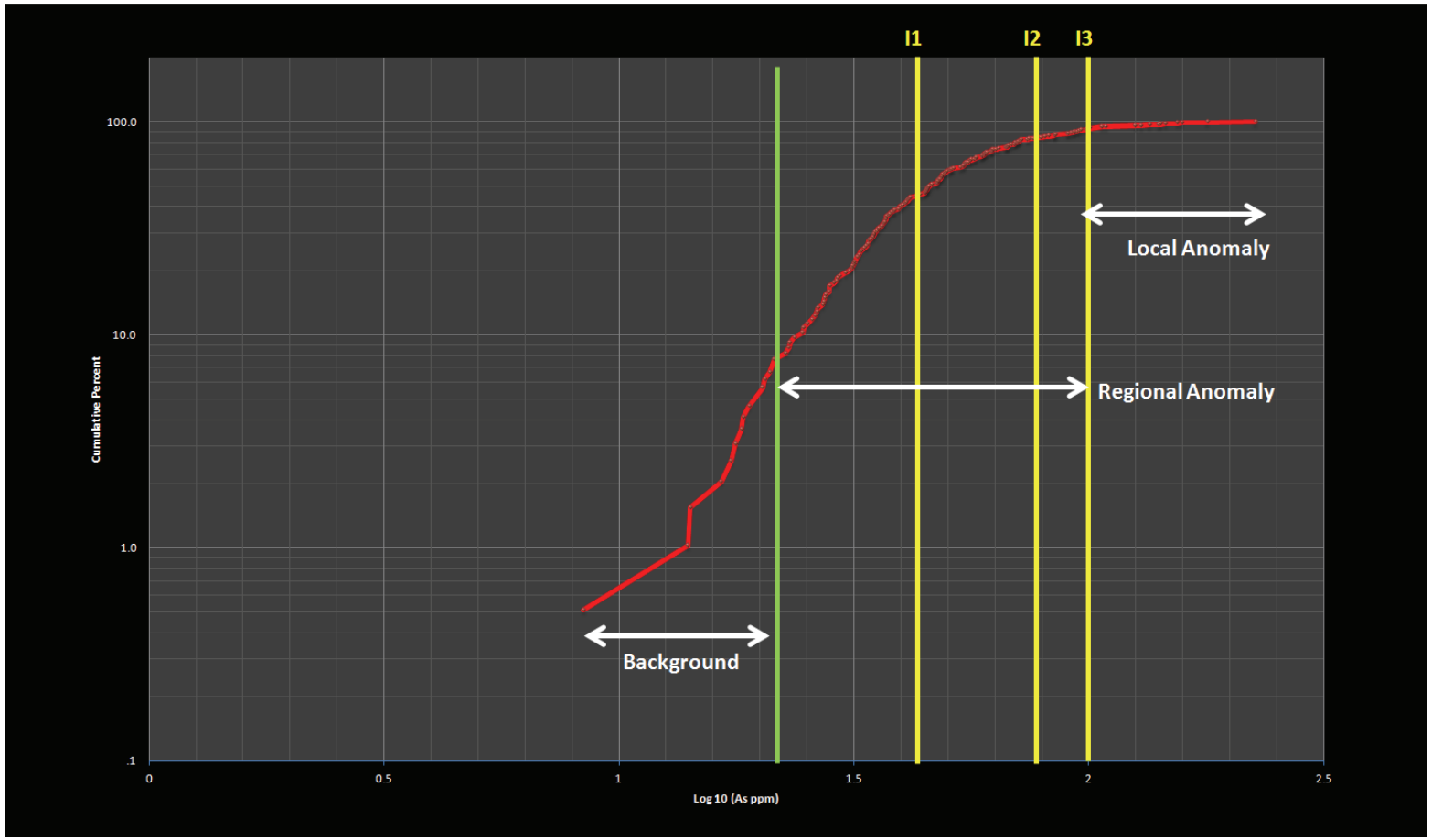

Figure 47. As probability graph (I1, I2, and I3: inflection points).

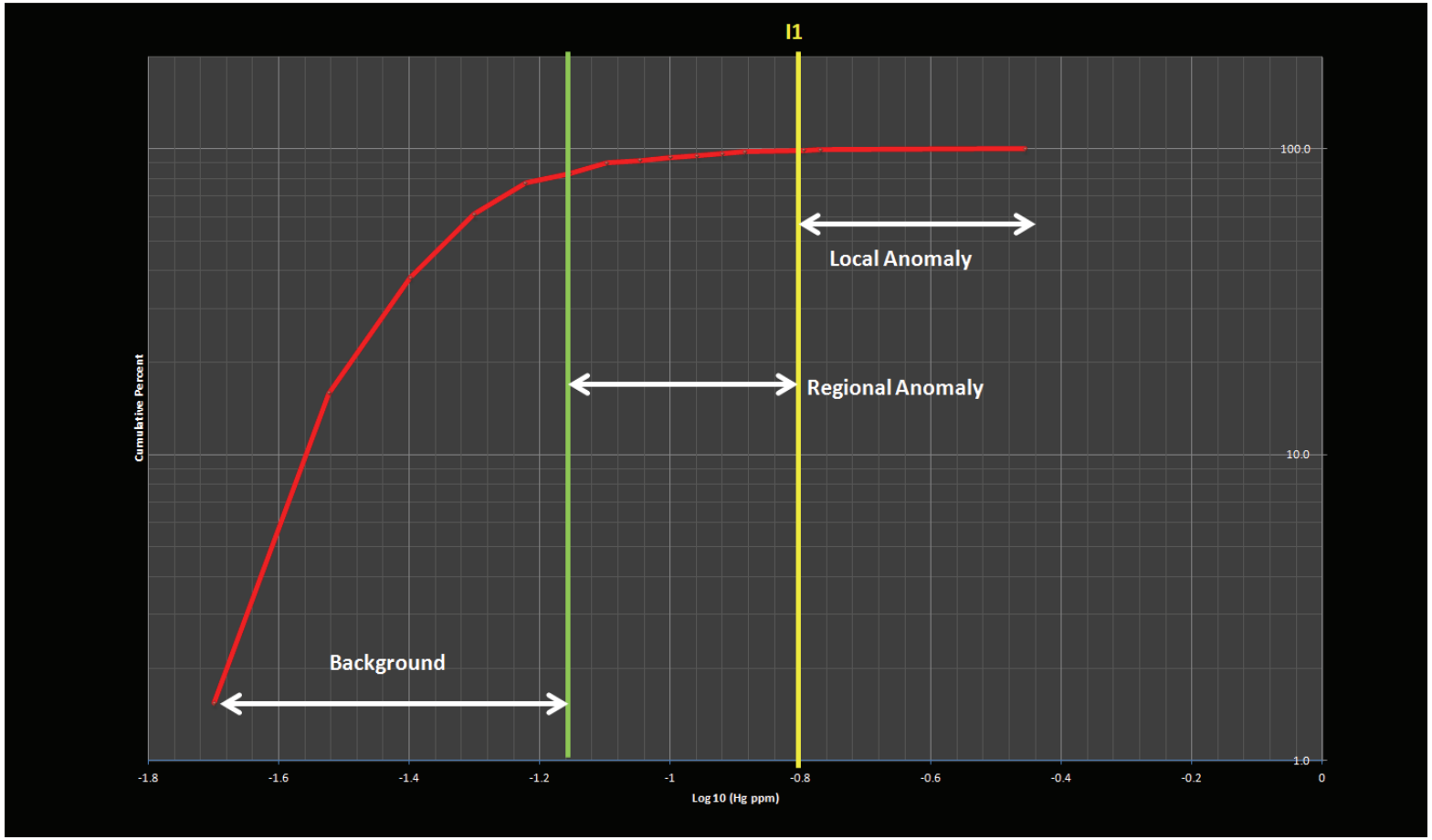

Figure 48. Hg probability graph (I1: inflection point).

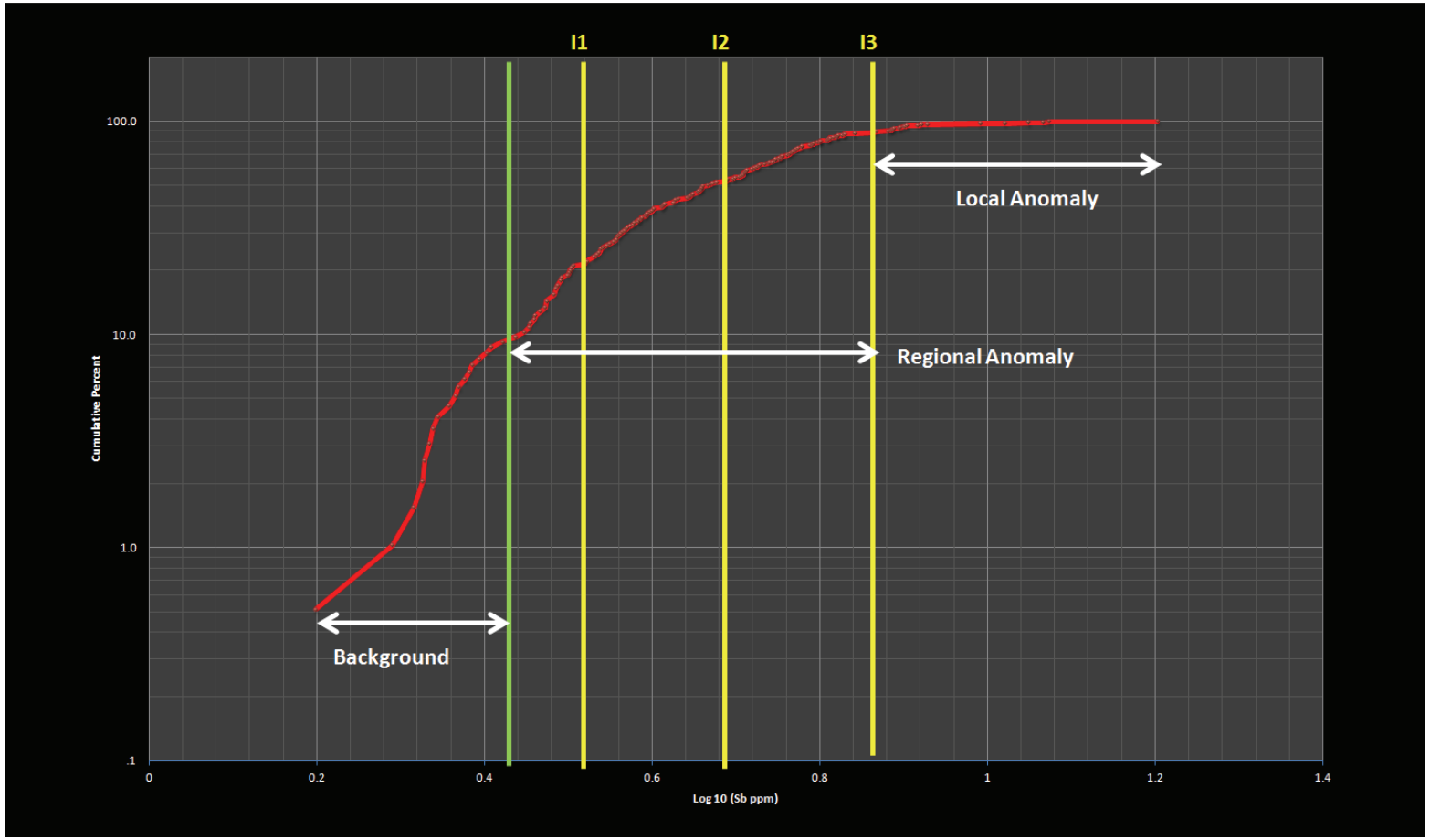

Figure 49. Sb probability graph (I1, I2, and I3: inflection points).

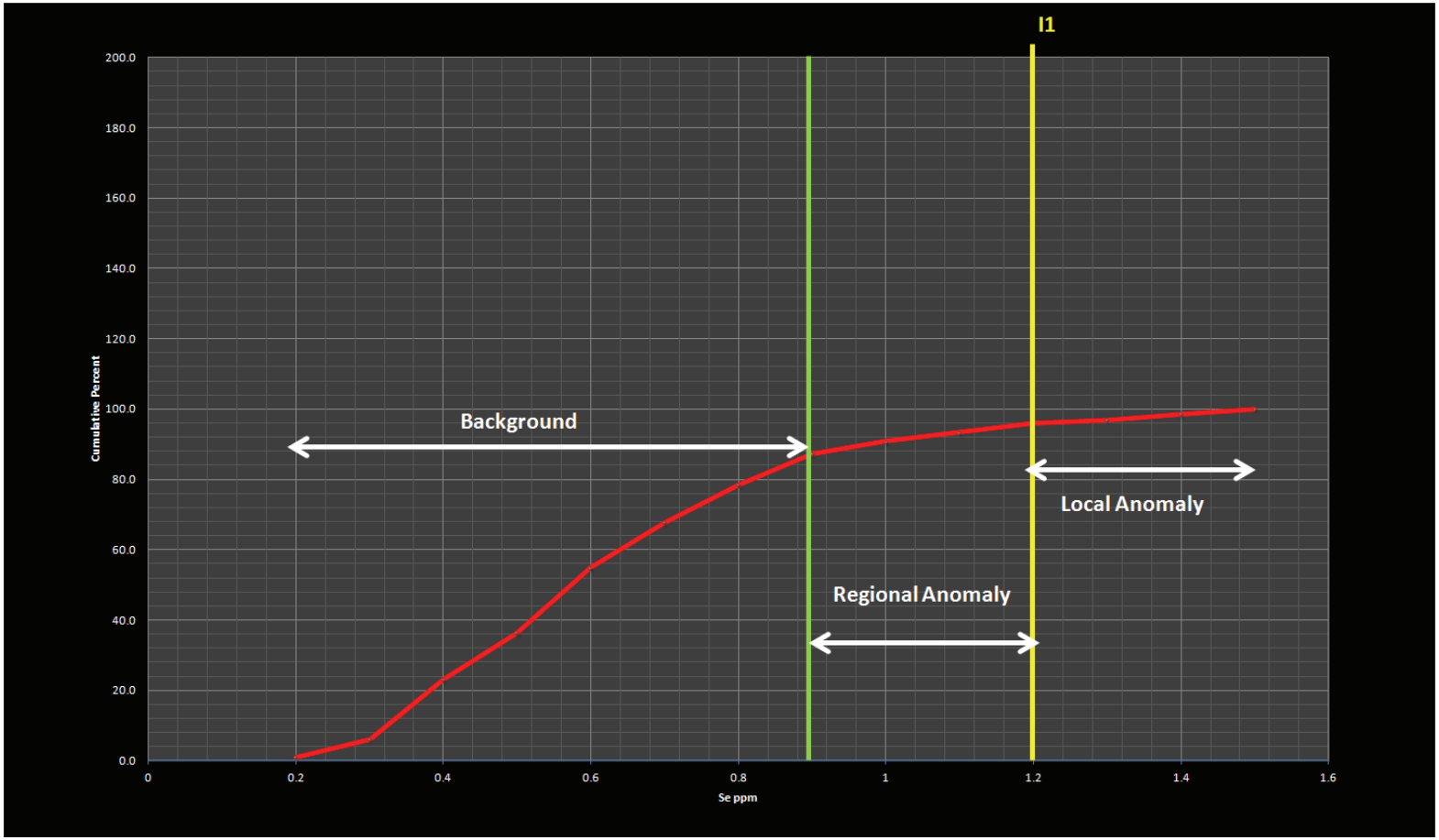

Figure 50. Se probability graph (I1: inflection point).

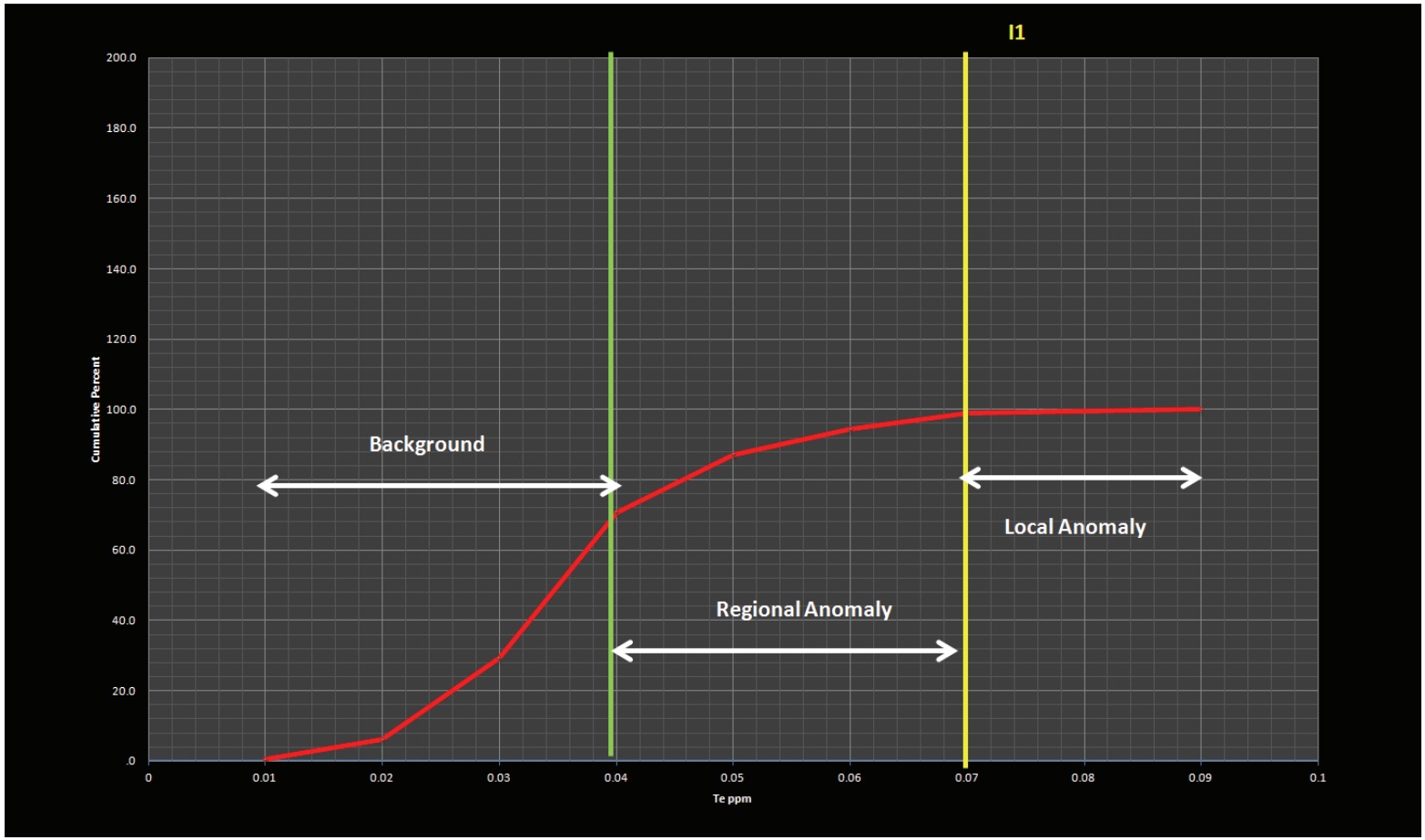

Figure 51. Te probability graph (I1: inflection point).

The threshold values calculated by mean plus two standard deviations, the threshold values calculated from box-and-whisker plots and the threshold values estimated from the cumulative probability graphs are shown in Table 4. Because the outliers are below 10% for Au (8.7%), Ag (5.1%), As (5.1%), and Sb (3%), the threshold values calculated from box-and-whisker plots are close to the threshold values estimated from the cumulative probability graphs. Results of Hg, Se and Te do not show any outliers. Therefore, the threshold values calculated by mean plus two standard deviations are almost same as threshold values estimated from the cumulative probability graphs.

Table 4. Anomaly values of Au, Ag, As, Hg, Sb, Se and Te (CPG: Cumulative probability graphs, SD: Standard Deviation)

	Au (ppb)	Ag (ppm)	As (ppm)	Hg (ppm)	Sb (ppm)	Se (ppm)	Te (ppm)
Mean+2SD	350	3.03	134	0.12	10	1.20	0.07
Box-and-Whisker Plot	104	0.86	81	0.07	7.23	0.95	0.06
CPG	155	1.90	97	0.16	7.20	1.20	0.07

In order to determine the element distribution, gridding maps were prepared for Au, Ag, As, Hg, Sb, Se, and Te based on their threshold values. Gridding maps were generated using interpolation kriging technique.

The gridding map of gold (Figures 54 and 55) shows that Au formed two strong and widespread anomalies (anomaly A and anomaly B) at the center of the area and four strong and small anomalies at the south, southwest and east side of the area. Anomaly A occurs at the lower parts of the main vein zone and it extends in the NE-SW direction which is parallel to the main vein trend. In area where anomaly B

found, no quartz veins are exposed at the surface. However, many quartz veins are observed in the trenches where the anomaly B occurs and east side of it. As a result, anomaly B could be associated with these found quartz veins. Besides, southeast of anomaly B is found in topographically lower area. Therefore, topography effect has also effect on these anomalies.

The gridding map of silver (Figure 56) shows three strong anomalies at almost the same area with the anomalies of Au. This situation implies that there is a close spatial relationship between Au and Ag.

In the As gridding map (Figure 57), strong anomalies were identified mainly in four different areas. The highest As concentration is found at south of the study area. Two of the anomalies are at east and west side of the field. The last highest one is found at the edge of the main zone.

Distribution map of Se (Figure 58) shows the presence of four strong anomalies at east and southeast parts of the field. There are small Sb anomalies in a wide area at the eastern part, southern part, and a few areas west of the field along NE-SW trending (Figure 59). Te and Hg do not form any strong anomalies (Figures 60 and 61).

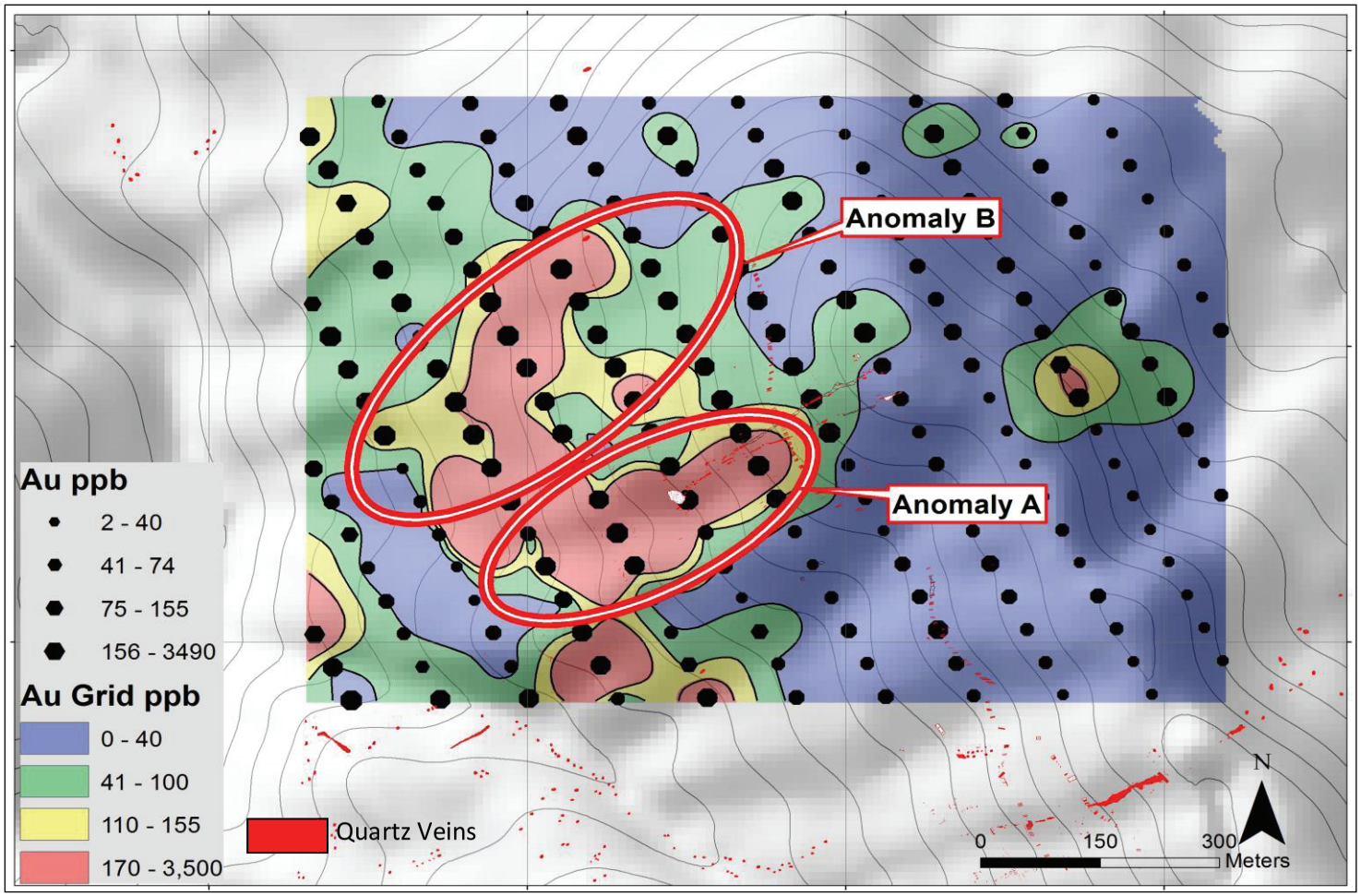

Figure 52. The Au soil anomaly map.

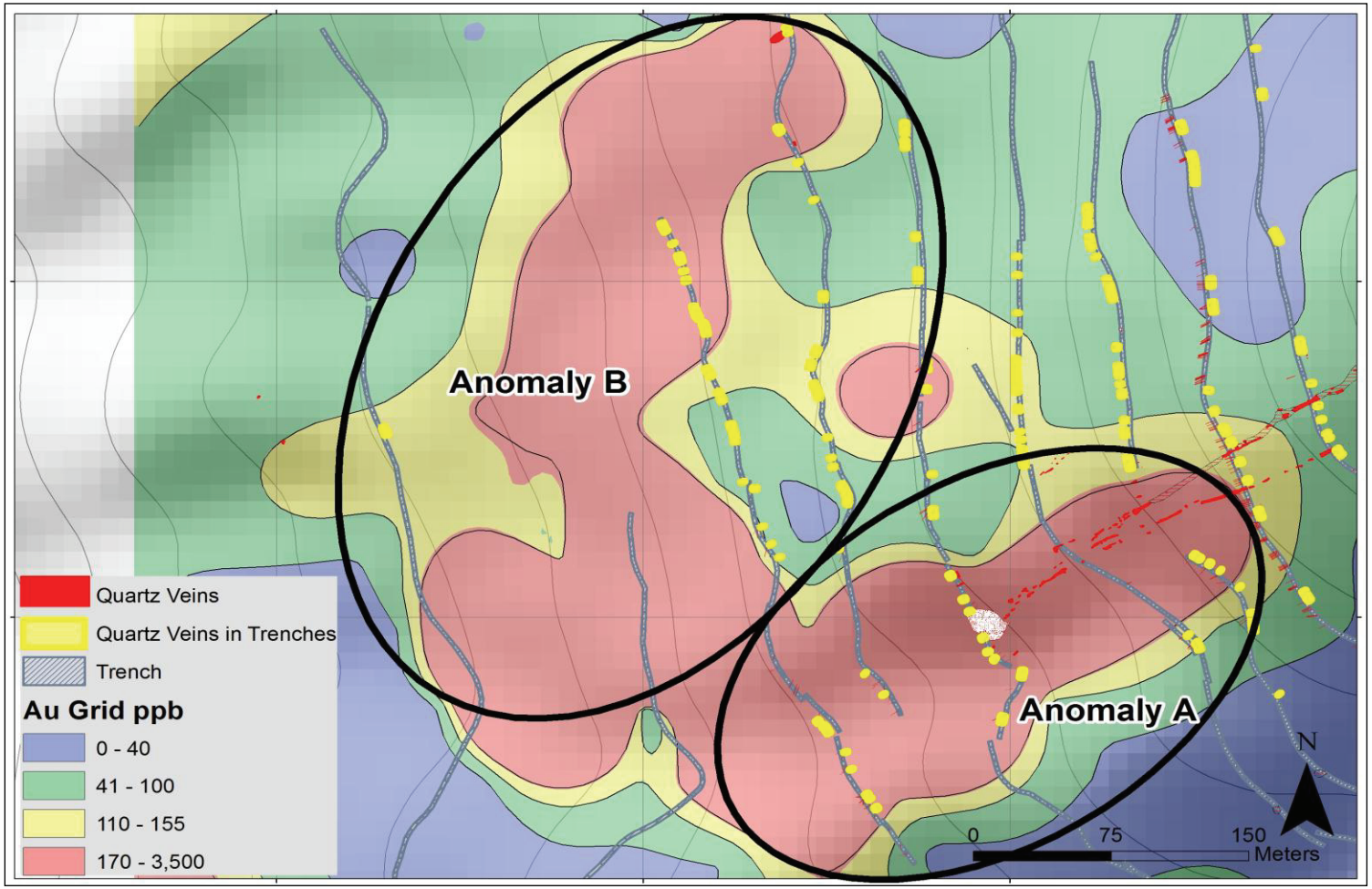

Figure 53. Anomaly A and Anomaly B with trenches.

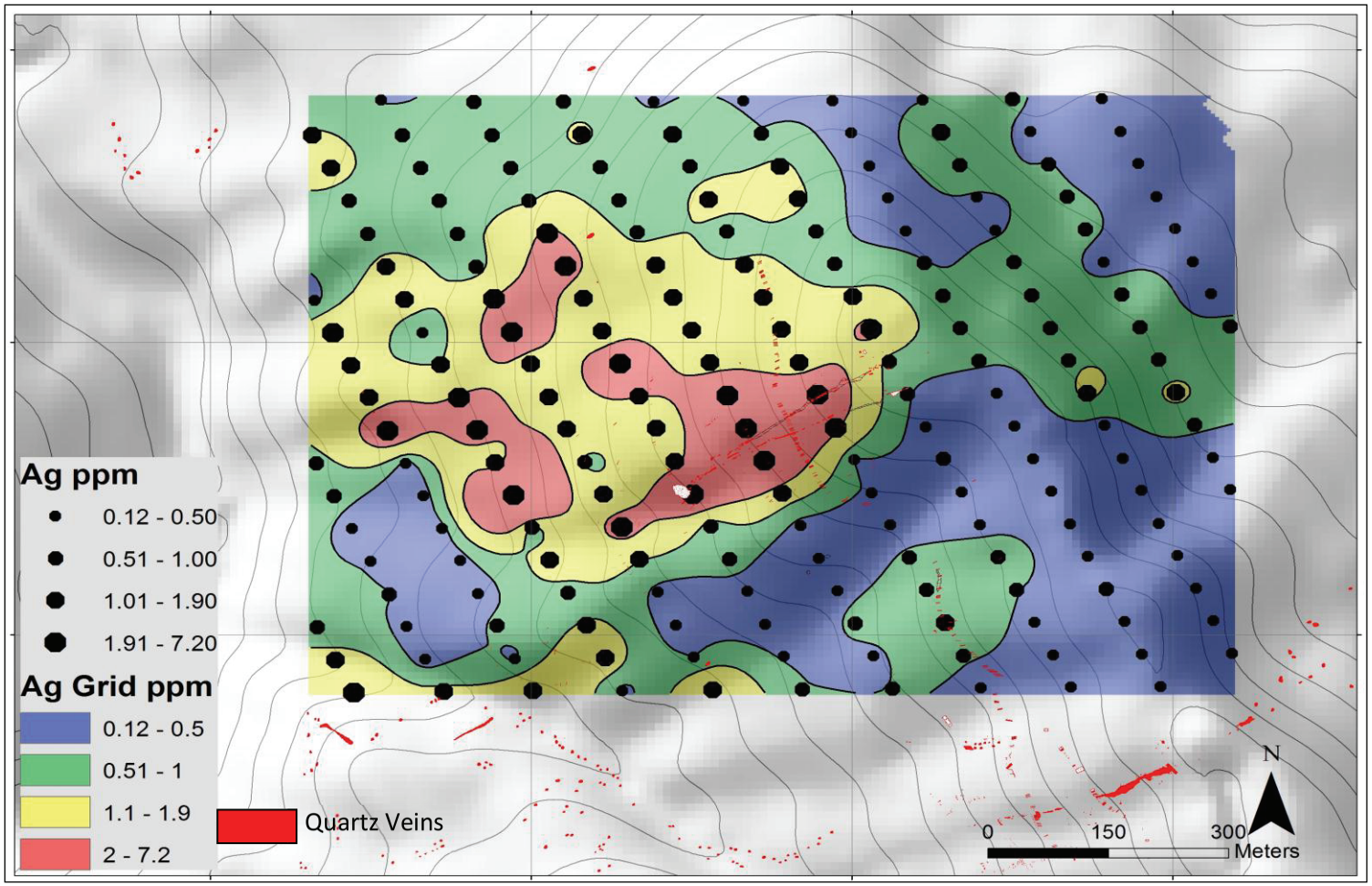

Figure 54. The Ag soil anomaly map.

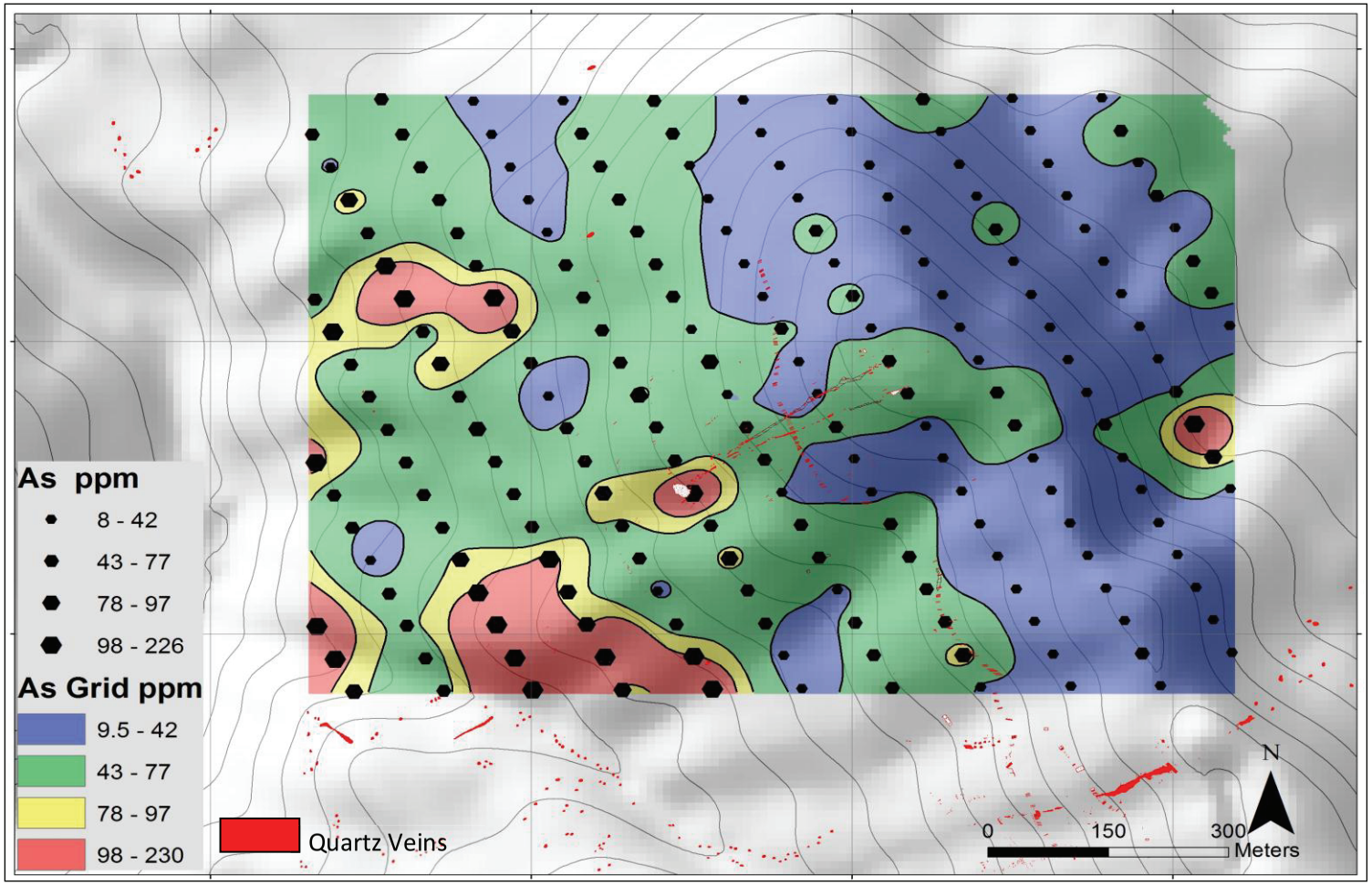

Figure 55. The As soil anomaly map.

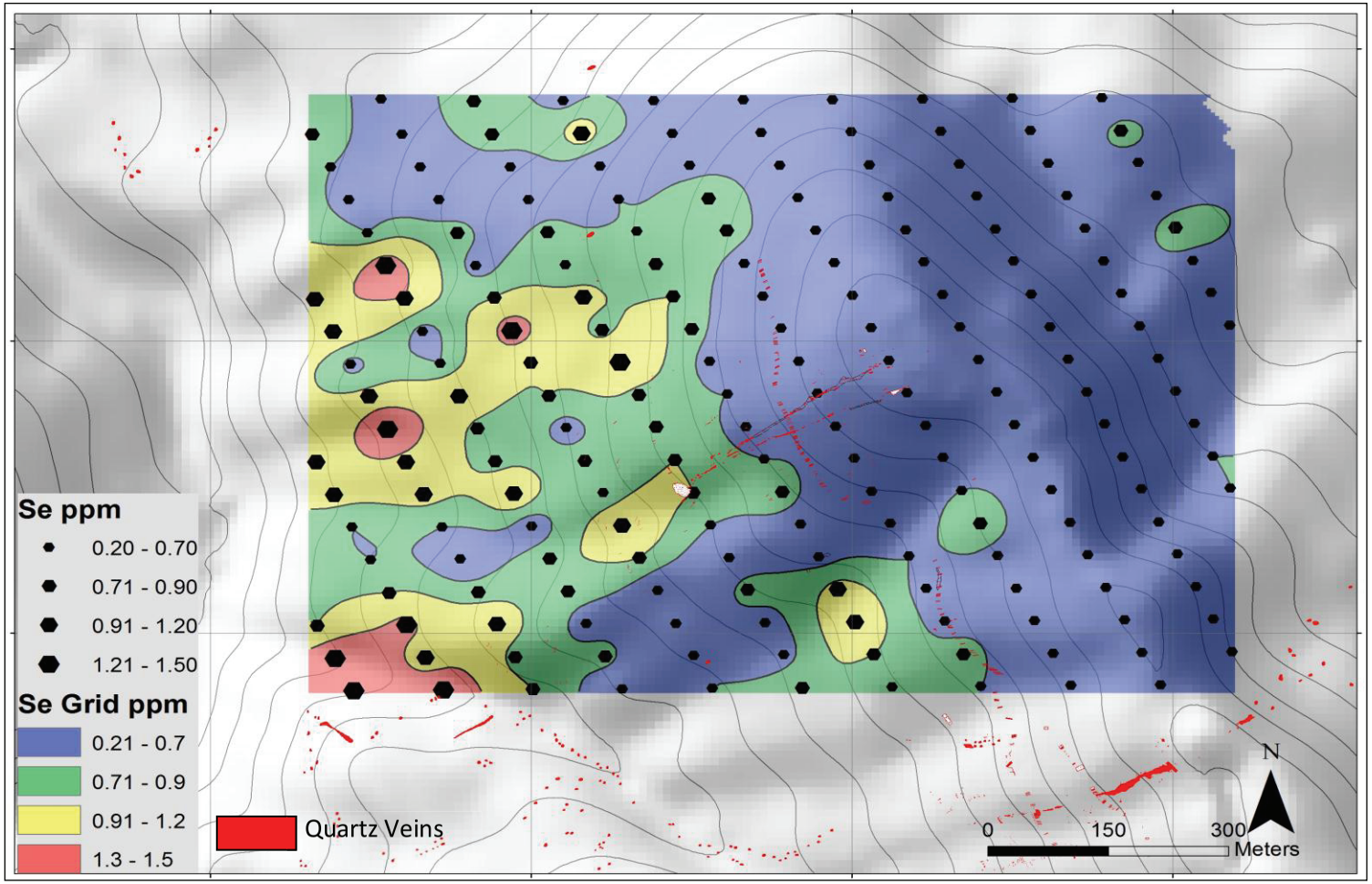

Figure 56. The Se soil anomaly map.

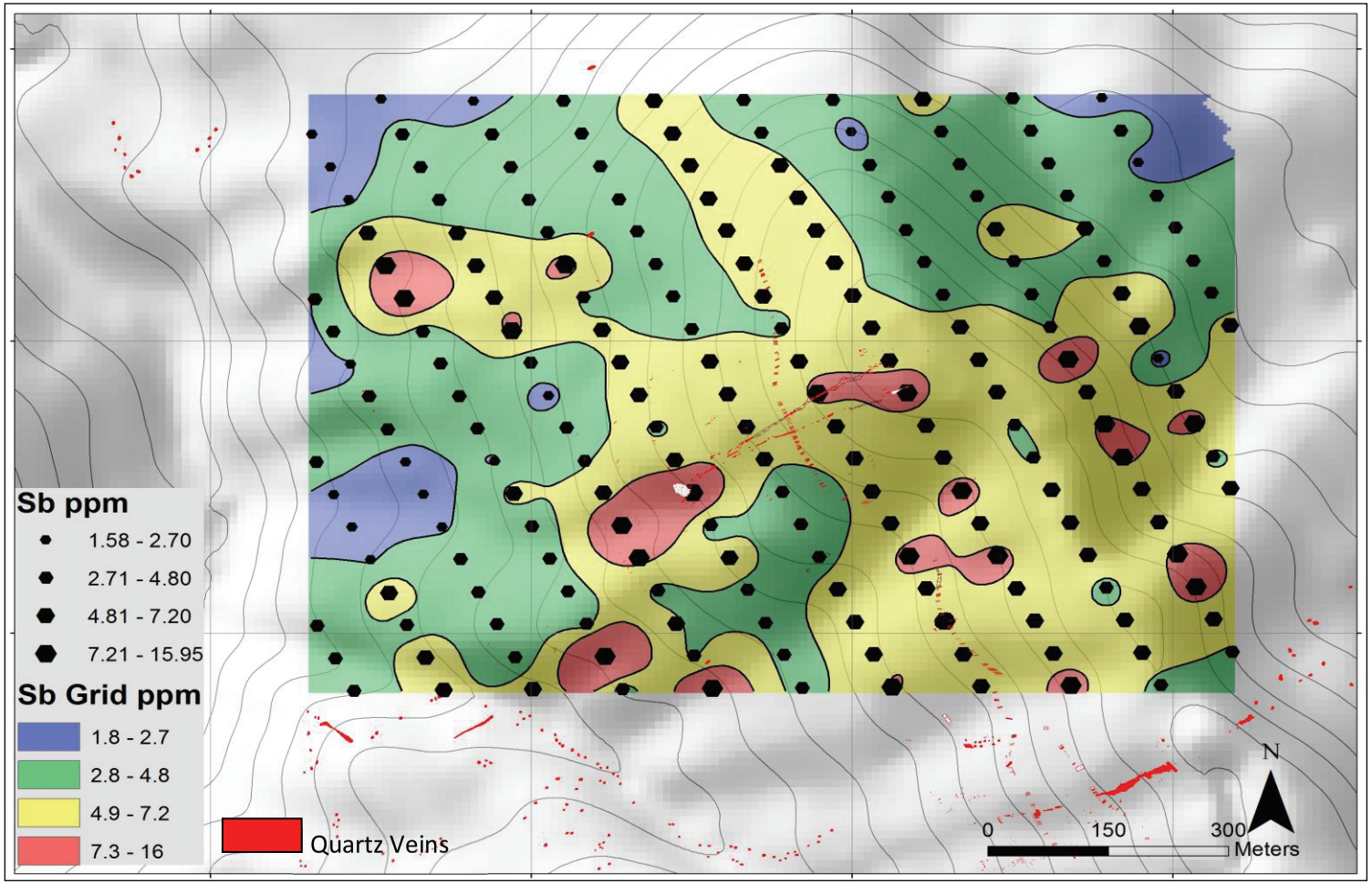

Figure 57. The Sb soil anomaly map.

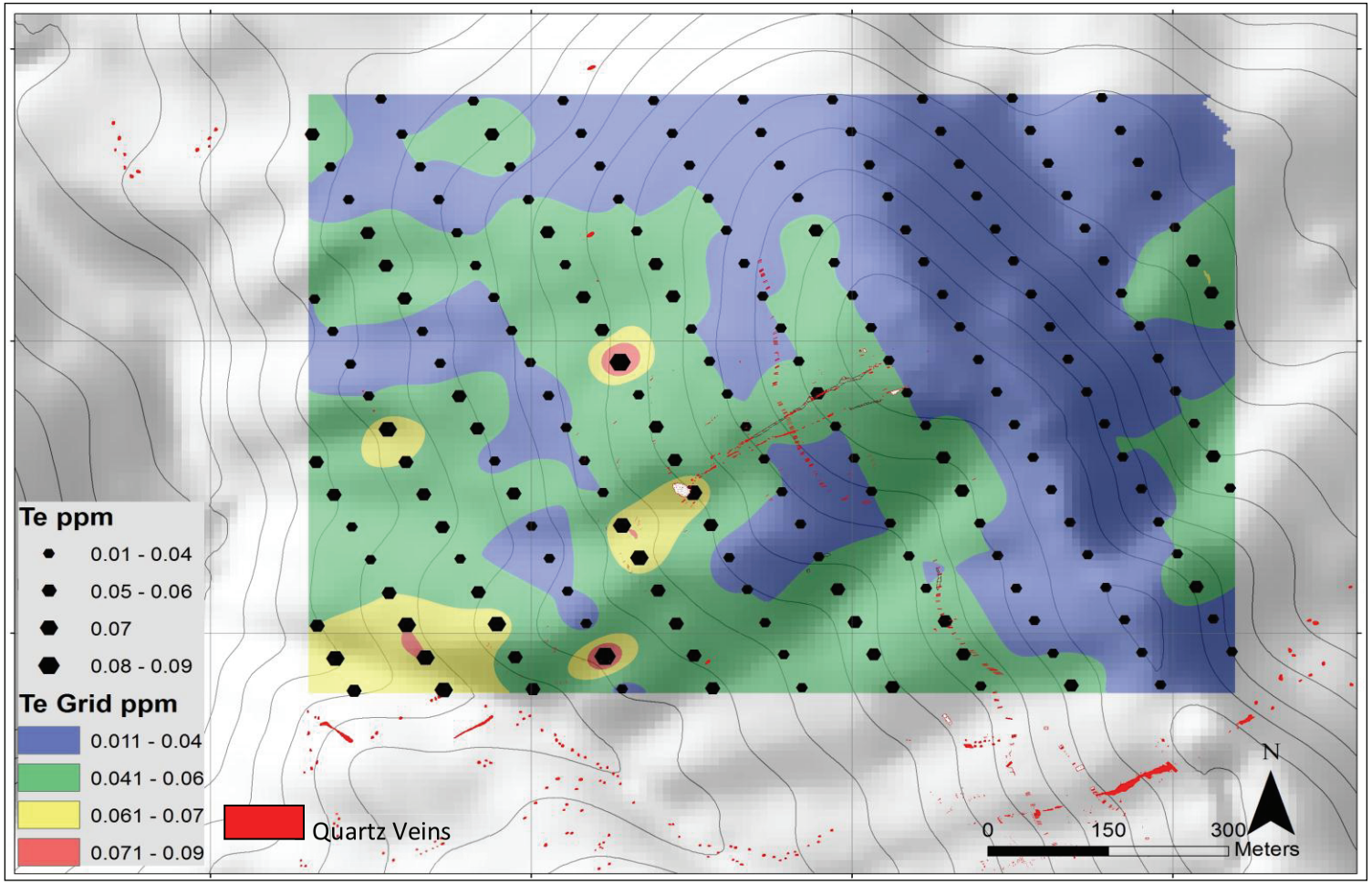

Figure 58. The Te soil anomaly map.

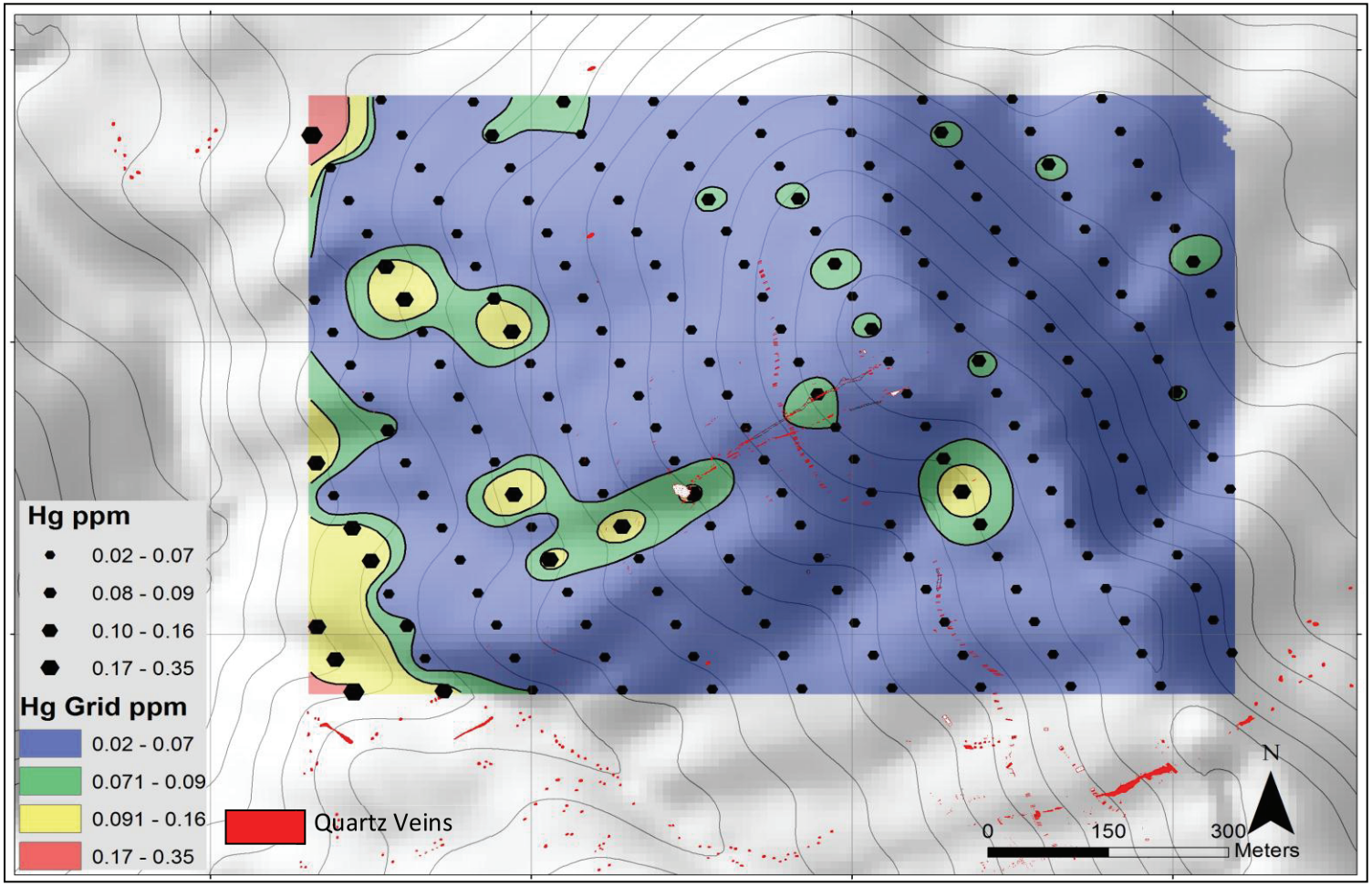

Figure 59. The Hg soil anomaly map.

In the dataset, there are more than two sub-populations for each element. Higher grade sub-population (higher backgrounds) may mask low grade sub-populations. Therefore, weaker anomalies may appear to be insignificant in terms of target generation for further exploration. In this study, in order to find out importance of the lower background populations, high geochemical values of the population with higher background was separated from the dataset for Au and Ag. Statistical methods were applied to the new dataset to determine new background, threshold and anomaly values to identify new target zones.

Figures 60-62 show the Q-Q plot, P-P plot and gridding map for Au, respectively. According to Q-Q plot, the raw data of Au deviated far from normal distribution. Hence, P-P plot and gridding map were created by using log-transformed data of Au. P-P plot shows that Au has three populations indicated by two inflection points I1 (30 ppb) and I2 (70 ppb). Anomaly values are above 70 ppb and the background values are below 20 ppb. In the comparison of two gold grid maps, one includes high-valued populations and the other does not, three new target areas were observed in the low-valued population map. The largest one is located the west part of the study are and the other is located at southeast of the area.

The Q-Q plot, P-P plot and gridding map for Ag are shown in Figures 62-64. Because the raw data of Ag does not follow normal distribution, P-P plot and gridding map were created based on log-transformed data. P-P plot shows that Ag is characterized by three populations indicated by two inflection points I1 (0.6 ppm) and I2 (1.0 ppm). Anomaly values are above 1.0 ppm and the background values are below 0.3 ppm. The gridding map of Ag shows that Ag forms a strong and widespread anomaly which is found in the same area as high population map. On the other hand, Ag formed two strong anomalies at west of the area and a strong anomaly at southeast of the area. These anomalies are located almost the same area with anomalies of Au.

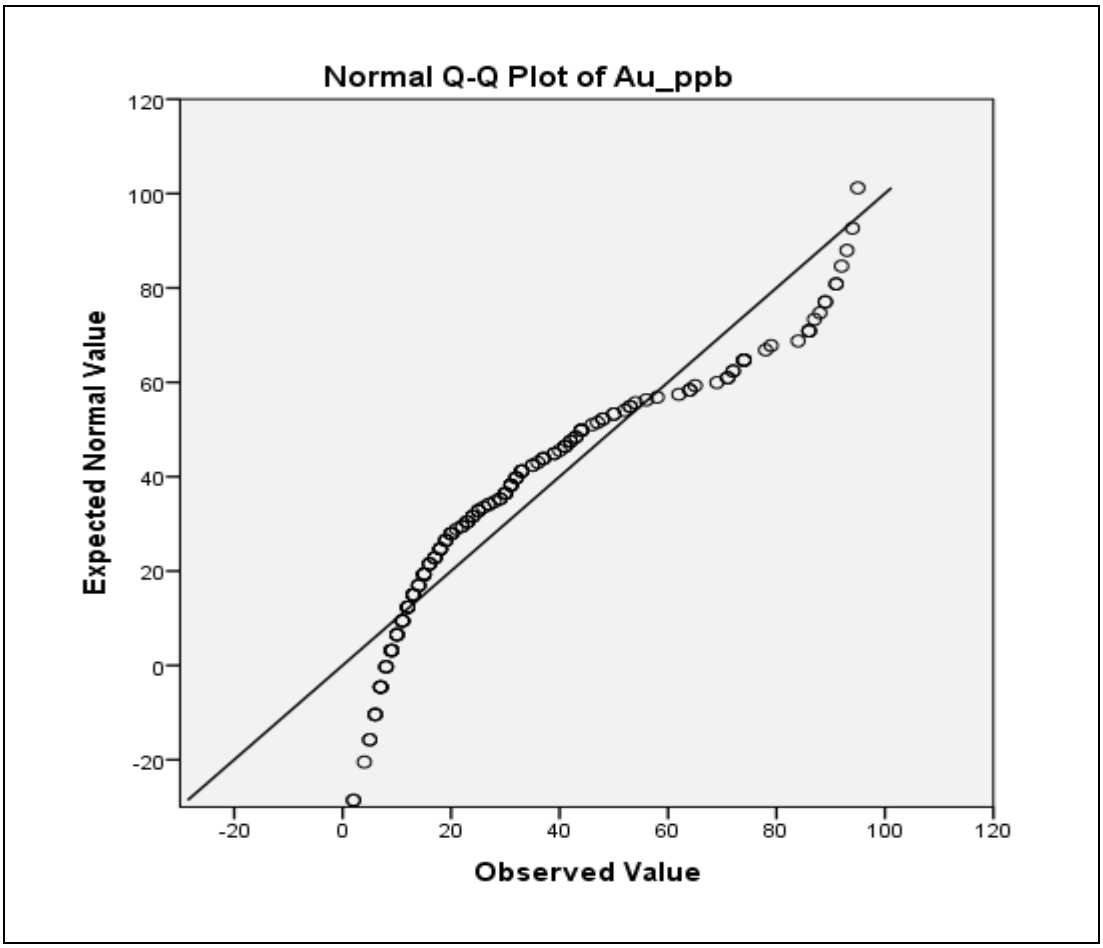

Figure 60. Q-Q plot for low geochemical Au values.

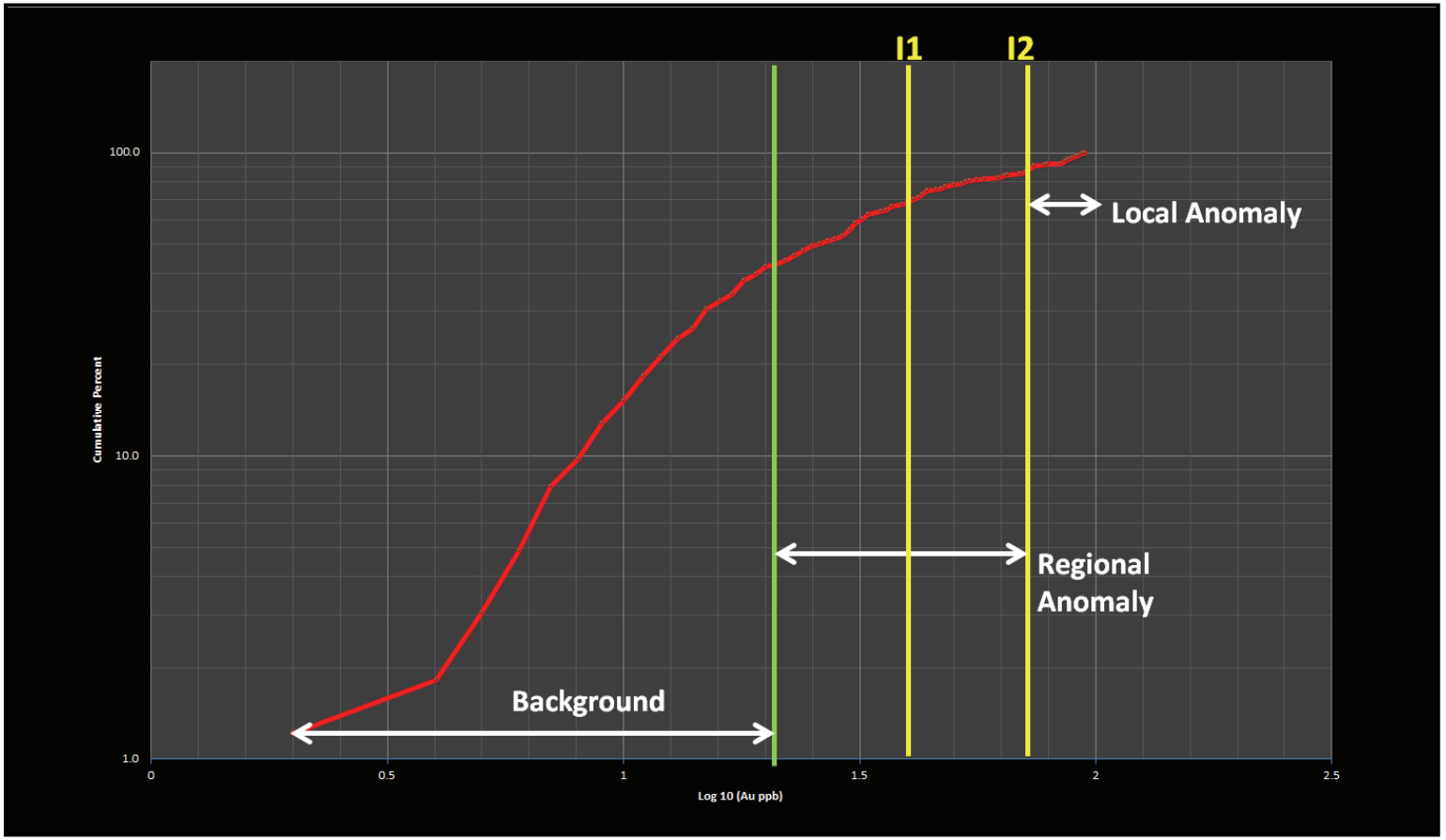

Figure 61. P-P plot for low geochemical Au values (I1 and I2: inflection points).

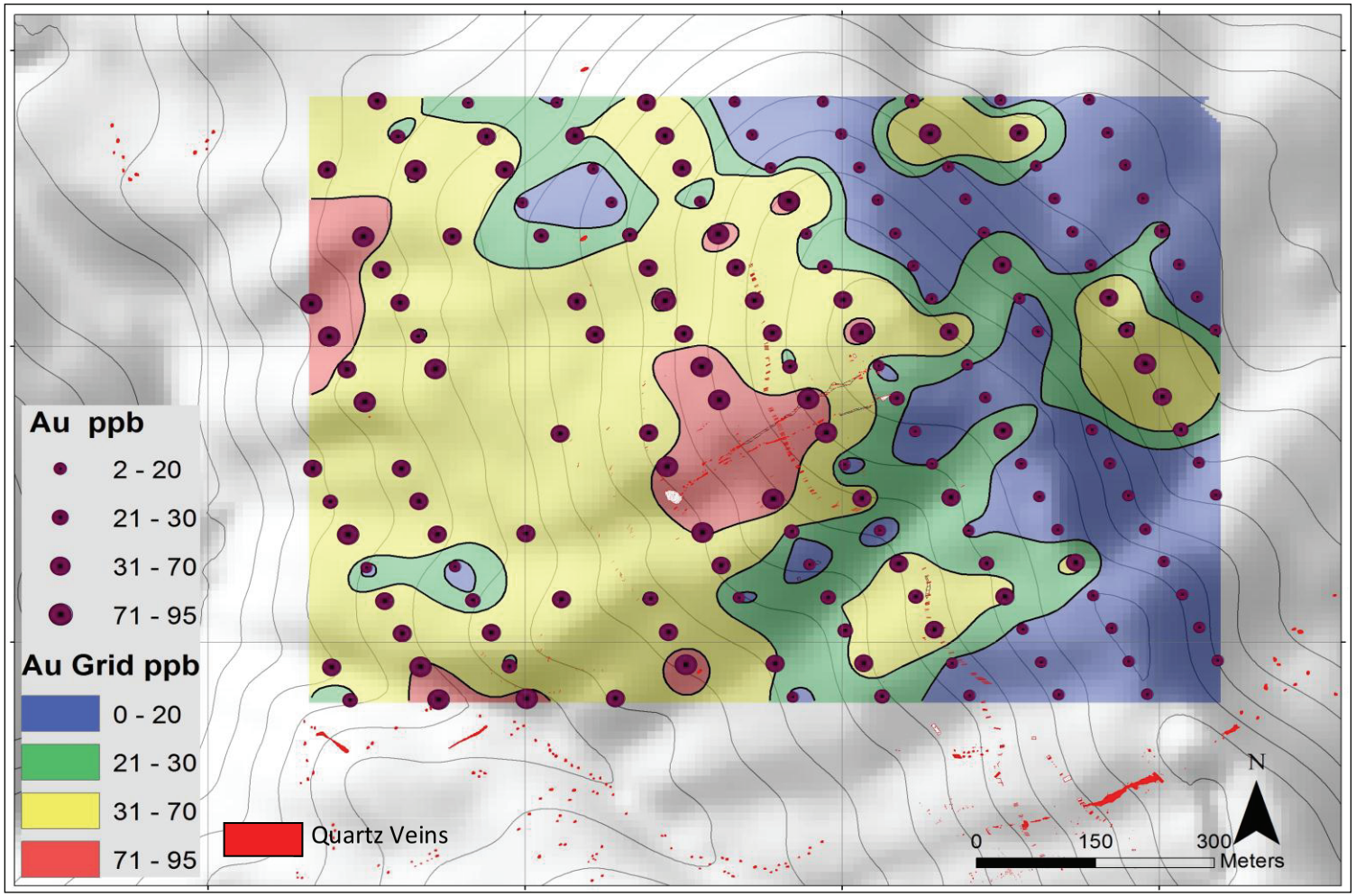

Figure 62. The low geochemical soil anomaly map for Au.

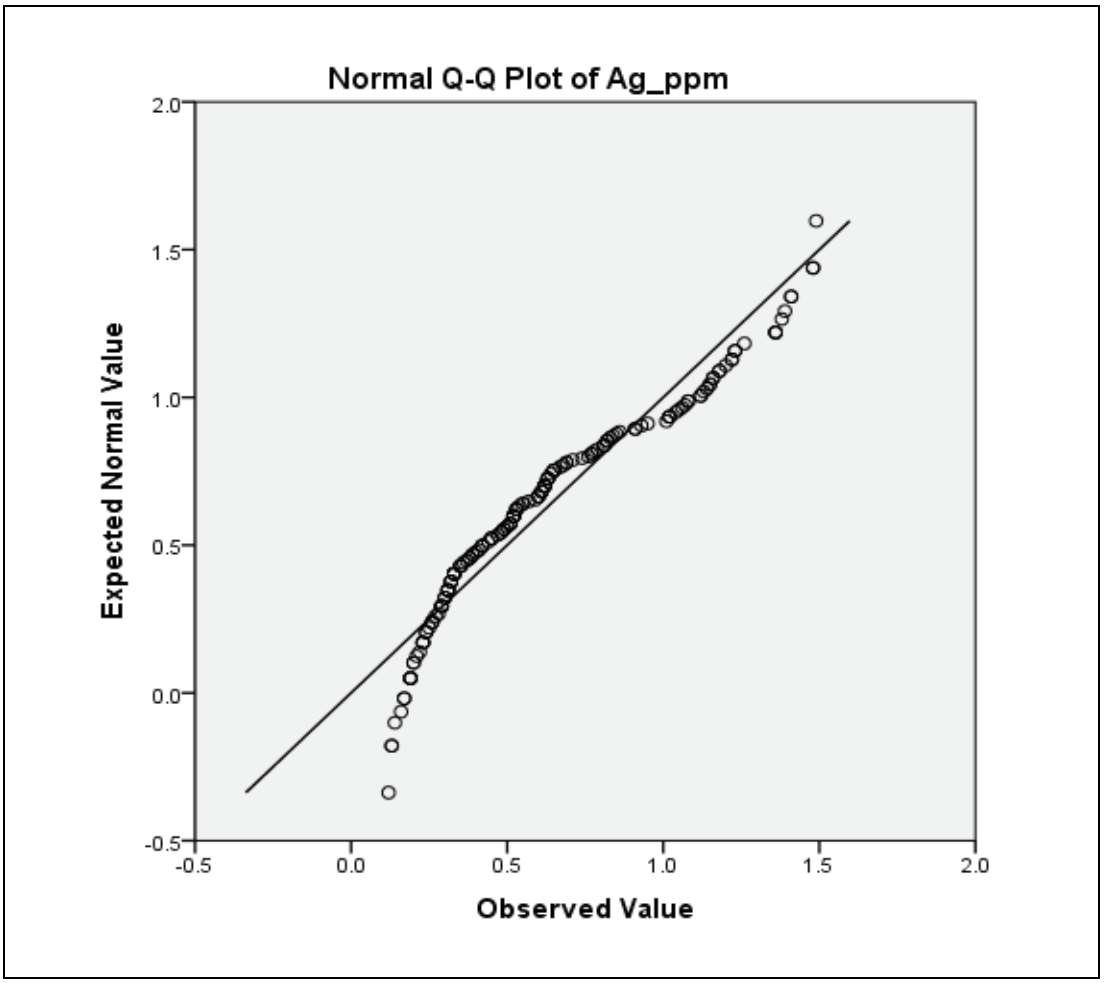

Figure 63. Q-Q plot for low geochemical Ag values.

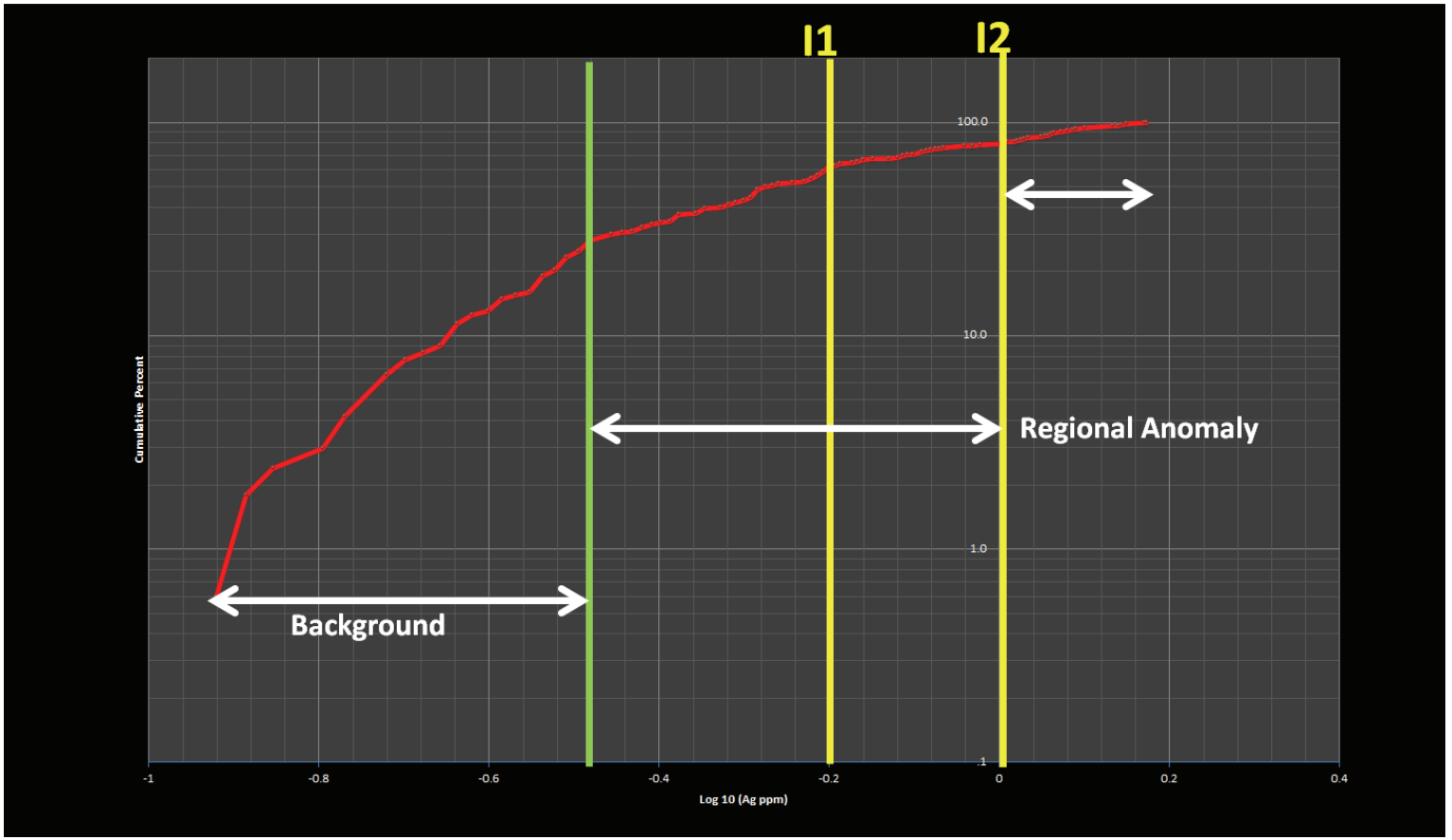

Figure 64. P-P plot for low geochemical Ag values (I1 and I2: inflection points).

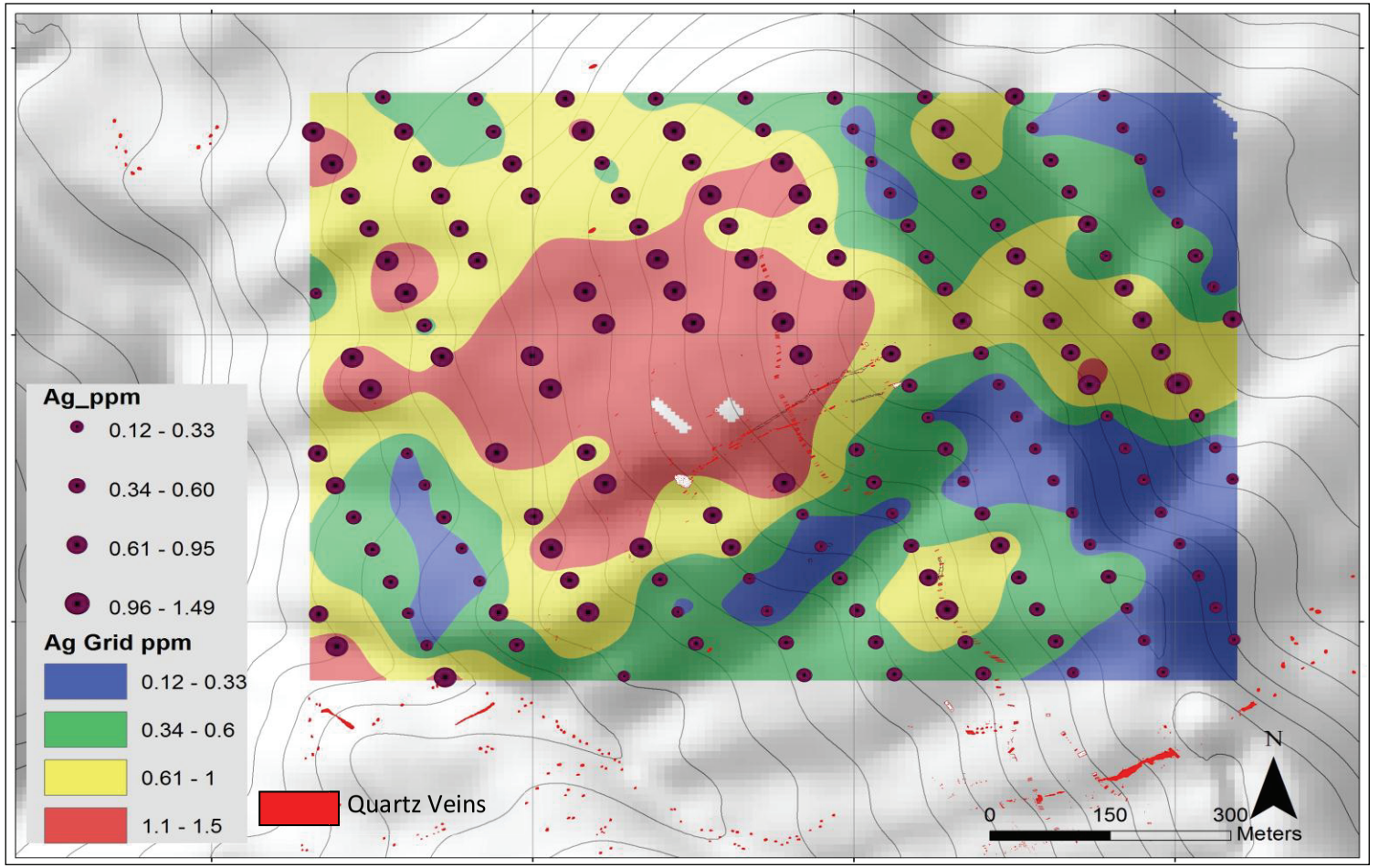

Figure 65. The low geochemical soil anomaly map for Ag.

CHAPTER 6

RESULTS AND CONCLUSIONS

In this study, geostatistical techniques were applied to interpret surface soil geochemical results and investigate Au, Ag, As, Hg, Sb, Se, and Te concentrations and their distribution patterns. Anomalous haloes were identified on gridding maps in order to select new Au targets for further exploration.

The conclusions of the geostatistical studies are:

- Descriptive statistics and histograms of the seven elements show that, Au, Ag, As, Hg, and Sb have non-normal distribution patterns while Se and Te have normal distribution patterns. To approach a normal distribution, raw data of Au, Ag, As, Hg, and Sb were logarithmically transformed (log10).
- Q-Q plots were used to examine datasets graphically whether geochemical data follow normal or log-normal distribution. According to Q-Q plots of the seven elements, datasets of Au, Ag, As, Hg, and Sb deviated far away from the normal distribution. However, datasets of Se and Te are close to normal, they do approximate straight line. These results are consistent with the results from descriptive statistics and histograms.
- The box and whisker boxes were used to show the distribution of datasets graphically and determine threshold values for seven elements. Au, Ag, As, Hg, Sb, and Se boxes show that the distributions of elements are skewed. However, the median of Te plots near the center of box, indicating that the data are close to a normal distribution.
- The correlation matrix was generated for all the variables to determine the relations between elements. According to matrix results, Au has only positive

moderate correlation with Ag. This aspect is also seen in the Au/Ag scatter plot. Silver has low correlation with Se and Te has moderate correlation with As and Se.

- Cumulative probability graphs were created to estimate background, local anomaly and regional anomaly values. The distribution of Au and Ag have five populations whereas As, and Sb have four and Hg, Se and Te have two. The samples close to the mineralized zone indicated the presence of local Au-Ag anomalies, whereas the widespread alteration caused regional Au-Ag anomalies.
- Finally, threshold values which were estimated from the calculation of mean plus two standard deviations, box and whisker boxes, and cumulative probability graphs were compared with each other. Because the outliers are below 10% for Au (3%), Ag (4%), As (5%), and Sb (3%), the threshold values calculated from box plots are close to the threshold values estimated from the cumulative probability graphs. Results of Hg, Se and Te do not show any outliers. Therefore, the threshold values calculated by mean plus two standard deviations are almost the same as threshold values estimated from the cumulative probability graphs. As a result, the threshold values which are estimated from the cumulative probability graphs were accepted as more precise results.

In order to determine the element distribution in the area, gridding maps were prepared for Au, Ag, As, Hg, Sb, Se, and Te based upon calculated threshold values by using the kriging method. The results can be summarized as follows:

- Au, Ag, As, Sb, and Se form strong anomalies while Hg and Te do not. Therefore, Te and Hg are not used as pathfinder elements for this study.
- Au, Ag and As show wider and stronger anomalies in comparison to other elements.
- The strong gold anomalies nearly coincide with the strong silver anomalies at the center of the area. Hereby, Ag is considered as an indicator element for this deposit.
- Au and Ag anomalies that are located at the lower parts of the main vein zone, extend in NE-SW direction. The extension of anomalies are parallel the extension of main vein zone.

- Au and Ag anomalies that are located at topographically lower elevations and away from the main vein zone, are closely related to unexposed quartz veins and topographic effect.
- Although Ag is very mobile in the weathering environment, Ag does not disperse over a wide area and it yields anomalies coinciding with the mineralization.
- Anomaly of Se occurs approximately at the same area as the anomaly of As. However, As anomalies are stronger and wider than Se anomalies.
- As and Se appear to be enclosed to the main Au anomalies. Therefore, As and Se could be used as a pathfinder elements for prospecting for gold.
- The dispersion of strong Sb anomalies are larger than the dispersion of strong Au, Ag, As and Se anomalies due mainly to its high mobility at surface condition.

In order to identify new target zones, higher background population was separated from the datasets for Au and Ag. Hereby, weaker anomalies that masked by higher background population were found out. Weaker anomalies may reveal a potentially important exploration targets in the area. As a result of this process, new three gold targets, NE, N and SE of the area, were identified for further exploration work.

REFERENCES

Belkhiri, L., Boudoukha, A., and Mouni, L., 2010, *A multivariate statistical analysis of groundwater chemistry data*, International Journal of Environmental Research, 5(2), p.537-544.

Berger, B.R., and Eimon, P.L., 1983, *Conceptual models of epithermal precious metal deposits, in Shanks, W.C. III,* Cameron volume on unconventional mineral deposits: New York, American Institute of Mining, Metallurgy and Petroleum Engineering, and Society of Mining Engineers, p. 191-205.

Bounessah, M., and Atkin, B.P., 2003, *An application of exploratory data analysis as a robust non-parametric technique for geochemical mapping in a semiarid climate,* Appl. Geochem., 18, p.1185-1195.

Buchanan, L. J., 1981, *Precious metal deposits associated with volcanic environments in the southwest,* Arizona Geologic Society Digest, Vol. 14, p. 237-261.

Chadwick, T.H., 2009, *Eurasian Minerals Inc.-Akarca and Aratepe gold projects, Western Anatolia, Turkey (unpublished).*

Corbett, G.J., and Leach, T.M., 1998, *Southwest Pacific Rim gold-copper systems: sructure, alteration and mineralization,* Society of Economic Geologists Special Publication 6, 236 p.

Davies, B., 2012, *Eurasian Minerals Inc.-Akarca Project basement targeting and trap site framework (unpublished).*

Davis, J. C., 1973, *Statistics and data analysis in geology,* Wiley, Newyork, p. 28-59.

Delaloye M. and Bingöl, E., 2000, *Granitoids from western and northwestern Anatolia: geochemistry and modelling of geodynamic evolution*, International Geology Review, v. 42, p. 241–268.

Dreier, J.E., and Soylu, M., 2011, *Akarca Gold-Silver Project Technical Report: Preliminary 43-101 report by Eurasian Minerals Inc.*

Edwards, A.L., 1976, *The correlation coefficient. In: Introduction to linear regression and correlation,* Chapter 4, W.H. Freeman and Company, San Francisco, p. 33–46.

Ferguson, 2013, *Eurasian Minerals Inc.-Structural and tectonic setting of the Akarca district, Bursa Province, Turkey (unpublished).*

Hedenquist, J.W., 1987, *Mineralization associated with volcanic related hydrothermal systems in the Circum Pacific Basin, in Horn, M.K.*, Transactions of the 4th circum Pacific energy and mineral resources conference, p. 513-523.

Hedenquist J.W., Arribas A.R., and Gonzalez-Urien G., 2000, *Exploration for epithermal gold deposits*, SEG Reviews in Economic Geology, v. 13, p. 245-277.

Hedenquist, 2011, *Eurasian Minerals Inc.-Observations on the Akarca epithermal Au prospect, Turkey (unpublished).*

Helvacı, C., 1994, *Mineral assemblages and formation of the Kestelek and Sultançayır borate deposits*, Proceeding of 29th International Geological Congress, Kyoto Part A, p. 245-264.

Hollister, F.V. 1985, *Discoveries of epithermal precious metal deposits,* AIME, Case histories of mineral discoveries, V.1, p. 168

Lepertier, C., 1969, *A simplified statistical treatment of geochemical data by graphical representation*, Econ. Geol., V.64, p. 538-550

Lindgren, W., 1933, *Mineral deposits*, Fourth Edition, McGrow-Hill, New York, 930p.

Matheron, G., 1971, *The theory of the regionalized variable and its application*, Cahier Fasc. 5, Centre de Geostatistique.

McGill, R., Tukey, J. W., and Larsen, W. A., 1978, *Variations of box plots*, The American Statistician, 32(1), p. 22-16.

Okay, A.İ., and Göncüoğlu, M. C., 2004, *The Karakaya Complex: A review of data and concepts,* Turkish Journal of Earth Sciences, p. 77-95.

Panteleyev, A., 1996, *Epithermal Au-Ag: Low Sulphidation,* Selected British Columbia Mineral Deposit Profiles, Volume 2, p. 41-44.

Reimann, C., Filzmoser, P., and Garrett, R., 2005, *Background and threshold: critical comparison of methods of determination,* Sci. Total Environ., 346, p.1-16.

Rose, A.W., Hawkes, H.E. and Webb, J.S., 1979, *Geochemistry in mineral exploration,* Academic Press, New York, N.Y., p. 490--517.

Sapancı, Ö., 2011, *Çataldağ (Balıkesir) granitoyidinin petrografik ve jeokimyasal özellikleri,* Master's Thesis, Kocaeli Üniversitesi, Fen Bilimleri Enstitüsü, Jeoloji Mühendisliği Bölümü, Kocaeli.

Shapiro, S. S., 1990, *How to test normality and other distribution assumptions*, Milwaukee, WI: American Society for Quality, p. 50-52.

Sillitoe, R. H., and Bonhom, H. F., 1984, *Volcanic landforms and ore deposits*, Econ. Geol., 79, p. 1286-1298.

Sillitoe, R.H., 1993. *Epithermal models: Genetic types, geometrical controls and shallow features,* Geological Association of Canada Special Paper 40, p. 403-417.

Sillitoe, R. H., and Hedenquist, W. J., 2003, *Linkages between volcanotectonic settings, ore-fluid compositions, and epithemal precious metal deposits*, Society of Economic Geologist, Special Publication 10.

Sinclair, A. J., 1974, *Selection of threshold values in geothermal data uusing probability graph*, Journal of Geochemical Exploration, p. 129-149.

Sinclair, A. J., 1991, *A fundamental approach to threshold estimation in exploration geochemistry*, probability plots revisited, J. Geochem. Explor., 41(1), p.1–22..

Taylor, B.E., 2007. *Epithermal gold deposits: in Goodfellow, W.D., ed., Mineral deposits of Canada: a synthesis of major deposit-types, district metallogeny, the evolution of geological provinces, and exploration methods*, Geological Association of Canada, Mineral Deposits Division, Special Publication, v. 5, p. 113-139.

Toprak, V., 2014, AMM-Lithological Logging of AkarcaProject, Bursa, *(unpublished)*.

Tosdal,R., 2010, *Eurasian Minerals Inc.-Evaluation of the current understanding of the low sulfidation style epithermal veins at the Akarca property, Western Anatolia, Turkey, (unpublished)*.

Tukey, J. W., 1977, *Exploratory data analysis,* Addison-Wesley, 1st ed.

White, N.C, and Hedenquist, J.W., 1995, *Epithermal gold deposits: Styles, characteristics and exploration*, SEG Newsletter, v. 23, p. 1, 9-13.

Yalçınkaya, S., and Avşar, Ö.P., 1980, *Mustafakemalpaşa (Bursa) ve dolayının jeolojisi,* MTA Rapor No: 6717.

APPENDIX A

DESCRIPTIVE STATISTICS TABLE

Table 5. Descriptive statistics for all elements.

	Range	Minimum	Maximum	Sum	Mean	Std. Deviation	Variance	Skewness	Kurtosis
Au (ppb)	3,488	2.00	3490.0	17,121	87.80	288.31	83,123.53	9.68	106.29
Ag (ppm)	7	0.12	7.2	171	0.88	0.82	0.67	3.29	18.73
Al %	2	0.23	2.1	186	0.96	0.30	0.09	1.01	1.86
As (ppm)	218	8.40	226.0	10,514	53.92	32.18	1,035.49	1.97	5.54
Ba (ppm)	280	30.00	310.0	15,560	79.79	38.50	1,482.43	2.34	8.49
Be (ppm)	5	0.29	5.6	232	1.19	0.46	0.21	4.79	43.94
Bi (ppm)	0	0.08	0.3	41	0.21	0.04	0.00	0.08	0.08
Ca %	1	0.02	0.6	26	0.13	0.11	0.01	2.05	4.61
Cd (ppm)	0	0.02	0.4	15	0.08	0.05	0.00	2.70	11.45
Ce (ppm)	72	8.95	81.3	9,071	46.52	12.91	166.64	0.24	-0.31
Co (ppm)	38	3.20	41.5	3,014	15.46	5.73	32.82	0.81	1.29
Cr (ppm)	161	17.00	178.0	14,095	72.28	26.42	698.10	1.63	3.21
Cs (ppm)	19	0.72	19.6	809	4.15	2.03	4.11	3.28	18.57
Cu (ppm)	39	4.80	43.3	3,526	18.08	5.95	35.41	1.12	1.95
Fe %	4	0.75	5.2	521	2.67	0.67	0.45	0.60	1.28

Table 5 (Cont'd)

	Range	Minimum	Maximum	Sum	Mean	Std. Deviation	Variance	Skewness	Kurtosis
Ga (ppm)	8	1.05	9.5	919	4.71	1.14	1.31	0.88	2.09
Ge (ppm)	0	0.05	0.1	11	0.05	0.01	0.00	2.21	4.76
Hf (ppm)	0	0.02	0.2	7	0.04	0.02	0.00	2.15	6.27
Hg (ppm)	0	0.02	0.4	11	0.06	0.03	0.00	4.38	32.00
K %	0	0.03	0.2	19	0.10	0.03	0.00	1.19	2.44
La_ppm	34	6.20	40.1	3,967	20.34	6.45	41.61	0.76	0.19
Li_ppm	42	2.80	44.6	1,765	9.05	4.73	22.36	3.42	19.09
Mg %	1	0.04	0.8	29	0.15	0.09	0.01	4.61	26.78
Mn (ppm)	4,024	146.00	4170.0	170,743	875.61	548.06	300,373.99	2.08	7.62
Mo (ppm)	7	0.34	7.0	144	0.74	0.50	0.25	10.37	126.70
Na %	0	0.01	0.0	2	0.01	0.00	0.00		
Nb (ppm)	1	0.09	1.5	108	0.55	0.24	0.06	0.98	1.16
Ni (ppm)	230	22.30	252.0	16,687	85.57	35.18	1,237.51	1.72	4.02
P (ppm)	1,040	150.00	1190.0	80,310	411.85	205.46	42,214.10	1.00	0.76
Pb (ppm)	75	7.80	82.6	4,152	21.29	7.06	49.82	4.12	31.20
Rb (ppm)	44	6.80	50.9	5,233	26.84	8.69	75.50	0.47	-0.29
S %	0	0.01	0.1	3	0.01	0.01	0.00	3.20	15.23
Sb (ppm)	14	1.58	16.0	966	4.95	2.04	4.17	1.47	4.52
Sc (ppm)	8	0.90	8.8	748	3.84	1.26	1.58	1.05	2.09
Se (ppm)	1	0.20	1.5	131	0.67	0.27	0.07	0.95	0.83
Sn (ppm)	1	0.20	1.4	166	0.85	0.19	0.04	0.44	0.38

Table 5 (Cont'd)

	Range	Minimum	Maximum	Sum	Mean	Std. Deviation	Variance	Skewness	Kurtosis
Sr (ppm)	55	3.20	58.3	1,795	9.20	5.72	32.70	4.24	29.14
Te (ppm)	0	0.01	0.1	8	0.04	0.01	0.00	0.88	1.66
Th (ppm)	6	0.40	6.5	625	3.20	1.05	1.11	0.47	0.44
Ti %	0	0.01	0.0	2	0.01	0.01	0.00	1.18	1.20
Tl (ppm)	8	0.08	7.6	161	0.83	0.75	0.56	4.96	37.54
U (ppm)	3	0.12	3.5	137	0.70	0.38	0.15	2.75	15.05
V (ppm)	66	13.00	79.0	9,213	47.25	10.99	120.88	0.23	0.07
W (ppm)	2	0.08	1.6	51	0.26	0.15	0.02	4.51	37.39
Y (ppm)	19	1.64	20.9	1,446	7.41	4.48	20.09	1.13	0.65
Zn (ppm)	67	17.00	84.0	7,831	40.16	10.76	115.73	1.16	1.88
Zr_ppm	4	0.50	4.0	184	0.95	0.64	0.41	2.25	6.25

APPENDIX B

SCATTER PLOTS

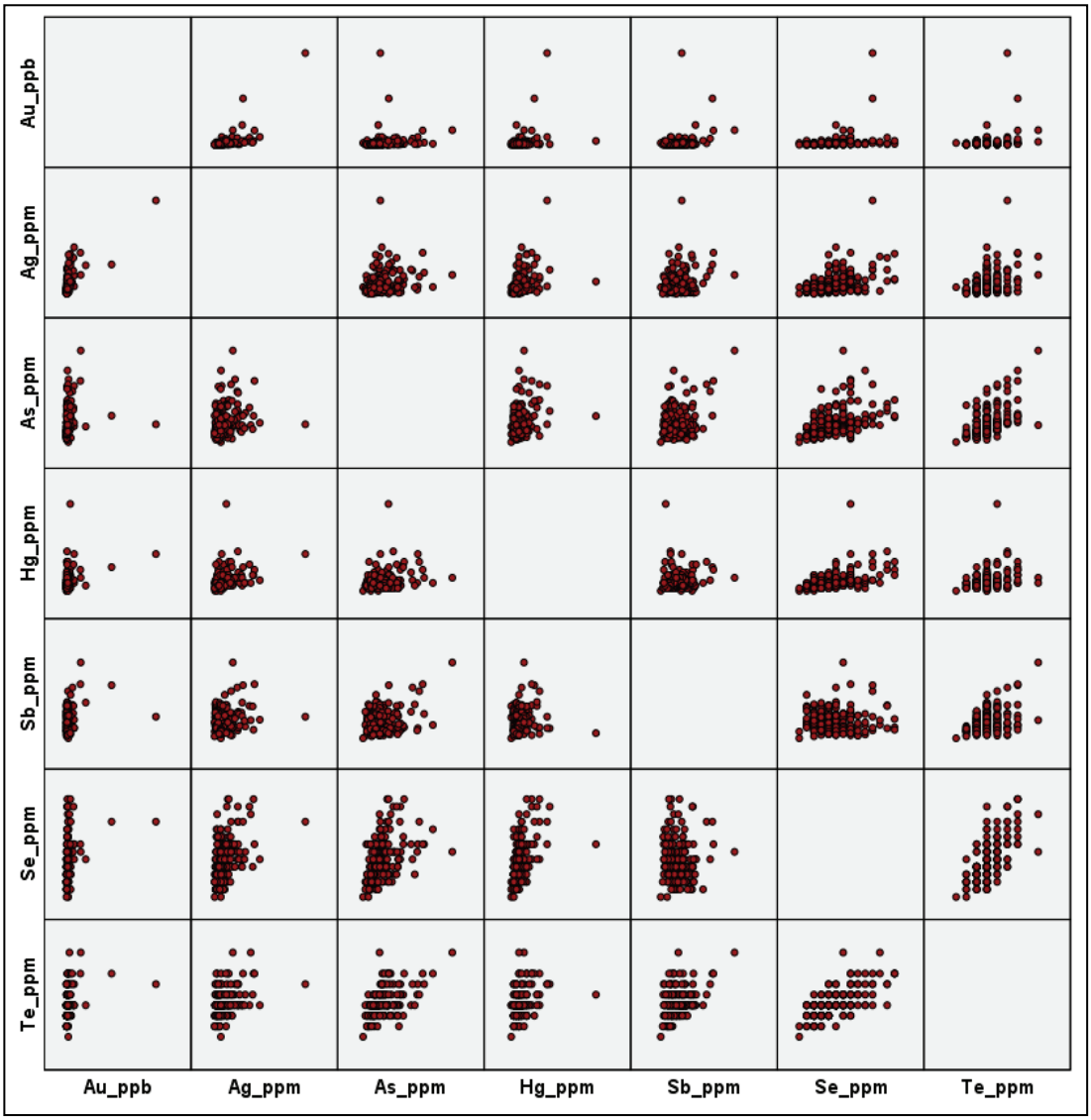

Figure 66. Scatter plots for selected elements.